UNIVERSITY OF OKLAHOMA

GRADUATE COLLEGE

SUB-SEISMIC REEF CHARACTERIZATION USING MACHINE LEARNING AND MULTI-ATTRIBUTE ANALYSIS

A THESIS

SUBMITTED TO THE GRADUATE FACULTY

in partial fulfillment of the requirements for the

Degree of

MASTER OF SCIENCE

By

CARL ROBERT BUIST

Norman, Oklahoma

2020

Downloaded from SHAREOK. Persistent Handle URL: https://hdl.handle.net/11244/325206

SUB-SEISMIC REEF CHARACTERIZATION USING MACHINE LEARNING AND MULTI-ATTRIBUTE ANALYSIS

A THESIS APPROVED FOR THE
SCHOOL OF GEOSCIENCES

BY THE COMMITTEE CONSISTING OF

Dr. Heather Bedle, Chair

Dr. John Pigott

Dr. Matthew Rine

© Copyright by CARL ROBERT BUIST 2020
All Rights Reserved.

Acknowledgements

I would first like to thank my committee members, Dr. Matt Rine and Dr. John Pigott, for all their help, guidance, and insight through this MS research. My research would not have been possible without them.

To the wonderful members of SDA and AASPI. Thank you for all your feedback and help during my practice presentations and for being so kind and friendly. To Dr. Kurt Marfurt, thank you so much for all your helpful comments and suggestions. Without your help, many interesting things discovered in this research would have remained unseen. And a big thank you to Ashley Tullius, Ginger Leivas, Leah Moser and Rebecca Fay for helping me as well. You all made OU warm and welcoming.

Next, I would like to thank all my friends that have been there for me and helped me throughout all these years. You were always there to lead an ear when I needed to talk and were always around when I needed some company. So, thank you so much to James Kubricht, Howard Lin, Casey Crews, Jami Marcum, Josh Davis, Ryne Quinn, Ana Rovira, Tina Vu, Nate and Emily Pitchford, Whitney Warneke, Joel Warneke, Josh Narabal, and Somaria Sammy, to name only a few. Because of you all, I was able to achieve everything I have so far without losing too much of my sanity.

To my Uncle Carl and Aunt Carol. Thank you for being supportive of me through my long academic journey. To my brother, Crash, thank you for being such a wonderful brother. You were always there to make me laugh when I needed some happiness. To my mom and dad, thank you for all your love and support. Thank you so much for always pushing me to follow my dreams, despite how long it took me to catch them. You two have taught me so many things that I will never forget and always cherish. I love you all dearly.

To my advisor and dear friend, Dr. Heather Bedle, thank you so much for all your patience and guidance through my long time spent in graduate school. Becoming your TA was the luckiest thing that could have happened to me. Not only have you taught me so much about geophysics, but you have also been a wonderful mentor and role model. Thank you for not

giving up on me when I was close to giving up on myself. Without you I would not be where I am today.

And to Amber. Thank you so much for everything you have done for me. You have always been supportive, encouraging, caring, understanding, and loving. You were always there to pick me up when I was getting down. You were always there to congratulate me when I succeeded. You have always been there to share my life with, and no amount of flowery phrasing or fancy wordplay can express how much I appreciate that. You mean the world to me and I love you with everything I have. Thank you.

Finally, to everyone else who has been there for me, thank you. Everything that has happened to me has been because of the kindness and support of all my friends and family.

Abstract:

Historically, Silurian reef complexes in the Michigan Basin have been largely identified using 2D seismic surveys with very little research focusing on characterizing these reefs (morphology, internal architecture, reservoir quality, etc.) using 3D seismic data. To date, the only 3D study, conducted by Toelle and Ganshin (2018), had sub-optimal resolution due to a thick glacial overburden, no core/petrophysical data, and a very small number of wells with geophysical logs for correlation. This study is the first to incorporate a high-resolution 3D dataset with a well-studied and data-rich reef reservoir that attempts to correlate seismic attributes to petrophysical properties through machine learning and self-organizing maps (SOMs). This study provides a workflow for quantitative seismic attribute analysis derived from a data-rich reef analog field in SE Michigan that can be used as a blueprint for characterizing reefs with less data (core/logs) for the purpose of future exploration, gas storage, and CO_2 sequestration efforts.

The workflow construction began by choosing the most data-rich reef reservoir, Puttygut reef, from a field on the SE side of the Michigan Basin. A suite of structural and frequency-based attributes were calculated from pre-stack time migrated (PSTM) seismic data. A subset of those attributes were then selected by an interpreter to be used as inputs to the SOM, which is an unsupervised machine learning algorithm. The SOM is able to take the input data that is usually viewed at the wavelet scale and transforms it to have beneficial information at the sample scale.

A strong relationship between certain combination percentages of attributes and certain sections of the reef with specific porosity (and potentially permeability) was found after the SOM was calculated and compared to the well log data in the Puttygut reef. Areas with high permeability and porosity correlated well with attribute combinations high in average frequency and spectral decomposition at 29 and 81 Hz. Areas with high porosity and varying permeability correlated well with attribute combinations high in average frequency and spectral decomposition at 29, 57, and 81 Hz. Areas with intermediate porosity correlated well with attribute combinations high in average frequency and spectral decomposition at 29 and 57

Hz. The created workflow was then applied to two nearby reefs. The results were very similar, showing the same attribute combinations correlating with the same sections of the reefs with similar porosity and permeability values.

The developed workflow from this study was able to consistently find a relationship between certain sections of a reef reservoir with a specific range of porosity and permeability on the SE side of the Michigan Basin.

Table of Contents

ACKNOWLEDGEMENTS ..... **IV**

ABSTRACT: ..... **VI**

CHAPTER 1: INTRODUCTION **1**

MOTIVATION 1

CHAPTER 2: PARADISE MACHINE LEARNING AND SOM WORKFLOW METHODOLOGY **6**

REGIONAL GEOLOGY 6

PURPOSED METHODS 14

PUTTYGUT DATA 23

PUTTYGUT SINGLE AND MULTI-ATTRIBUTE RESULTS 25

DISCUSSION 40

CONCLUSIONS **44**

CHAPTER 3: APPLICATIONS OF WORKFLOW TO DIFFERENT AREAS **48**

IRA 3D 49

LENOX 3D 57

CHAPTER 4: CONCLUSIONS AND FUTURE WORK **63**

APPENDIX A: ATTRIBUTES ON PUTTYGUT PRE-STACK TIME MIGRATED DATA **66**

EXTRACTED SINGLE ATTRIBUTES ONTO OTHER EXPERT PICKED HORIZONS 66

APPENDIX B: PREVIOUS PUTTYGUT SOM RUNS **83**

HORIZON SLICES OF SOM RUN NUMBER ONE: FULL INLINE AND CROSSLINE EXTENT 84

HORIZON SLICES OF SOM RUN NUMBER TWO: CROPPED INLINE AND CROSSLINE EXTENT 86

SIDE BY SIDE OF SOM RUNS ONE AND TWO IN VERTICAL SECTION 88

APPENDIX C: INLINE VIEWS OF FINAL PUTTYGUT SOM **96**

APPENDIX D: WELL LOGS **106**

APPENDIX E: 3D SURVEY DESIGN, ACQUISITION PARAMETERS, AND PROCESSING WORKFLOW **111**

REFERENCES **115**

List of Tables

Table 1: Guelph formation facies classification table provides a more detailed explanation of the lithology in each reef section. FWB is the fair-weather wave base and SWB is the storm wave base. Modified from Rine (2019). 11

Table 2: List of all available well logs and which wells have them. See Figure 9 for well locations. 24

Table 3: List of available core data turned to logs and which wells have them. See Figure 9 for well locations. 24

Table 4: Two neurons from each SOM run from Figure 14 were chosen that characterized an interesting structural feature (which is outlined in a white dashed line). The table shows the percentages of each attribute that was used to create each neuron. Notice that there is neuron 23 listed twice but that it has different distributions of the attributes. Neuron 23 having different distributions was because each SOM had different input parameters, which caused the final results to differ. 35

Table 5: List of relevant neurons along the four wells in Figure 19. 43

Table 6: The filtered neurons for the Ira frequency SOM. While the exact percentages and attribute ratios are not exactly the same, the presence of the dominant attributes in the blends is the same. Neuron 6 is like case three from Puttygut. Neuron 16 is like case two from Puttygut. Neuron 23 is like case one from Puttygut. 53

Table 7: The filtered neurons for the Lenox frequency SOM. While the exact percentages and attribute ratios are not exactly the same, the presence of the dominant attributes in the blends is the same. Neuron 23 is like case one from Puttygut. Neuron 24 is like case two from Puttygut. 60

Table 8: Comparative table showing the attribute contribution percentages for each case at each different reef. The blue highlighting represents the attribute with the highest contribution for each SOM at each reef. The green represents the second most contributing attribute, the yellow represents the third highest contributor, and finally the orange represents the fourth highest contributor. 64

Table 9: Puttygut acquisition parameters. 111

List of Figures

Figure 1: Map of Michigan with the Michigan Basin overlain from Rine (2019). The yellow star indicates the area of interest for this research. The bottom image is a zoomed in view of the Puttygut reef with all wells shown where the pink outline represents the reef extent. 4

Figure 2: Map of Michigan showing the area of interest with a yellow star. Arbitrary well cross section over the Puttygut reef showing the gamma ray, permeability, and porosity logs. The two-way time structure map is of the Brown Formation. The fillings on the permeability log: yellow is between 1 and 10 mD, green is between 10 and 50 mD, and blue is greater than 50 mD. The fillings on the porosity logs: pink is between 0 and 3 %, yellow is between 3 and 6%, green is between 6 and 10%, and blue is greater than 10%. Uncolored logs found in Appendix D. 5

Figure 3: An abridged and modified version of the depositional history from Rine (2019). T-3 depicts bioherm initiation with the rise in sea level. T-5 and T-6 illustrate a rapid sea level rise which begins pinnacle reef growth and puts them in the "keep up" stage. T-10 marks the end of the relevant depositional history where the A-1 Evaporite, A-1 Carbonate, Rabbit Ear Anhydrite, and the A-2 Evaporite sections are deposited on top of the reefs. 7

Figure 4: Generalized stratigraphic column of the reefs in the southern trend of the Michigan Basin (Rine, 2019). 8

Figure 5: Arbitrary line through the Puttygut 3D dataset. The path can be seen on the TWT map in Figure 2. The top image is the arbitrary line without interpretation, the bottom is with horizon interpretation. The A-2 Anhydrite, A-1 Carbonate, Brown, and Gray Formations are very difficult to resolve and require a great deal of apriori geologic and structural knowledge of the area to pick accurately. The A-1 Carbonate and Clinton horizons are much easier to resolve. The A-2 Salt is shown on the flanks of the reef. 9

Figure 6: Location map for the Flower Garden Banks pinnacle reefs from NOAA Flower Garden Banks National Marine Sanctuary website. 13

Figure 7: A) West Flower Garden Bank and B) East Flower Garden Bank pinnacle reefs habitat classification by color. Maps from NOAA Flower Garden Banks National Marine Sanctuary website. 14

Figure 8: The "SOM bakery". The top right shows the original bakery with “seismic wiggle” overlay. We see that there is a clear contrast between the bread and the empanadas, resulting in a large “acoustic impedance”. The classic donuts and the jelly filled donuts are mixed up and chaotic, resulting in less of a contrast. The left grid shows the “neurons” that were created from the sweet/savory and filled/empty attributes. The bottom right image is the result after classification. Each sample point (baked good) is now classified into one of the four output neurons. 17
Figure 9: Map of Puttygut reef approximate location with all wells labeled with well flow rankings. Map from M. Rine (personal comm., 2020). 25
Figure 10: The SOM outputs voxels that are 55 by 55 feet in lateral area and 1 millisecond vertically, which is equivalent to the bin size and sample rate of the input data. 28
Figure 11: The top image shows the inline and cross line extent of the SOM runs with Bing Maps Hybrid Imagery overlay. The green box encompasses all the inlines and crosslines. The blue box is the cropped survey extent with a range from Inline 38 to 116 and from Crossline 45 to 85 and the pink outline is the mapped outline of the reef. The bottom image, at 20 times vertical exaggeration, shows the vertical extent of each SOM run. The green and blue shaded areas are associated with the green and blue boxes from the upper image and vertically constrain the data between the A-2 Carbonate and the Clinton Formation. The yellow shaded area represents the vertical extent of the third SOM run. It is laterally constrained by the blue box but vertically it is between the A-1 Carbonate and the Gray Formations. 29
Figure 12: A) The two-way time map for the Brown horizon. B) The pre-stack time migrated (PSTM) amplitude data extracted onto the Brown horizon. C) Energy ratio similarity (ERS). D) Negative curvature. E) Aberrancy. F) Grey level co-occurrence matrix (GLCM) homogeneity. Pink outline marks the outer reef boundary as defined by the A-1 Carbonate horizon. 32
Figure 13: A) Average frequency. B) Cosine of the instantaneous phase. C) Continuous wavelet transform (CWT) spectral decomposition at 29 Hz. D) CWT spectral decomposition at 57 Hz. E) CWT spectral decomposition at 81 Hz. Pink outline marks the outer reef boundary as defined by the A-1 Carbonate horizon. 33

Figure 14: Structure SOMs with a more gradational color bar. Left image was created between A-2 Carbonate and Clinton horizons. Right image is a SOM created between the A-1 Carbonate and the Gray horizons. Both SOMs are shown on the Brown horizon. Both SOMs were created with the cropped inline and crossline extent discussed in Figure 11. The white dots represent four wells that penetrate the reef. From north the south they are: P-106, P-201, P-102, P-103. Refer to text for description of white-dashed area and white arrows. The black area surrounding the SOMs is the background color for the software where there is no information being shown.....36
Figure 15: Frequency SOMs with random color bar. Left image was created between A-2 Carbonate and Clinton horizons. Right image is a SOM created between the A-1 Carbonate and the Gray horizons. Both SOMs are shown on the Brown horizon. Both SOMs were created with the cropped inline and crossline extent discussed in Figure 11. The white dots represent four wells that penetrate the reef. From north the south they are: P-106, P-201, P-102, P-103. The black area surrounding the SOMs is the background color for the software where there is no information being shown. 37
Figure 16: Structure SOMs with a more gradational color bar. Left image was created between A-2 Carbonate and Clinton horizons but visually cropped between the A-1 Carbonate and the Gray horizons. Right image is a SOM created between the A-1 Carbonate and the Gray horizons. Both VSDs are Inline 92 through well P-201, which is marked by the white vertical line. Both SOMs were created with the cropped inline and crossline extent discussed in Figure 11. The black area surrounding the SOMs is the background color for the software where there is no information being shown. 38
Figure 17: The mound feature with only relevant neurons turned on. The left SOM created the feature using five neurons while the right SOM produced it with eight neurons. The black area surrounding the SOMs is the background color for the software where there is no information being shown.....39
Figure 18: Frequency SOMs with a random color bar. Left image was created between A-2 Carbonate and Clinton horizons but visually cropped between the A-1 Carbonate and the Gray horizons. Right image is a SOM created between the A-1 Carbonate and the Gray horizons. Both

VSDs are Inline 92 through well P-201, which is marked by the white vertical line. Both SOMs were created with the cropped inline and crossline extent discussed in Figure 11. The black area surrounding the SOMs is the background color for the software where there is no information being shown.....40
Figure 19: Qualitative well/SOM correlation. Porosity (right log) and permeability (left log) logs were stretched and squeezed between SOMs at inlines that the wells are located. The blue box on well P-106 indicates an area with great permeability and porosity. The red boxes on wells P-106 and P-102 indicate areas of poor permeability and poor to intermediate porosity. The green boxes on wells P-201 and P-102 are areas of widely varying permeability but good to great porosity. The yellow boxes on well P-103 show two areas. Both with good to great porosity but with opposite permeabilities.....43
Figure 20: Relating the SOM neurons to the geology. Top image from Garrett (2016) shows a facies distribution on cross section line A-A' within the Puttygut reef and in 2D map view. Bottom shows the results from the Puttygut SOM in both map view and on cross section line B-B'. B-B' goes from "2" to "5" on the A-A' line. Black dashed lines show where the edges of the model meets the edge of the SOM.....46
Figure 21: Top and bottom images from Garrett (2016) showing the calculated porosity (top image) and permeability (bottom image) for a reef model. Black dashed lines show where the edges of the model meet the edge of the SOM. Hotter colors indicate more porosity or permeability. When comparing those models to the SOM we see a good correlation between the two. The reef talus, reef core, and bioherm all have higher values of porosity and permeability when compared to the rest of the model. These are also the areas where the SOM neurons are focused.....47
Figure 22: Locations of the two reef complexes used to test the developed workflow. Ira lies to the south and slightly east of Puttygut while Lenox lies to the southwest. Bing Maps Hybrid Imagery overlay is displaying satellite imagery.....48
Figure 23: Ira reef in map view. Refer to Figure 22 for location or reef in relation to other reefs. The survey boundary is seen in the green box. The pink line represents the boundary of the reef. The blue box represents the boundary of the SOM survey. The inline range is from 58 to

106 and the crossline range is from 33 to 81. Bing Maps Hybrid Imagery overlay is displaying satellite imagery.....51
Figure 24:Ira reef approximate location with all wells labeled with well flow rankings. Map from M. Rine (personal comm., 2020). 52
Figure 25: Ira 3D seismic survey: Inline 82 at 20 times vertical exaggeration through the center of the reef with the horizons on. 53
Figure 26: Ira frequency SOM on the Brown horizon. The left image is with all neurons active while the right image only has neurons 6, 16, and 23 turned on. 55
Figure 27: Ira frequency SOM in VSD. Top let is Inline 82 and top right is Crossline 58. The vertical white lines are five wells that are located on Crossline 58. From left to right they are I-104, I-202, I-201, I-111, I-108. Below each of those is the same inline and crossline with only neurons 6, 16, and 23 turned on. 56
Figure 28: Lenox reef in map view. Refer to Figure 22 for location or reef in relation to other reefs. The survey boundary is seen in the green box. The pink line represents the boundary of the reef. The blue box represents the boundary of the SOM survey. The inline range is from 43 to 68 and the crossline range is from 60 to 84. Bing Maps Hybrid Imagery overlay is displaying satellite imagery.....58
Figure 29: Lenox reef approximate location with all wells labeled with well flow rankings. Map from M. Rine (personal comm., 2020). 59
Figure 30: Lenox 3D seismic survey: Inline 56 at 20 times vertical exaggeration through the center of the reef with the horizons on. 60
Figure 31: Lenox frequency SOM on the Brown horizon. The dominant neurons for the reef can clearly be seen as neurons 23 and 24. 61
Figure 32: Lenox frequency SOM in VSD through the center of the reef at Inline 56. There is a clear dominance of neuron 24 in the reef core at this inline with neuron 23 making up more of the outer reef.....62
Figure 33: Cross section through the reef at 20 times vertical exaggeration showing the horizons that constitute the reef and the four key wells, P-103, P-102, P-201, and P-106. The path can be

seen on the TWT map in Figure 2. The top image is the arbitrary line without interpretation, the bottom is with horizon interpretation. 67
Figure 34: TWT maps for the expert picked horizons. Contour lines are 2 ms. A) A-2 Carbonate B) A-2 Anhydrite C) A-1 Carbonate D) Brown E) Gray F) Clinton.....68
Figure 35: A-2 Carbonate horizon with extracted single structural attributes. A) PSTM amplitude B) Aberrancy C) Negative curvature D) ERS E) GLCM homogeneity Pink outline marks the outer reef boundary as defined by the A-1 Carbonate horizon. 69
Figure 36: A-2 Carbonate horizon with extracted single frequency attributes. A) PSTM amplitude B) CWT 29 Hz C) Cosine of the instantaneous phase D) CWT 57 Hz E) Average frequency F) CWT 81 Hz Pink outline marks the outer reef boundary as defined by the A-1 Carbonate horizon. ...70
Figure 37: A-2 Anhydrite horizon with extracted single structural attributes. A) PSTM amplitude B) Aberrancy C) Negative curvature D) ERS E) GLCM homogeneity Pink outline marks the outer reef boundary as defined by the A-1 Carbonate horizon. 71
Figure 38: A-2 Anhydrite horizon with extracted single frequency attributes. A) PSTM amplitude B) CWT 29 Hz C) Cosine of the instantaneous phase D) CWT 57 Hz E) Average frequency F) CWT 81 Hz Pink outline marks the outer reef boundary as defined by the A-1 Carbonate horizon. ...72
Figure 39: A-1 Carbonate horizon with extracted single structural attributes. A) PSTM amplitude B) Aberrancy C) Negative curvature D) ERS E) GLCM homogeneity Pink outline marks the outer reef boundary as defined by the A-1 Carbonate horizon. 73
Figure 40: A-1 Carbonate horizon with extracted single frequency attributes. A) PSTM amplitude B) CWT 29 Hz C) Cosine of the instantaneous phase D) CWT 57 Hz E) Average frequency F) CWT 81 Hz Pink outline marks the outer reef boundary as defined by the A-1 Carbonate horizon. ...74
Figure 41: Stratal slice one (Mid-Reef) with extracted single structural attributes. A) PSTM amplitude B) TWT map C) Aberrancy D) Negative curvature E) ERS F) GLCM homogeneity Pink outline marks the outer reef boundary as defined by the A-1 Carbonate horizon. 75
Figure 42: Stratal slice one (Mid-Reef) with extracted single frequency attributes. A) PSTM amplitude B) CWT 29 Hz C) Cosine of the instantaneous phase D) CWT 57 Hz E) Average frequency F) CWT 81 Hz Pink outline marks the outer reef boundary as defined by the A-1 Carbonate horizon. 76

Figure 43: Stratal slice two (Bioherm) with extracted single structural attributes. A) PSTM amplitude B) TWT map C) Aberrancy D) Negative curvature E) ERS F) GLCM homogeneity Pink outline marks the outer reef boundary as defined by the A-1 Carbonate horizon. 77
Figure 44: Stratal slice two (Bioherm) with extracted single frequency attributes. A) PSTM amplitude B) CWT 29 Hz C) Cosine of the instantaneous phase D) CWT 57 Hz E) Average frequency F) CWT 81 Hz Pink outline marks the outer reef boundary as defined by the A-1 Carbonate horizon. 78
Figure 45: Gray horizon with extracted single structural attributes. A) PSTM amplitude B) Aberrancy C) Negative curvature D) ERS E) GLCM homogeneity Pink outline marks the outer reef boundary as defined by the A-1 Carbonate horizon. 79
Figure 46: Gray horizon with extracted single frequency attributes. A) PSTM amplitude B) CWT 29 Hz C) Cosine of the instantaneous phase D) CWT 57 Hz E) Average frequency F) CWT 81 Hz Pink outline marks the outer reef boundary as defined by the A-1 Carbonate horizon. 80
Figure 47: Clinton horizon with extracted single structural attributes. A) PSTM amplitude B) Aberrancy C) Negative curvature D) ERS E) GLCM homogeneity Pink outline marks the outer reef boundary as defined by the A-1 Carbonate horizon. 81
Figure 48: Clinton horizon with extracted single structural attributes. A) PSTM amplitude B) CWT 29 Hz C) Cosine of the instantaneous phase D) CWT 57 Hz E) Average frequency F) CWT 81 Hz Pink outline marks the outer reef boundary as defined by the A-1 Carbonate horizon. 82
Figure 49: Structure SOM with full inline and crossline extent on: A) A-2 Anhydrite B) A-1 Carbonate C) Brown D) Gray 84
Figure 50: Frequency SOM with full inline and crossline extent on: A) A-2 Anhydrite B) A-1 Carbonate C) Brown D) Gray 85
Figure 51: Structure SOM with cropped inline and crossline extent on: A) A-2 Anhydrite B) A-1 Carbonate C) Brown D) Gray 86
Figure 52: Frequency SOM with cropped inline and crossline extent on: A) A-2 Anhydrite B) A-1 Carbonate C) Brown D) Gray 87

Figure 53: Inline 105, intersecting well P-106, of the full lateral extent SOM (left image) and the cropped lateral extent SOM (right image). Both images are displaying the SOMs created by using structural attributes. 88
Figure 54: Inline 105, intersecting well P-106, of the full lateral extent SOM (left image) and the cropped lateral extent SOM (right image). Both images are displaying the SOMs created by using frequency attributes. 89
Figure 55: Inline 92, intersecting well P-201, of the full lateral extent SOM (left image) and the cropped lateral extent SOM (right image). Both images are displaying the SOMs created by using structural attributes. 90
Figure 56: Inline 92, intersecting well P-201, of the full lateral extent SOM (left image) and the cropped lateral extent SOM (right image). Both images are displaying the SOMs created by using frequency attributes. 91
Figure 57: Inline 79, intersecting well P-102, of the full lateral extent SOM (left image) and the cropped lateral extent SOM (right image). Both images are displaying the SOMs created by using structural attributes. 92
Figure 58: Inline 79, intersecting well P-102, of the full lateral extent SOM (left image) and the cropped lateral extent SOM (right image). Both images are displaying the SOMs created by using frequency attributes. 93
Figure 59: Inline 56, intersecting well P-103, of the full lateral extent SOM (left image) and the cropped lateral extent SOM (right image). Both images are displaying the SOMs created by using structural attributes 94
Figure 60: Inline 56, intersecting well P-103, of the full lateral extent SOM (left image) and the cropped lateral extent SOM (right image). Both images are displaying the SOMs created by using frequency attributes 95
Figure 61: Base map showing inlines through Puttygut reef at an interval of five. Apart from Inline 92, which was included to show well P-201. 96
Figure 62: Inline 40....97
Figure 63: Inline 45....97
Figure 64: Inline 50....98

Figure 65: Inline 55.....98
Figure 66: Inline 60.....99
Figure 67: Inline 65.....99
Figure 68: Inline 70.....100
Figure 69: Inline 75.....100
Figure 70: Inline 80. Vertical purple line is location of well P-102. 101
Figure 71: Inline 85.....101
Figure 72: Inline 90.....102
Figure 73: Inline 92. Vertical red line is location of well P-201. 102
Figure 74: Inline 95.....103
Figure 75: Inline 100.....103
Figure 76: Inline 105. Vertical green line is location of well P-106. 104
Figure 77: Inline 100.....104
Figure 78: Inline 115.....105
Figure 79: The locations of the four key wells in map view. The TWT map is of the Brown Formation. 106
Figure 80: Permeability and porosity logs for well P-106 107
Figure 81: Permeability and porosity logs for well P-201 108
Figure 82: Permeability and porosity logs for well P-106 109
Figure 83: Permeability and porosity logs for well P-106 110
Figure 84: Puttygut pre-plot design. 112
Figure 85: Sterling processing scope of work. 113
Figure 86: Puttygut PSTM SEGY header. 114

Chapter 1: Introduction

Motivation

The focus of this study was to characterize features in ancient reef reservoirs that are below seismic resolution by creating a machine learning and multi-attribute analysis workflow. A seismic attribute is a measurement derived from seismic data, most commonly based on time, amplitude, frequency, and/or attenuation. The primary use for attributes is that they can help an interpreter see features, relationships, or patterns that might go unnoticed (Brown, 2011). An ideal area to develop and test such a workflow is in the Michigan Basin on Niagara-Lower Salina pinnacle reefs. The reefs form a sublinear trend on the northern and southern rims of the basin at depths between 900 and 2200 meters (Sears and Lucia, 1979). As of 2019, these reefs have produced over 500 million barrels of oil and over 3 trillion cubic feet of natural gas (Michigan Department of Environmental Quality, 2019). In addition to what has already been produced, there is still great potential for secondary oil recovery through water, CO_2, or gas injection. Michigan reef reservoirs have an approximate 26% average primary recovery and an approximate 12.5% average secondary recovery and only around 5% of the discovered fields here have gone past primary production (Brock et al., 1995). In addition to the production related motivation to better characterize these reef reservoirs, they have also been used for gas storage and CO_2 sequestration over the past 50 years (Rine, 2019).

The reefs on the southern edge of the basin were initially focused on. In addition to the apriori geologic knowledge, a great deal of geophysical data were provided, which included 3D pre-stack and post-stack time migrated seismic data over multiple reefs with well logs, and in some cases very detailed core analysis and descriptions (personal communication, Matt Rine, 2019). One reef, Puttygut, was chosen as the initial reef for workflow development, as it has the most complete and well-rounded dataset, with the most detailed core analysis of the reefs available. The Puttygut reef complex is approximately 150 acres in areal extent and 325 feet tall with a capacity of 14.6 BCFG. Figure 1 illustrates the area of interest with the top image from Rine (2019) of Michigan with the Michigan Basin overlain. The yellow star seen on the top image represents a zoom in of the reefs of interest. The bottom image shows the outline of the

Puttygut reef (represented by the pink outline) with all the wells shown. Figure 2 displays an arbitrary well cross section through four key wells in the Puttygut reef. The two-way time structure map is of the Guelph Formation (referred to herein as the Brown Formation, driller's terminology) within the reef interval. The logs shown are gamma ray, permeability, and porosity. There are areas in the logs that are 10% porosity or greater and regions that also have permeabilities of 50 mD or greater on average. For reefs in this basin, rock properties near these values are very desirable. These areas are relatively thin, however, sometimes only reaching thicknesses of 5 feet, usually thinner. In general, well log data have very good vertical resolution, but the lateral coverage they provide is extremely limited. On the other hand, seismic data have lateral coverage that is magnitudes greater. In addition, seismic data are much cheaper to acquire when compared to drilling and logging a well. The seismic volume for the Puttygut reef has roughly 60 to 80 feet vertical resolution at depths comparable to the logs. Under normal circumstances, it is impossible to resolve the thin high porosity and permeability features. Machine learning and multi-attribute analysis can potentially be utilized to drastically improve the vertical resolution of seismic data. Seismic data can be used to create a suite of attributes that can, in turn, be used as inputs for a machine learning algorithm that creates self-organizing maps (SOMs). Attributes output their results at the wavelet scale, which can cause difficulty when comparing them side by side. SOMs, on the other hand, have the potential to analyze these attributes together all the way down to the sample interval of the data (Roden et al., 2017). Once at that scale, SOMs then characterize data points into clusters based on their similarity. The SOM process greatly increases the resolution of the data and consequently allows for more apt comparisons to the well log data.

It is important to increase the vertical resolution of seismic data to advance our understanding of the subsurface. With machine learning and multi-attribute analysis, it is possible to reexplore preexisting seismic data through a new lens and see features at much finer detail than previously possible. Machine learning can open new doors to exploring our geologic past and to increase our understanding of smaller scale events and processes. It can aid us in identifying and characterizing features of interest that were previously hidden in the data, and it is possible to use this method on any geologic regime. More practically, the

machine learning method can be used to reduce the cost and increase the likelihood of success when drilling a well. That well could be used for oil and gas exploration and production, it could be used for gas storage and CO_2 sequestration, production, etc. In any case, if a well is drilled in a location with undesirable rock properties and/or fluid properties, then money and resources have been wasted. The workflow from this research was developed in an attempt to reduce uncertainty when interpreting seismic data and lower risk associated with planning and drilling a well. Overall, if you have seismic data, a way to calculate attributes, and a method of machine learning, you will be able to explore that seismic data with increased detail and clarity that was not possible before with just the data and attributes.

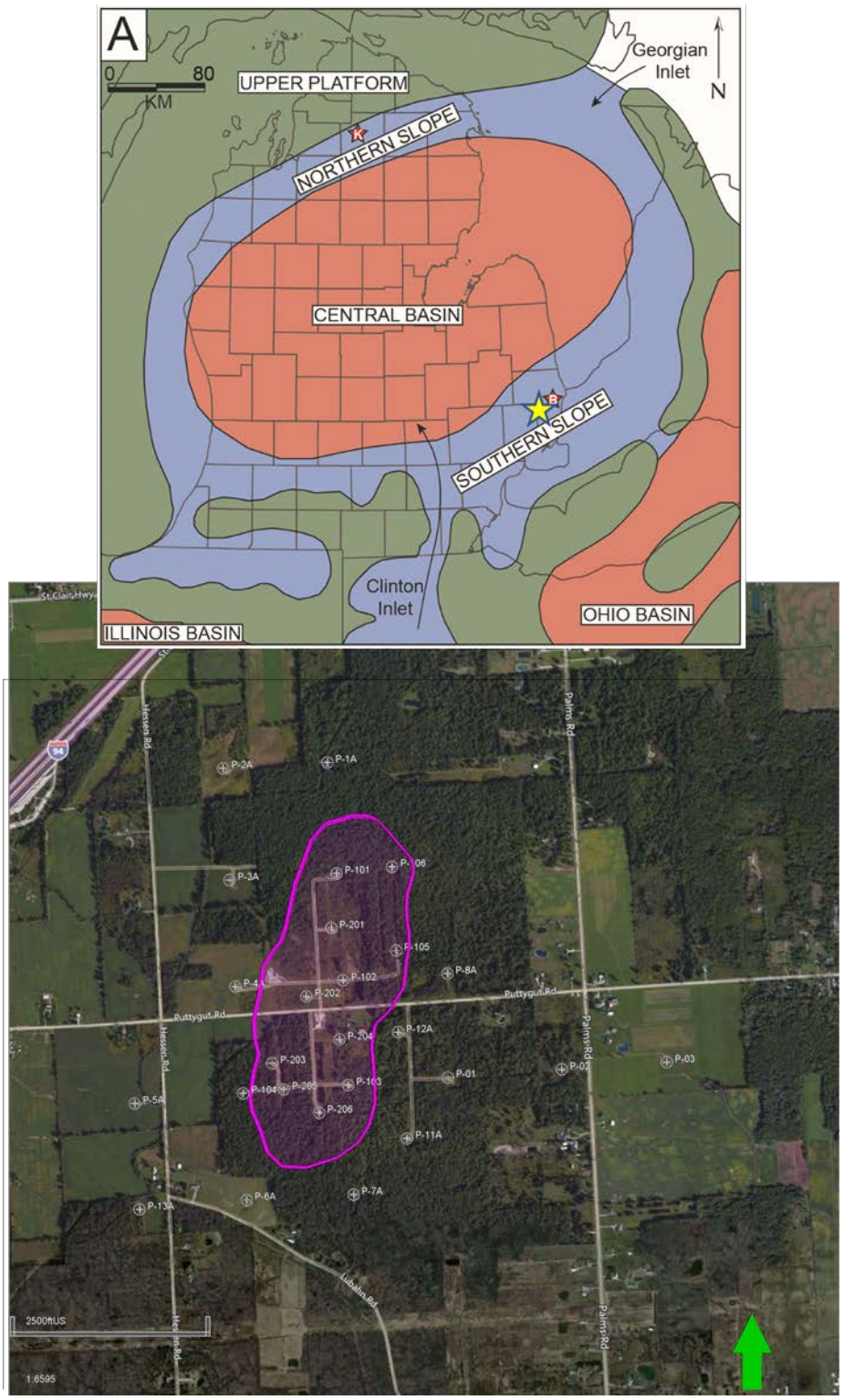


Figure 1: Map of Michigan with the Michigan Basin overlain from Rine (2019). The yellow star indicates the area of interest for this research. The bottom image is a zoomed in view of the Puttygut reef with all wells shown where the pink outline represents the reef extent.

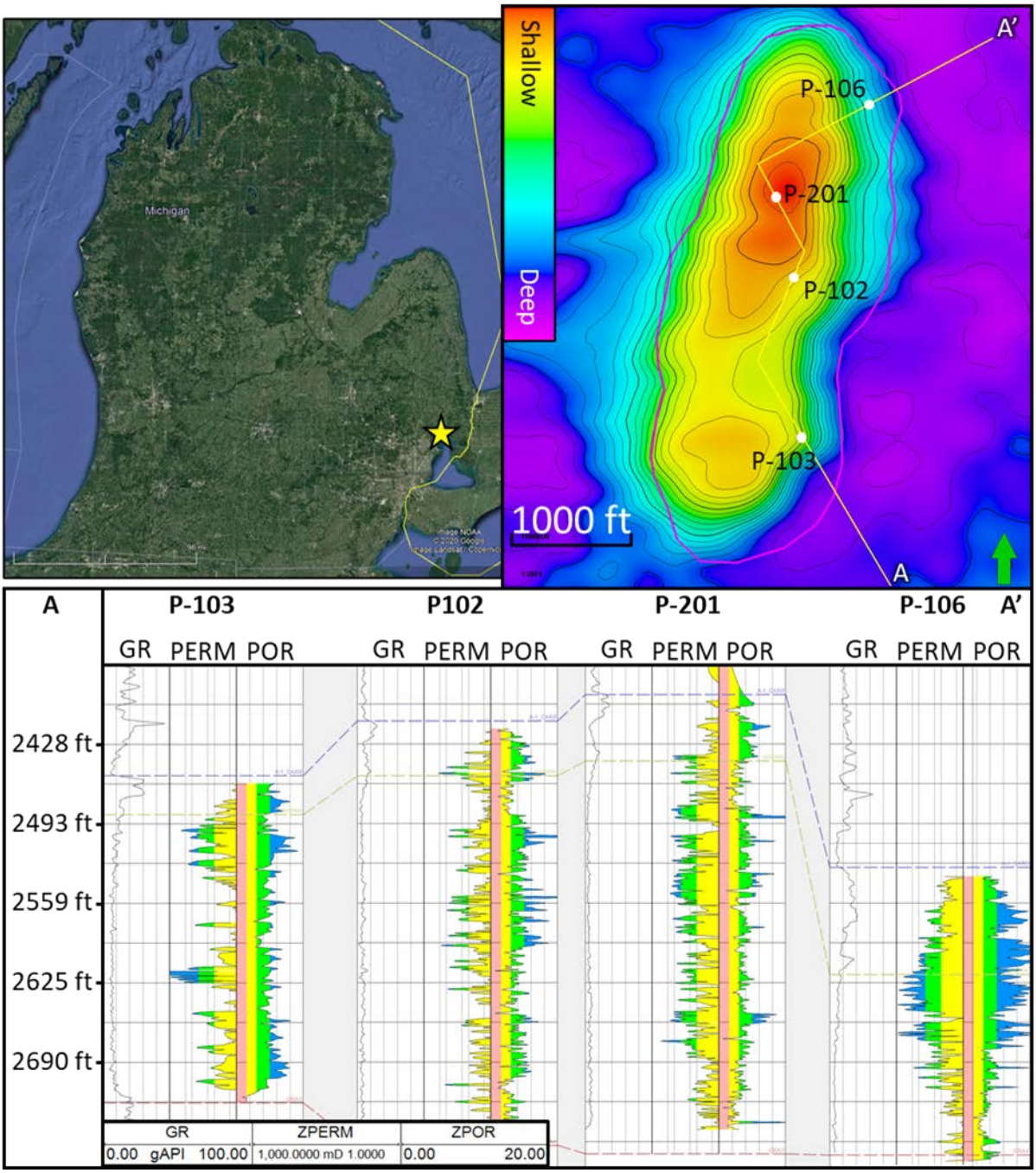


Figure 2: Map of Michigan, from Google Earth, showing the area of interest with a yellow star. Arbitrary well cross section over the Puttygut reef showing the gamma ray, permeability, and porosity logs. The two-way time structure map is of the Brown Formation. The fillings on the permeability log: yellow is between 1 and 10 mD, green is between 10 and 50 mD, and blue is greater than 50 mD. The fillings on the porosity logs: pink is between 0 and 3 %, yellow is between 3 and 6%, green is between 6 and 10%, and blue is greater than 10%. Uncolored logs found in Appendix D.

Chapter 2: Paradise machine learning and SOM workflow methodology

Regional geology

The Michigan Basin was formed during the Silurian when North America was a shallow sea. It is a circular basin that covers an area of ~316,000 km^2 (Catacosinos et al., 1991). The reefs in this basin occur in the upper Niagaran age and form a sublinear trend on the northern and southern rims at depth between 900 and 2200 meters (Sears and Lucia, 1979). The general stratigraphy of the reefs in the southern trend of the basin can be seen in Figure 4 below (Rine, 2019). The reef is overlain by multiple anhydrite and carbonate layers and is underlain by the Lockport dolomite. A time-step basin wide depositional evolution of the Michigan Basin developed by Rine (2019) is as follows: Through a time of sea level oscillations the first formation to be deposited in the basin is the Lockport formation. Eventually, a sea level fall exposes the Lockport and ends its deposition. Following is a sea level rise which coincides with the initiation of the bioherm mounds and marks the beginning of the lower Guelph Formation. Next, sea level falls again which exposes the bioherm mounds and causes significant wasting. That is what creates the flat tops seen today. A rapid sea level rise follows initiating the pinnacle reef growth in the upper Guelph. Tidal flat facies begin to be deposited as the basin experiences restriction. Relative sea level fall in the basin results in A-1 Evaporite deposition. Sea level rises, falls, and rises again resulting in the deposition of the lower A-1 Carbonate, the Rabbit Ear Anhydrite (REA), and the upper A-1 Carbonate, respectively. Also at this point in time, the reefs are completely covered in sediment. The A-2 Evaporite section is then deposited with another fall in sea level. Finally, through another rise and fall in sea level, the A-2 Carbonate and the B-Salt are deposited, respectively, which marks the end of the relevant sequence. Figure 3 shows an abridged and modified version of this depositional history from Rine (2019). In summary, while the primary depositional model for these reefs is relatively well know, the post-depositional diagenetic history of these reefs is still relatively unknown. Since the reefs in SE Michigan have been 100% dolomitized and are partially salt plugged, the primary depositional facies are not the only factors that contribute to the petrophysical properties and in turn, seismic attribute creation.

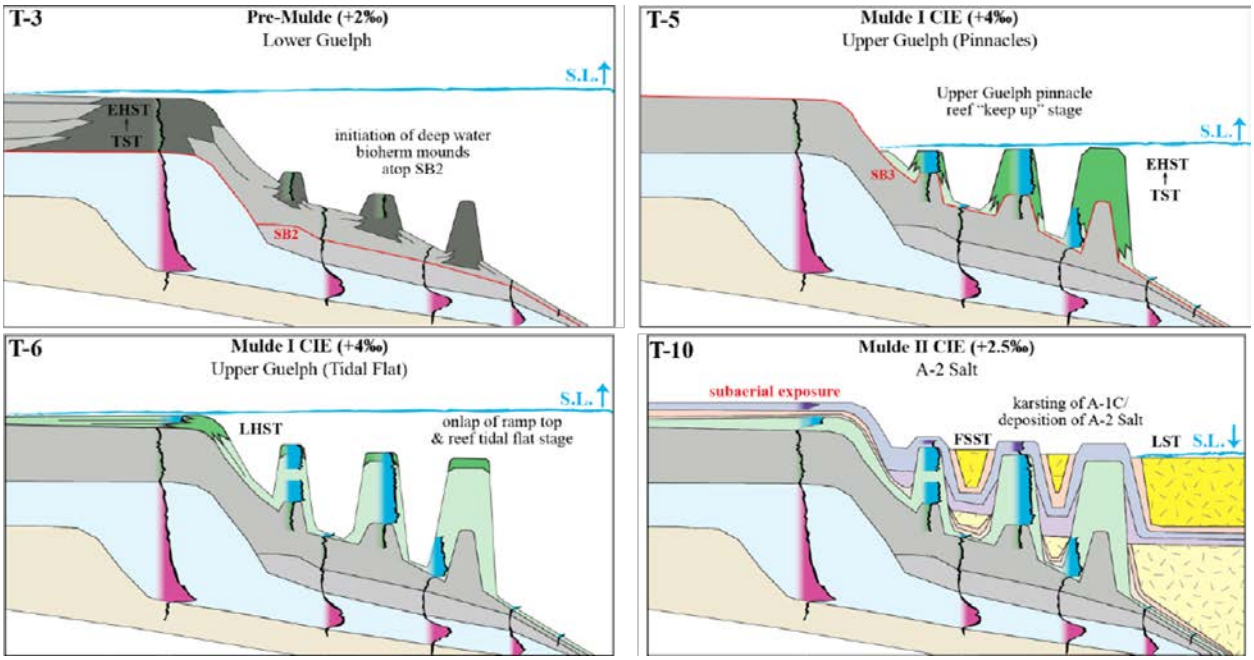


Figure 3: An abridged and modified version of the depositional history from Rine (2019). T-3 depicts bioherm initiation with the rise in sea level. T-5 and T-6 illustrate a rapid sea level rise which begins pinnacle reef growth and puts them in the "keep up" stage. T-10 marks the end of the relevant depositional history where the A-1 Evaporite, A-1 Carbonate, Rabbit Ear Anhydrite, and the A-2 Evaporite sections are deposited on top of the reefs.

The interval of interest for these reefs can been seen in Figure 4 from the A-1 Carbonate down to the Gray Formation. Due to the fact that these formations are below seismic resolution, it is very difficult to determine where to pick these horizons by looking at the seismic data alone. Figure 5 shows an arbitrary line through the Puttygut reef. The seismic horizons were picked by an expert geologist in the area with substantial apriori geologic and structural knowledge of the Michigan Basin to achieve the most accurate horizon picks. The A-2 Carbonate and Clinton Formation are easily seen due to their thickness and acoustic impedance contrast to their surroundings. The A-2 Anhydrite, A-1 Carbonate, Brown, and Gray Formations however are not so easy to resolve. They are detectable at points along the line but are not confidently pickable without the prerequisite geologic and structural knowledge in the area. Coincidently, the horizons that are more difficult to pick are the horizons that we are interested in. The reef core and bioherm between the A-1 Carbonate and the Gray Formation are

commonly the areas where the highest quality reservoirs are found. Areas of high permeability and porosity tend to exist in the skeletal wackestone and reef boundstone of the reef core. The thrombolitic bindstone facies within the A-1 Carbonate that caps the reef complex in the reef crest position is also an area of high permeability and porosity (Rine, 2019).

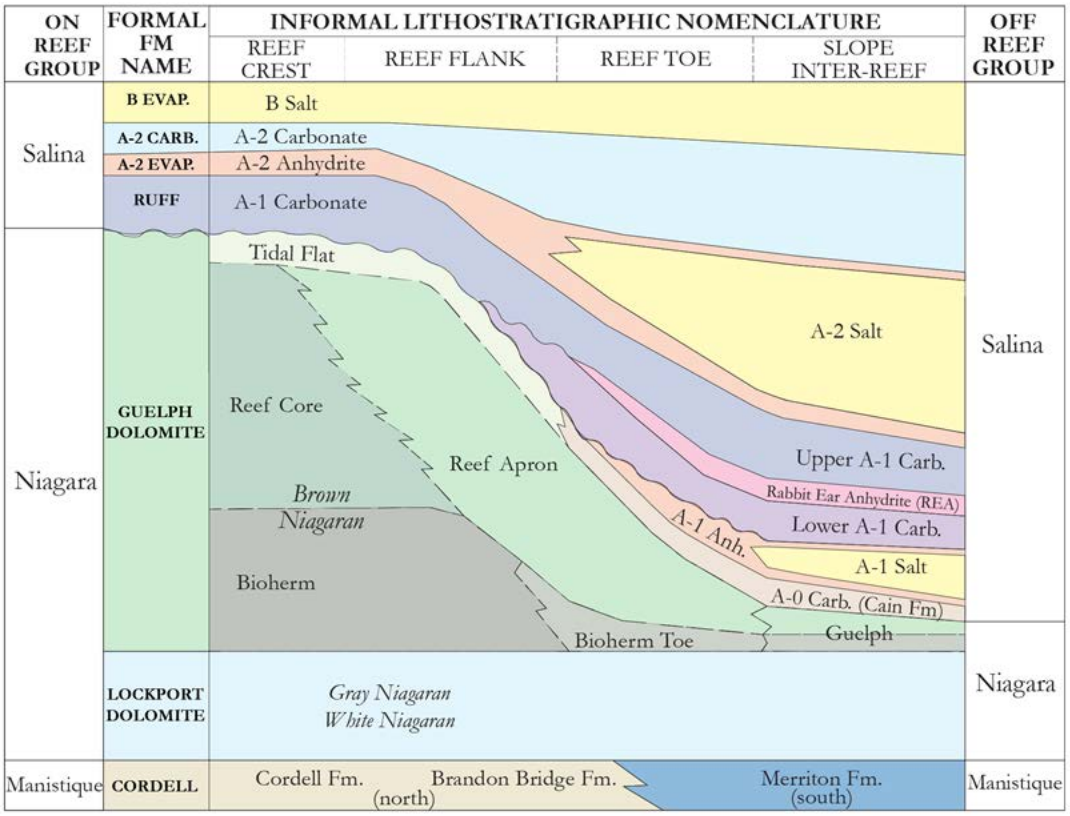


Figure 4: Generalized stratigraphic column of the reefs in the southern trend of the Michigan Basin (Rine, 2019).

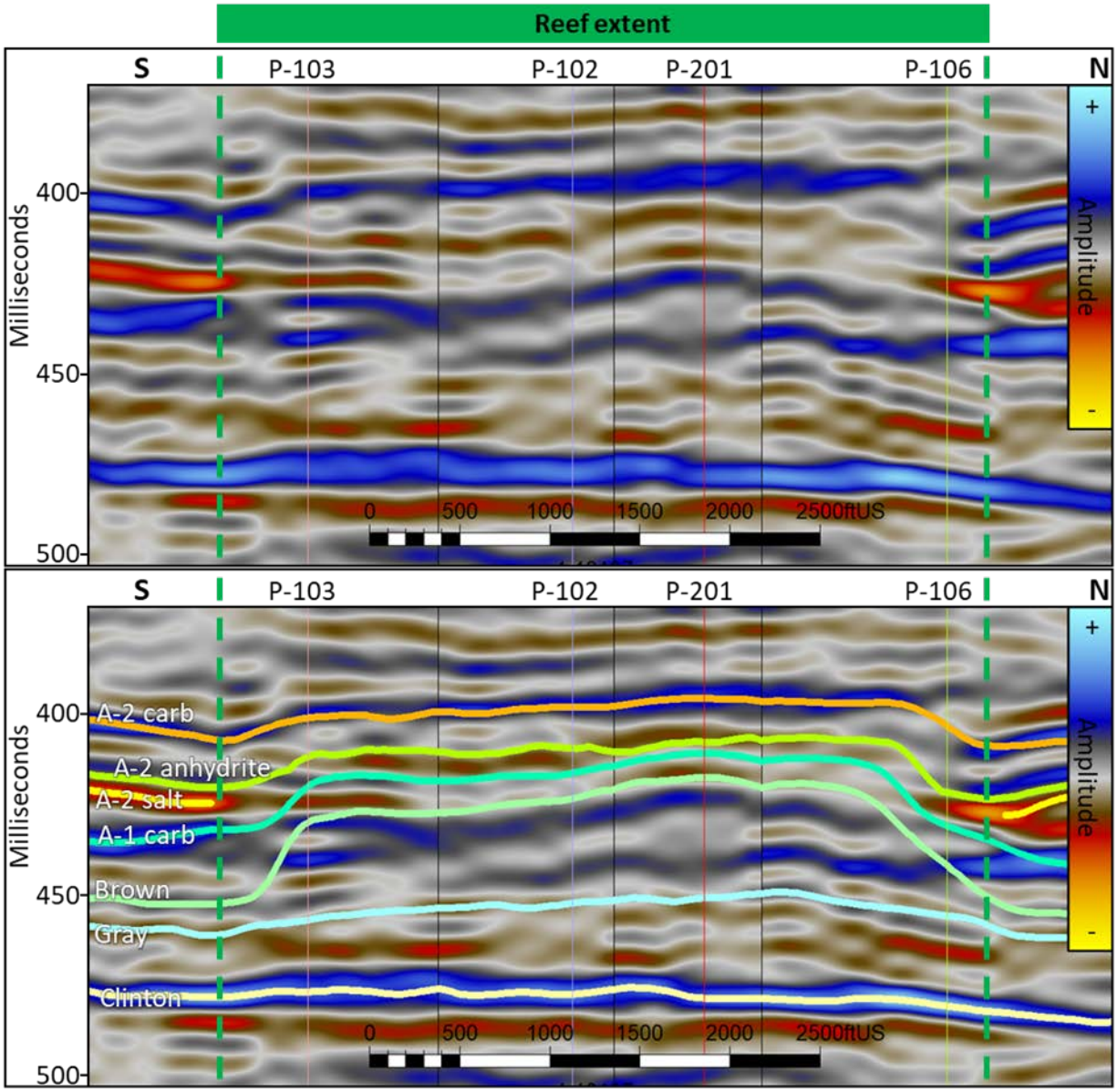


Figure 5: Arbitrary line through the Puttygut 3D dataset. The path can be seen on the TWT map in Figure 2. The top image is the arbitrary line without interpretation, the bottom is with horizon interpretation. The A-2 Anhydrite, A-1 Carbonate, Brown, and Gray Formations are very difficult to resolve and require a great deal of apriori geologic and structural knowledge of the area to pick accurately. The A-1 Carbonate and Clinton horizons are much easier to resolve. The A-2 Salt is shown on the flanks of the reef.

A major part of this work will involve identifying small scale features within the Michigan pinnacle reefs. As such, it is pertinent to include information about the internal structure of said reefs from both historical and modern examples. The most obvious example is to characterize the Michigan pinnacle reefs themselves from recent geologic work. Rine (2019) proposed a new model for these reefs by analyzing numerous cores and well logs in the basin, concluding that they are asymmetrical, due to interaction with a strong paleo-wind at the time of reef growth, as well as having internal facies distributions that follow regular predictable patterns. The paleoreefs are divided into three main paleobiologic sections: the stromatolitic cap, the reef complex, and the biohermal complex (Rine, 2019). Table 1 includes a more detailed explanation of the lithofacies and lithologic attributes in each of these sections.

Reef Growth Stage	Depositional Environment	Lithofacies	Lithologic Attributes	Water Depth
3 Stromatolitic Cap	Tidal Flat	*hemispheroid stromatolitic bindstone*	Dark brown, laterally-linked hemispheroid stromatolites	Above FWB to Intertidal
		skeletal wackestone	Skeletal fragments composed of reef core organisms (tabulate corals, brachiopods, bryozoan); abundant cements	Above FWB to Intertidal
	Windward Proximal Foreslope	*stromatolitic intraclastic rudstone*	Large (pebble to cobble), tightly packed stromatolite clasts *(flat pebble conglomerate)* ; poorly sorted	Below SWB
	Windward Distal Foreslope	*stromatolitic intraclastic floatstone*	Small (granule to pebble), infrequent stromatolite clasts in a micrite matrix	Below SWB
2 Reef Complex	Leeward Toe-of-slope	*skeletal mudstone*	Minor skeletal fragments in a micrite matrix; anhydrite-filled vugs; <10 m thick	Below SWB
	Leeward Distal Reef Apron	*skeletal mudstone*	Minor skeletal fragments; abundance of drusy calcite spar cement lining vuggy porosity; >10 m thick	Below SWB
	Leeward Proximal Reef Apron	*skeletal mudstone*	Minor skeletal fragments; abundance of drusy calcite spar cement lining vuggy porosity	Between SWB and FWB
		skeletal wackestone	Disarticulated fossils (tabulate corals, brachiopods, bryozoans, crinoids) in a micrite matrix	Above FWB
	Reef Core	*coral/stromatoporoid boundstone*	Frame-building organisms (tabulate corals, stromatoporoids)	Above FWB
		skeletal wackestone	Intra-reef faunal assemblages (bryozoans, brachiopods, crinoids, rugose corals); 50-75% micrite matrix	Between SWB and FWB
	Windward Proximal Foreslope	*coarse lithoclastic floatstone*	Large, dark gray angular clasts in light gray micrite matrix; abundant crinoids	Below SWB
		skeletal intraclastic rudstone	Large clasts composed of tabulate corals, brachiopods, and crinoids; moldic porosity	Below SWB
	Windward Distal Foreslope	*skeletal mudstone*	Occasional skeletal fragments and small (pebble), angular clasts in a micrite matrix; anhydrite-filled vugs	Below SWB
1 Biohermal Complex	Bioherm	*crinoidal mudstone*	Mottled gray and white; abundant crinoids in a micrite matrix; abundant stromatactis	Below SWB
		skeletal wackestone	Mottled gray and white; bryozoans, tabulate corals, rugose corals and crinoids in a micrite matrix; abundant stromatactis	Between SWB and FWB
	Bioherm Toe	*crystalline dolomite*	Devoid of fossils; composed of dolomite rhombs; intercrystalline porosity	Below SWB

Table 1: Guelph formation facies classification table provides a more detailed explanation of the lithology in each reef section. FWB is the fair-weather wave base and SWB is the storm wave base. Modified from Rine (2019).

Next, modern analogous examples of pinnacle reefs are discussed to shine light on the internal structure and workings of living pinnacle reefs. The Flower Garden Banks reefs in the Gulf of

Mexico (see Figure 6) are good examples of modern pinnacle reefs. Figure 7 shows both the west and east reef, color coded by habitat classification from the NOAA Flower Garden Banks National Marine Sanctuary website. These reefs have formed on the surface expressions of underlying salt domes. A brief summary of the types of organisms that are found in each section of the reef is as follows: Coral reef zone (yellow) - primarily coral assemblages with leafy, coralline, and filamentous algae occurring on the reef substrate. Sponges are found throughout the reef in this area in crevices and cavities. Reef derived sediments (carbonate sands) are also found in this area, along with sand patches and channels. Coralline algal reefs (green) and algal nodules (red) - Crustose coralline algae are dominate in this section. The main difference between the two colors is whether the crustose coralline algae forms into algal nodules or rhodoliths (algal nodules section) or if they form into large plates and ridges that develop into massive reef structures (algal reefs section). In either case a variety of sponges are plentiful here as well. Deep coral zone (blue) - These are areas that do not support active photosynthesis and have a diverse collection of corals, sponges, bryozoans, etc., but lack coralline algal growth. In general, these reefs mimic the reefs of old, with a central reef core housing the frame-building organisms with less life moving out towards open water. More examples of modern pinnacle reefs can be found at Key Biscayne in Biscayne National Park. There are over 3,000 patch reefs located within the national park with two main morphologies present, flat top and pinnacle. Both morphologies of the patch reefs are composed of hermatypic corals (Reich et al., 2009). The pinnacle reefs tend to be in the deeper waters, taller and narrower when compared to the flat top reefs in the shallower waters. The narrow and tall morphology is consistent with a relatively rapidly rising sea level that restricted the lateral growth of the reef (Brock et al., 2008). Pinnacle reefs have their characteristic tall and narrow morphology because they are growing during a time of sea level rise. They are unable to expend the resources to grow laterally because if they do, the sea level will continue to rise while the reef remains at the same depth, which will result in the reefs being drown. So, the pinnacle reefs are in a state of “keeping up” with the rising sea level (Neumann and Macintyre, 1985). If they cannot keep up, then they will drown. The growth patterns of these modern pinnacle reefs are a good proxy to how pinnacle reefs would have grown in the past.

Contingent upon the initial mineralogy and subsequent diagenetic events, the taller and more narrow geometry can result in a concentration of coral that is ideal for the creation of permeable and porous reservoir. Those areas can either be within that main reef or immediately surrounding it. As the reef begin to drown and die, parts of it will break off and settle around the reef core, creating comparable areas of porosity and permeability. With this in mind, areas of high initial porosity and permeability are expected to be found in a more localized area within or immediately surrounding the reef when looking at the Puttygut reef in seismic. One final note is that the reefs that were created in the Silurian time were made during a greenhouse period, which resulted in low levels of aragonite. Modern reefs are currently being formed during a time how high levels of aragonite. The difference in aragonite composition is an important reminder that these modern reef analogs should not be relied too heavily upon. While many comparisons can be drawn from the modern, the fundamental difference in chemical makeup must also be remembered.

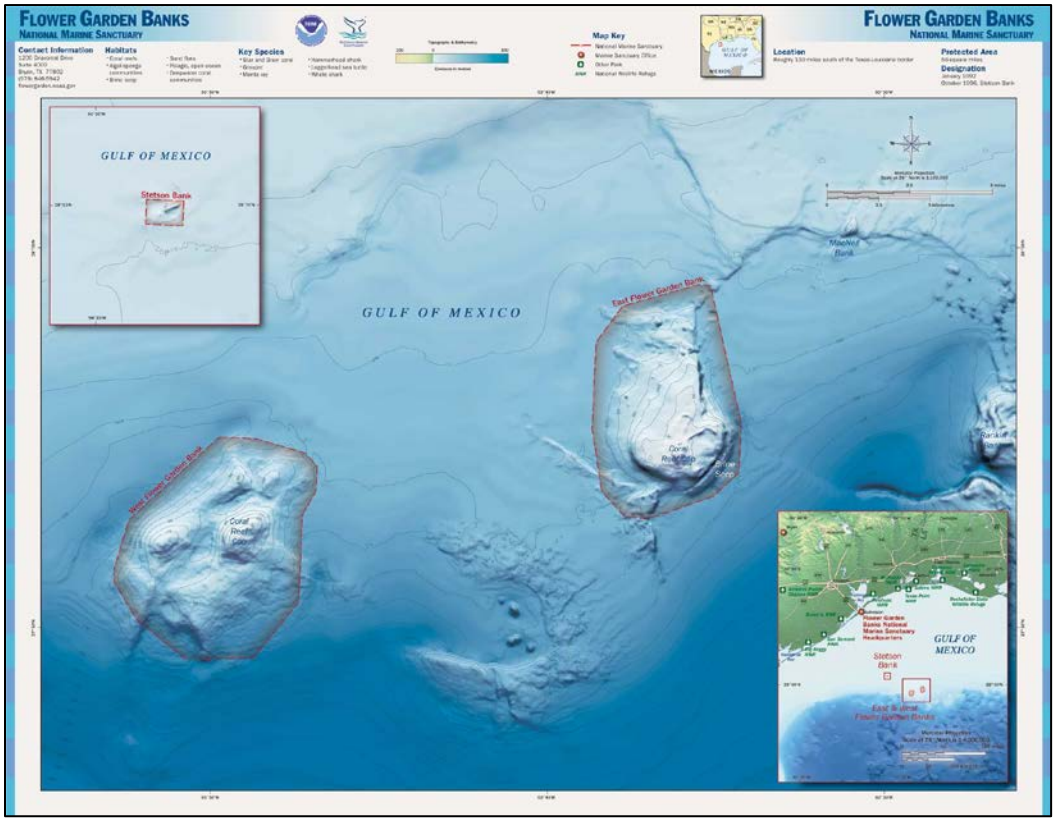


Figure 6: Location map for the Flower Garden Banks pinnacle reefs from NOAA Flower Garden Banks National Marine Sanctuary website.

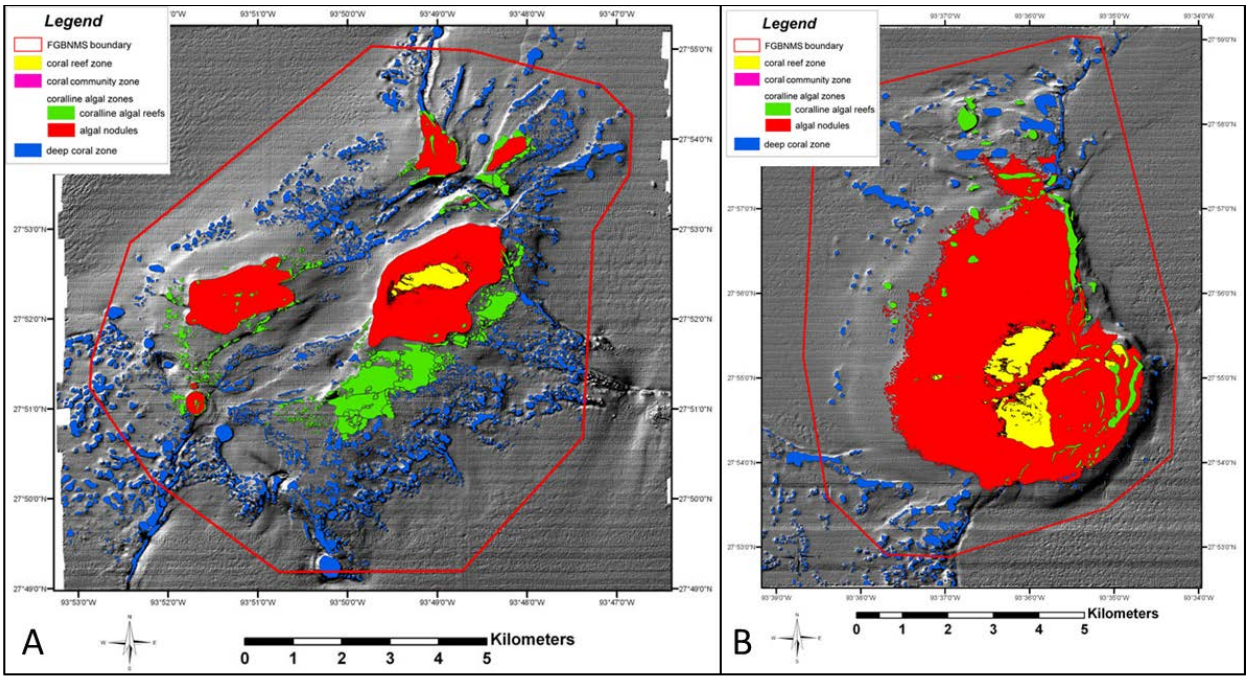


Figure 7: A) West Flower Garden Bank and B) East Flower Garden Bank pinnacle reefs habitat classification by color. Maps from NOAA Flower Garden Banks National Marine Sanctuary website.

Purposed methods

The initial proposed workflow was to run a large suite of attributes on the pre-stack 3D volume around the Puttygut reef. Additional details regarding the 3D survey design, acquisition parameters, and processing workflow are located in Appendix E. Geologically, we are primarily interested in improving the mapping of continuous areas of high porosity and permeability found in the sub-seismic formations that comprise the reef core and bioherm. Seismically, these areas are difficult to detect, so areas of interest with high permeability and porosity are initially chosen using core and well log data. There is one limitation with this approach however, as the core and well log data are in depth and the seismic data are in time. There are no reliable sonic logs and no density logs in the area. So, producing a reliable well tie is particularly challenging without making assumptions that drastically effect the reliability of the results. Horizons were created and provided by Dr. Rine (personal comm., 2020). The workflow for picking sub-seismic horizons was as follows: 1) Pick formation tops from geophysical logs and cores. 2) Tie the wells to the seismic using a VSP from the P-201 well and synthetic

seismograms generated from wells with DT and RHOB logs outside of the survey. 3) Shift the wells to time using key horizons (i.e. A-2 Carbonate, A-2 Salt, A-1 Carbonate, Clinton), 4) Pick sub-seismic horizons that cross-cut reflectors based on well control (i.e. Brown Niagaran, Bioherm, Gray Niagaran). From there, the smaller, sub-seismic horizons were mapped through apriori structural geologic knowledge and using the pseudo-tied wells to aid in picking locations. While this situation is not ideal, there is a very high level of confidence with the accuracy of these provided horizons. So, with these limitations and assumptions seismic attribute analysis can begin.

Attributes were evaluated by the interpreter to determine how effective they were at displaying minute details within the target reef. Attributes that exceled at revealing the internal, less detectable aspects, of the paleoreef were then selected for multi-attribute analysis in the form of self-organizing maps (SOMs) to achieve sub-seismic resolution. All single attributes were calculated in the AASPI software and then converted to SEGY format and imported into Petrel for visualization and evaluation. After the best attributes were determined they were ported into Paradise for SOM creation and interpretation. The theory of using SOM's and multi-attribute analysis to image and interpret sub-seismic resolution has been successfully tested and proven in the past (Roden et al., 2017). Most commonly SOM's were calculated over unconventional plays, such as in the Denver-Julesburg Basin and in the Eagle Ford shale, (Laudon et al., 2019, Roden and Sacrey, 2015, Santogrossi, 2017). They have also been tested in other areas, such as for interpreting DHI (direct hydrocarbon indicator) characteristics, classifying carbonate facies, and recognizing geologic patterns with varying degrees of success (Roden and Chen, 2017; Roden and Santogrossi, 2017; Roden et al., 2015). A SOM, or a self-organizing map, was explored in detail by Teuvo Kohonen (Kohonen, 1995) in his book "Self-organizing Maps," where a very mathematical description of self-organizing maps can be found. Kohonen describes SOMs as "nonparametric regressions" where a number of ordered discrete reference vectors are fit to a distribution of vectorial input samples. In order to approximate continuous functions though, the reference vectors are used to define nodes, or neurons, in a hypothetical elastic network. Local interactions between these neurons along the neural network create that essence of elasticity. By setting up the map in this way, the neurons

develop into specific detectors of signals in the input space. Even more, these detectors are formed in the map in a meaningful order as if falling into place on a feature coordinate system. These resultant feature maps are used for the preprocessing of patterns for recognition (Kohonen, 1997). Stated simply, SOMs require some number “m” of input characteristics and a desired number “n” of output “detectors”. These output detectors are then fit to the input characteristics such that they both attempt to classify the data and are influenced by the other detectors. What is made in the end is a map that is organized in a meaningful manner that can be used for potential pattern recognition. These inputs can be anything from variations of textures in an image, to the variations in the quality of life between nations (an example created by Kohonen), to the different attributes that can be created using seismic data. As mentioned previously, these SOMs analyze the input data at the sample interval level. Let us examine a heuristic example solved using SOMs.

Image you are in a bakery but do not know where anything is. You want to analyze and categorize the layout of the store so that you can decide on what to eat. The bakery could be completely disorganized, with sweet jelly filled donuts right next to the empanadas! So, you develop a small list of attributes that you think describe a majority of baked goods. 1) Is it sweet of savory? 2) Is there a filling or not? With this list of attributes, you create a SOM in your mind with an output of four neurons. After calculations, you are now able to see the patterns associated with the pastry positions. All the filled savory foods are on the counter to the left with all of the fresh breads are above them. But the donuts on the shelf to the right are mixed between being filled or not. So the patterns that you see are two large neuron clusters to the left that separate the filled from unfilled savory pastries and a chaotic mixture of two neurons representing the sweet pastry shelf where the filled and unfilled donuts are not organized.

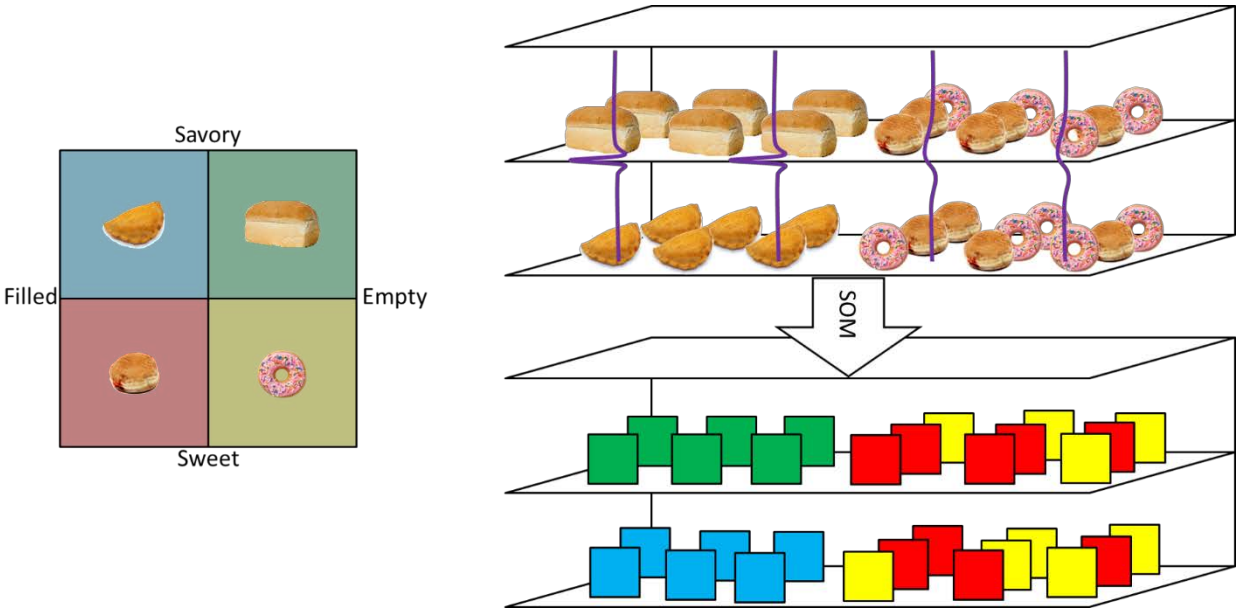


Figure 8: The "SOM bakery". The top right shows the original bakery with "seismic wiggle" overlay. We see that there is a clear contrast between the bread and the empanadas, resulting in a large "acoustic impedance". The classic donuts and the jelly filled donuts are mixed up and chaotic, resulting in less of a contrast. The left grid shows the "neurons" that were created from the sweet/savory and filled/empty attributes. The bottom right image is the result after classification. Each sample point (baked good) is now classified into one of the four output neurons.

In machine learning, for a desired anthropologically reasoned outcome, it is optimal to take advantage of the interpreter's knowledge when choosing SOM attributes and parameters. In this case, two categories were decided upon when initially analyzing single attributes. Structural based attributes and frequency-based attributes. The structural based attributes were graded on how well they illuminated the internal structure of the reefs. The frequency-based attributes were graded on how well they distinguished unique sections of the reef. Highlighting the sub-seismic internal structure of the reef and identifying different sections of the reef via frequency content potentially create the key to isolating areas of higher porosity and permeability. Narrowing down the attributes to a smaller set is also useful in the SOM stages later in the workflow. It is not necessarily beneficial to have more attributes when conducting multi-attribute analysis as many attributes are calculated in similar ways and show similar features. If all the attributes that were calculated are used in one SOM then there would

be a great amount of unnecessary redundancy. In addition, using more data in the calculations will increase the amount of time required to complete a SOM. With these factors in mind, the chosen set of attributes are defined below:

Structural attributes: The following structural defining attributes were chosen because they all excelled at defining some form of structure (internal or boundary) and because they are all calculated in reasonably different ways, which is important later during the multi-attribute analysis step.

Energy ratio similarity (ERS): An attribute that is designed for edge-detection. ERS is similar to other coherence attributes except that it is calculated along the structure and that it uses analytic traces instead of just the real traces. ERS is the ratio of the energy of the Karhunen-Loève filtered data over the total unfiltered energy of the input data within the analysis window (Chopra and Marfurt, 2007a). For the purposes of this research, ERS was the best at highlighting the reef outer boundary as well as some internal features that other attributes were unable to detect. The idea for reef edge and internal structure detection by use of coherence or similarity attributes has been tested extensively in the past. Chopra and Marfurt (2007a) showed its effectiveness on pinnacle reefs in Alberta, Canada. As well as on reefs in the Zama basin, northern Alberta, Canada, and a Winnepegosis reef in Saskatchewan, Canada. Skirius et al. (1999) also used coherency for edge detection for some carbonate reefs, reservoirs, and a slump.

Aberrancy: Defined as the third derivative of structure, it is the measure of the asymmetry of a curve about its normal (Schot, 1978). Aberrancy measures the lateral changes in the curvature along a surface and is also able to detect faults that are below seismic resolution (Qi and Marfurt, 2018). Qi and Marfurt (2018) calculated aberrancy on a data volume over the Barnett shale gas reservoir in Fort Worth Basin, Texas. With this attribute they were able to identify small karst features that were too smooth to be picked up by coherency. Yet in practice, it is best to use aberrancy in conjuncture with other attributes, such as coherency or curvature, as together they can show a more complete image of the subsurface. Aberrancy was

able to define smaller and more internal reef structures than other structural attributes for the purpose of this study.

Curvature: Defines how positively or negatively curving a feature is. Curvature is a second derivative calculation of the phase of the seismic waveform. If a feature has a positive curvature then it has an anticlinal expression, but if a feature has a negative curvature it has a more synclinal expression. Chopra and Marfurt (2007b) used most-positive and most-negative curvature to highlight differential compaction over channels. Duan et al. (2010) used most-positive to map the flanks/edges of a paleokarst collapse and the most-negative curvature to map the thalweg of the collapse. The collapse they mapped was in an Ordovician carbonate rock layer in the Ordos Basin. Wallet (2016) mapped channel forms in a hybrid carbonate turbidite system off the coast of Western Australia. Wallet used single attributes to aid in this mapping, one of which was the most negative principal curvature (k2). Since the bottoms of these channel expression are synclinal/valley features, the most negative curvature was able to highlight them well.

Grey level co-occurrence matrix (GLCM): Is a statistical textural attribute that essentially compares a sample point within an analysis window to the other sample points within that same window. Textural attributes aid an interpreter comparable to a similarity attribute. Eichkitz et al. (Feb. 2015) used a combination of a GLCM-based energy attribute calculated in four different directions in a comprehensive workflow to identify areas with high and low degrees of anisotropy. Eichkitz et al. (March 2015) later used this attribute to help extract more information about channel interiors while using a coherence attribute to distinguish the edges of the channels. GLCM was useful for identifying additional features within the reef core that were unnoticed by the other structural attributes.

Frequency attributes: The following frequency attributes were chosen based on how well they differentiated the internal reef structure.

Cosine of Instantaneous phase: Instantaneous phase attribute provides the interpreter with the phase of the wavelet at a certain location in the data. Yet instantaneous phase is cyclical in nature, wrapping around from -180° to +180°, and is also mathematically

discontinuous. Cosine of the phase is implemented in order to remove those discontinuities (Barnes, 2016). Taking the cosine of the instantaneous phase also removes the cyclical nature of the attribute, creating a scale from -1 to +1, which is better later on when being used in a SOM. Sukmono et al. (2006) used instantaneous phase and cosine of the phase in the Melandong Field, Indonesia, to help enhance differentiation of three facies reflectors within the reef. Sukmono et al. (2006) also used these attributes to aid in direct hydrocarbon indicator (DHI) signature analysis because they enhance weak reflectors and highlight phase reversals associated with flat spots and gas column/gas-oil contacts, respectively. Huang et al. (2011) calculated the instantaneous phase of a 3D dataset over the Upper Permian Changxing formation carbonate located in southern China using a couple of different methods. They found that the instantaneous phase helped identify the platform margin reef facies. When run on the Puttygut volume, cosine of instantaneous phase enhanced the differentiation of internal reef facies.

Average frequency: Instantaneous frequency is a measure of the frequency of the wavelet of the seismic trace at a given location in the data (Barnes, 2016). Toelle and Ganshin (2018) found a relationship between the instantaneous frequency of seismic data and the amount of porosity present in reefs located in the northern Michigan Basin. They found that the instantaneous frequency decreased from 73 Hz to 45 Hz as the porosity increased from 5% to 20%. They interpreted this decrease in frequency to be associated with frequency attenuation from the increase in porosity. Huang et al. (2011) calculated the instantaneous frequency of a 3D dataset over the Upper Permian Changxing formation carbonate located in southern China using a couple of different methods. They found that this attribute helped to identify the zoning in the area. Sarhan (2017) created a variety of attributes on fifteen 2D seismic lines over the central part of Abu Gharadig Basin in the NW desert of Egypt in order to differentiate between a massive, non-porous carbonate and a non-massive, porous carbonate. One attribute they implemented was instantaneous frequency. They found that low values of instantaneous frequency were present in the porous carbonate, potentially due to the absorption effects from the presence of fractures. Yet instantaneous frequency tends to have spikes and noise that can mask important information. One way to counter this is to take the average of that

instantaneous frequency. The reduction in noise and spikes in this attribute from averaging outweigh the potential loss of resolution (Barnes, 2000). The average frequency from the Puttygut volume produced pockets of low frequency near wells with higher porosities and sections of high frequency in other areas.

Spectral decomposition (continuous wavelet transform (CWT)): This is an attribute that separates the amplitude seismic data cube into different frequency cubes. There are a few ways to calculated spectral decomposition, but the CWT is a linear form that is based on the short time Fourier transform (STFT). Nejad et al. (2009) used spectral decomposition fast Fourier transform (FFT) and CWT to help identify reef structure as well as areas of high or low porosity in Abadan plain southwest of Iran. They also state that these spectral decomposition methods produce comparable results to that of acoustic impedance inversions, with the main difference being that the acoustic impedance takes more time to compute. Saadatinejad et al. (2012) conducted a spectral decomposition study using the FFT and CWT methods over an oilfield in the northwestern part of the Persian Gulf and found that FFT discovered hidden reef structures that were unseen by traditional seismic and that CWT detected low frequency shadows associated with oil and gas. The Puttygut seismic volume was decomposed into 25 different volumes with frequencies of 5 Hz to 101 Hz at intervals of 4 Hz. Spectral decomposition was chosen for this study as it showed significant variation within the reef at different frequencies.

One of the ultimate goals of this research is to attempt to map/identify areas of high permeability and porosity within the reef reservoirs using machine learning and multi-attribute analysis. Yet these two characteristics of reservoirs are difficult to find using attributes (permeability more so than porosity). Past research has attempted to map these properties with varying degrees of success (Goloshubin et al., 2008; Kozlov, 2007; Pramanik et al., 2004; Iturrarán-Viveros, 2012; Schuelke et al., 1998). The main idea is that using attributes that are frequency focused in nature is the key. Goloshubin et al. (2008) derived a frequency-dependent attribute based off the fluid flow and scattering effect in order to estimate reservoir permeability. Kozlov (2007) used two main attributes that were found to be proportional to permeability. The first, S', was modeled after Lichman and Goloshubin (2003), and it was used to measure the "steepness of the spectrum's left-hand slope" of the seismic data. The thinking

here is that the calculation will give insight into the fluid mobility within the reservoir. There will be a different result depending on whether the reservoir is more permeable, which would allow or hinder the flow of the fluid. They found that there was a relative increase in the low-frequency content as the energy reflected within and/or near a reservoir, especially if gas-saturated. The second was developed within the framework of parameterized spectral decomposition. The relationship used to predict permeability is a ratio of the reflected amplitude spectrum from the minimum to the median with the reflected spectrum from the median to the maximum. Both attributes are calculated or measured from the frequency of the reflected wave energy. Pramanik et al. (2004) found that using a PNN-based (probabilistic neural network) approach with the 10 sample-based attributes produced the best results when attempting to predict effective porosity. To determine the amount and best attributes to use, they designed a multi-attribute stepwise linear regression using 19 sample-based attributes and discovered that 10 attributes was the most efficient. The final attributes are inverse of acoustic impedance, average frequency, filtered seismic 25/30-35/40, dominant frequency, instantaneous phase, amplitude envelope, amplitude-weighted cosine phase, raw seismic, integrated absolute amplitude, and instantaneous frequency. Adding more than ten attributes began to cause an increase in average validation error even though the average training error was still decreasing. Iturrarán-Viveros (2012) conducted a smooth regression using the Gamma test for data analysis to aid in the construction of ANN (artificial neural network) models to predict effective porosity using seismic attributes. They found that the best set of attributes out of 18 proposed to estimate the effective porosity was the following 12: time data, seismic of synthetic trace (STK), envelope (ENV), phase (PH), instantaneous frequency (IFR), second derivative of the phase (D2PHA), decay, second derivative of the envelope (D2ENV), weighted mean frequency (WMF), thin bed indicator (TBI), acceleration (ACC), and reflectivity of p-wave from AVO processing (Rp). The second-best set was very similar to the first, except it removed PH and D2PHA and added in quality factor (QF), totaling 11 attributes. The difference in MSError between the two sets was 0.005. Schuelke et al. (1998) used a combination of instantaneous phase, instantaneous frequency, instantaneous Q factor, chaotic reflection, and parallel bedding indicator in addition to traditional seismic acoustic impedance in neural

networks to significantly improve porosity estimations within a Devonian reservoir located in the Pegasus field, Permian Basin, West Texas. All this past research has one thing in common when attempting to map or predict permeability or porosity: the attributes chosen are mostly derived from or related to the frequency and/or phase of the seismic data. In order to determine if the frequency-based attribute approach at identifying permeability and porosity is effective for the study area of this research, all attributes will be looked at initially on the provided high confidence horizons that represent the reef lithofacies. These detailed horizons make it possible to accurately estimate the location of high permeability and porosity zones surrounding wells that penetrate the reef. From there, it should be possible to work out from each well into the reef to determine how much variability in permeability and porosity there is. Four value ranges were set to differentiate "great" from "poor" permeability and porosity. The ranges for porosity are: 0% - 3% is poor, 3% - 6% is intermediate, 6% - 10% is good, and greater than 10% is great. The ranges for permeability are: < 1 mD is poor, 1 - 10 mD is intermediate, 10 - 50 mD is good, and greater than 50 mD is great.

Puttygut Data

This dataset is fairly rich in data, but not entirely as complete as would be ideal. There are two 3D seismic volumes acquired and processed in 2019 (one is pre-stack time migrated and the other is post-stack time migrated) using the Michigan South 2113 projection system. The inline and crossline spacing is 440 feet, with shot and receiver spacing of 110 feet, a final bin size of 55 by 55 feet, and a sample rate is 1 millisecond. Additional details regarding the 3D survey design, acquisition parameters, and processing workflow are located in Appendix E. The vertical resolution of the data at the reef level is approximately 60 to 80 feet. These values were calculated using the equation: $VR = \frac{\lambda}{4}\ where\ \lambda = \frac{v}{f}$ where the peak frequency was between 40-50 Hz and an interval velocity range at the depth of interest was 11,971.9-12,910.1 ft/sec. There are 30 wells in the area drilled within and around the reef. All 30 wells have at least a gamma ray log. Table 2 below lists all other well logs available in the area in order of most common to least. Table 3 shows core data that was compiled and transferred into LAS format.

Well log name	Wells that have the log
Neutron porosity	**14** (P-4A, 23494, 23900, P-105, P-102, P-106, P-3A, P-101, P-01, P-03, P-02, P-202, P-204, P-206)
Resistivity	**2** (23494, 23900)
SNP	**1** (P-201)
DT	**1** (P-4A)
D13C	**1** (P-105)

Table 2: List of all available well logs and which wells have them. See Figure 9 for well locations.

Core data name	Number of wells (well name)
ZPERM	**11** (P-101, P-102, P-103, P-104, P-105, P-106, P-201, P-3A, P-4A, P-11A, P-12A)
ZPOR	**11** (P-101, P-102, P-103, P-104, P-105, P-106, P-201, P-3A, P-4A, P-11A, P-12A)
ZOILSAT	**9** (P-102, P-103, P-105, P-106, P-201, P-3A, P-4A, P-11A, P-12A)
ZWATSAT	**9** (P-102, P-103, P-105, P-106, P-201, P-3A, P-4A, P-11A, P-12A)
ZPERM_90	**4** (P-3A, P4-A P-11A, P-201)

Table 3: List of available core data turned to logs and which wells have them. See Figure 9 for well locations.

In addition to these well logs, there are also 18 core analyses (P-101, P-102, P-103, P-104, P-105, P-106, P-201, P-01, P-1A, P-2A, P-3A, P-4A, P-5A, P-6A, P-7A, P-8A, P-11A, P-12A) and five in depth core profiles (P-105, P-106, P-201, P-4A, P-11A). These wells are marked on Figure 9 below. In addition to all this well data and 3D seismic data, there is a vertical seismic profile (VSP) at well P-201.

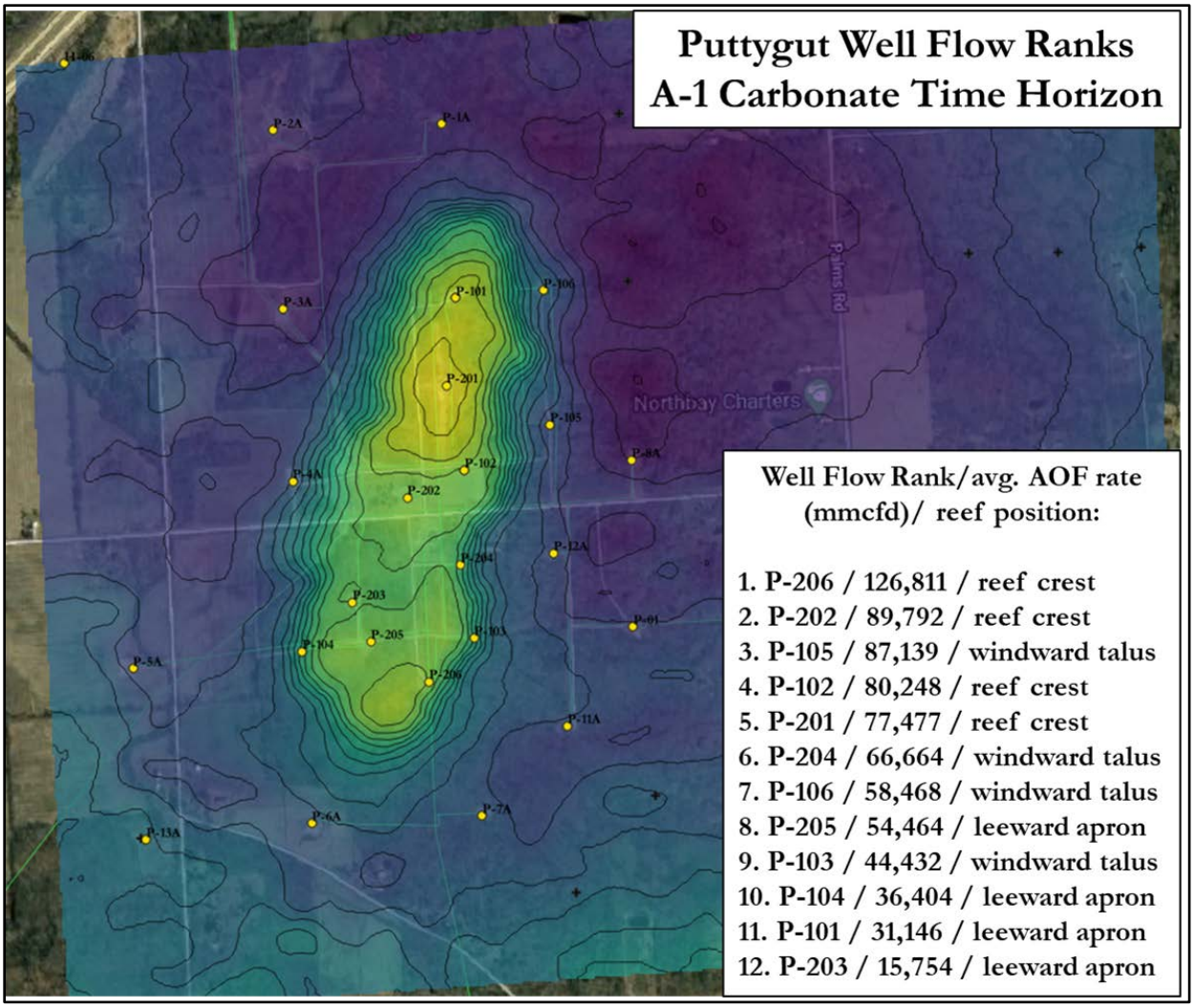


Figure 9: Map of Puttygut reef approximate location with all wells labeled with well flow rankings. Map from M. Rine (personal comm., 2020).

Puttygut single and multi-attribute results

A wide range of single attributes were calculated in AASPI and compared by the interpreter to decide which attributes best showed features of interest in the reef. There are other methods for attribute selection, such as the PCA (principal component analysis) method, but they were not implemented as interpreter apriori knowledge was used to select the optimal set of attributes. PCA, and other such methods, use mathematical approaches which can aid the interpreter if apriori knowledge is lacking. The goal is to attempt to identify sub-seismic features in one of two ways: 1) Using attributes that help define the geometry of the

subsurface. 2) Using attributes that are calculated in the frequency realm. Using PCA to choose the attributes will not differentiate between attributes that specialize in structural identification and those that are useful in the frequency domain, it will give attributes that show the most variability in the data regardless of their specialization. Designating the attribute selection to the interpreter is the easiest way to avoid mixing the two categories of attributes. Therefore, after much consideration, the following attributes were deemed most worthy. Structural: energy ratio similarity, negative curvature, aberrancy, and GLCM homogeneity. Frequency: cosine of instantaneous phase, average frequency, continuous wavelet transform (CWT) spectral decomposition at frequencies of 29 Hz, 57 Hz, and 81 Hz. The approximate thickness ranges these frequencies correspond to with velocities at the reef interval are 107 feet, 55 feet, and 38 feet for 29 Hz, 57 Hz, and 81 Hz respectively.

The following section of the chapter details observations of the single attributes and multi-attribute results extracted onto horizons picked by an expert geologist that works in the Michigan Basin. Initially, stratal slices were used to estimate the locations of the different facies within the reef, but upon consultation it was discovered that the geometry of the reef interior changes dramatically from the horizons that encase it. These encasing horizons were used as the boundaries to create the stratal slices and because of this the internal geometry change was not recorded. First, the single attributes that were calculated in AASPI are extracted onto the Brown horizon slice in Petrel and initial observations are recorded. Appendix A contain the single attributes extracted onto the other formation horizons. Second, six total SOMs were calculated in Paradise. All six SOM calculations were output with a 5x5 neuron grid. Three of the six SOM runs used the aforementioned structural attributes in addition to the PSTM amplitude while the other three used the aforementioned frequency attributes without the PSTM amplitude. The amplitude was removed from the frequency SOM runs because it tended to dominate the results. After its removal, there was a greater variability in which attribute contributed the most for each cluster of data. The first two (one structure and one frequency) SOM runs were restricted between the A-2 Carbonate and Clinton layers and utilized all the inlines and crosslines. The next two (one structure and one frequency) were restricted between the same two horizons but the inlines and crosslines were restricted to isolate the reef from the

surrounding geology. That range is from Inline 38 to 116 and from Crossline 45 to 85. The final two SOM runs (one structure and one frequency) used the same inline and crossline restrictions as the second set of SOMs but were further confined vertically to be between the A-1 Carbonate and the Gray layers. Figure 11 shows the SOM boundaries in both map view and in cross section. The last two batches of SOM runs were then extracted onto the Brown horizon slice. SOM run number one can be found in Appendix B. There are six horizons that compose the reef boundary and internal structure, but the Brown horizon is the focus of the single and multi-attribute analysis. The Brown horizon is the top of the Guelph reef complex (the top of the Reef Core, Reef Apron, and Reef Talus geobodies), which made it the most important horizon for displaying the attribute maps because it is the most representative of the morphology of the Guelph reef complex. Observing the single and multi-attributes at this level gave the best insight into the reef possible. The horizon observations are followed by initial observations of the SOMs shown in vertical seismic display. The goal of this section is to identify areas and attribute combinations of interest, namely areas along well bores where there is permeability and porosity data. Four type wells that had the most complete suite of porosity and permeability data were chosen for this task: P-106, P-201, P-102, and P-103. All SOM results output the data into voxel sizes that were 55 by 55 feet laterally and 1 millisecond vertically. Figure 10 shows an example of the data and the voxel sizes.

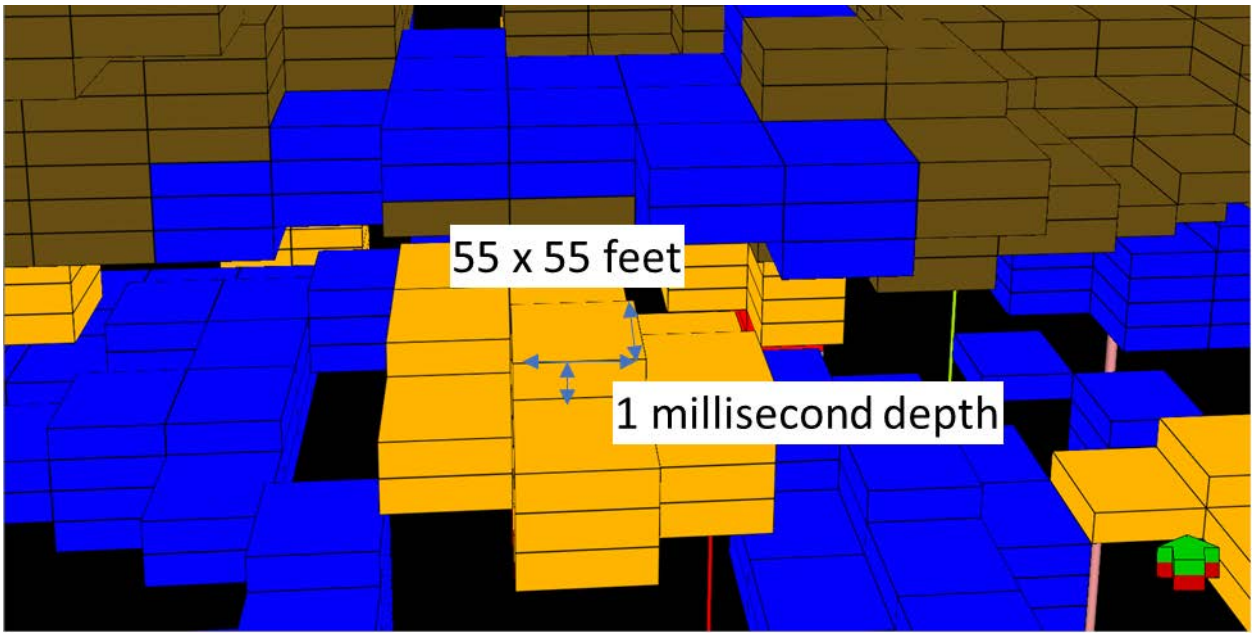


Figure 10: The SOM outputs voxels that are 55 by 55 feet in lateral area and 1 millisecond vertically, which is equivalent to the bin size and sample rate of the input data.

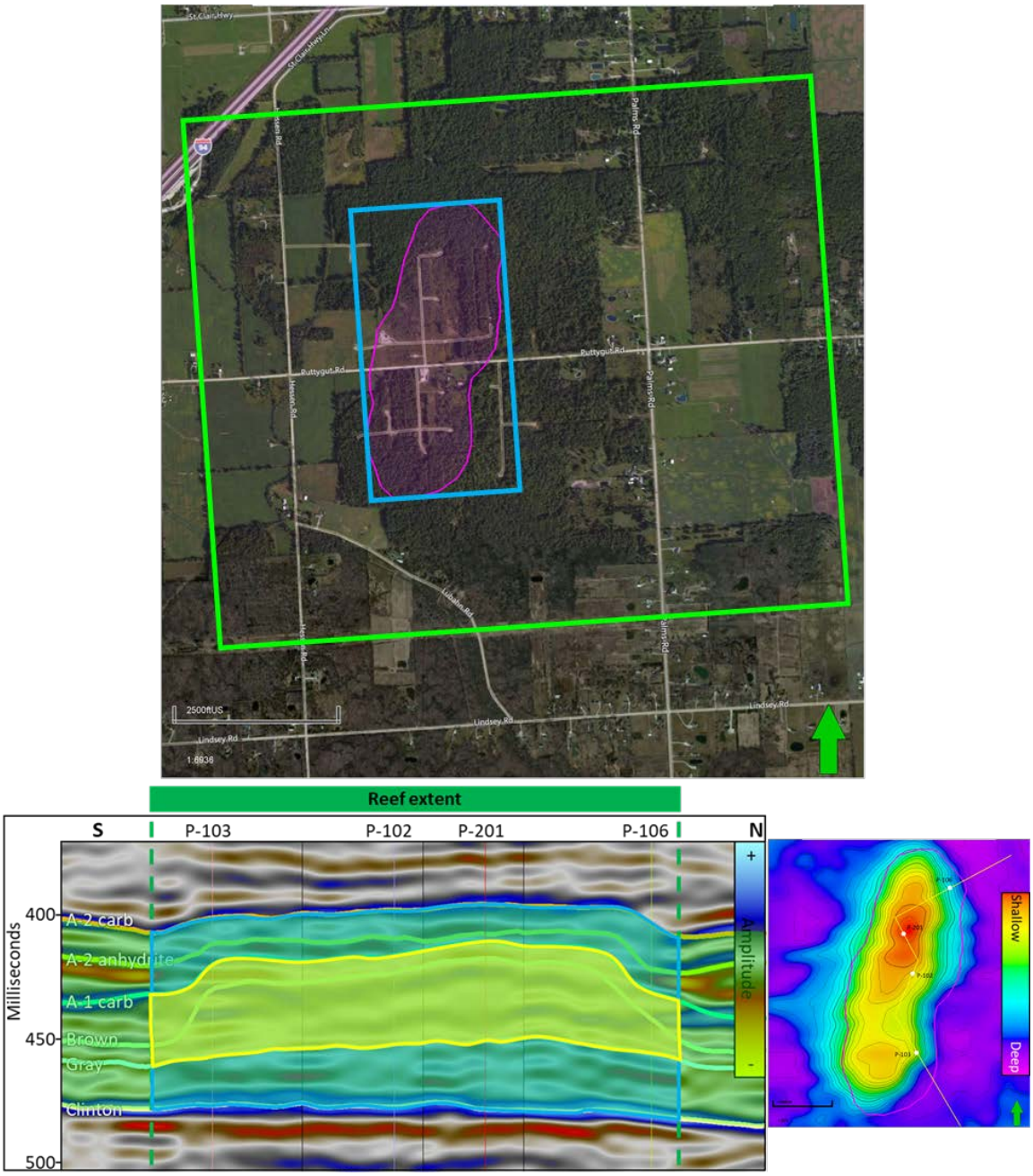


Figure 11: The top image shows the inline and cross line extent of the SOM runs with Bing Maps Hybrid Imagery overlay. The green box encompasses all the inlines and crosslines. The blue box is the cropped survey extent with a range from Inline 38 to 116 and from Crossline 45 to 85 and the pink outline is the mapped outline of the reef. The bottom image, at 20 times vertical exaggeration, shows the vertical extent of each SOM run. The green and blue shaded areas are associated with the green and blue boxes from the upper image and vertically constrain the data between the A-2 Carbonate and the Clinton Formation. The yellow shaded area represents the vertical extent of the third SOM run. It is laterally constrained by the blue box but vertically it is between the A-1 Carbonate and the Gray Formations.

Single attributes on Brown

Figure 12 shows an enlargement of the structural attributes extracted onto the Brown horizon in Petrel. The light pink outline in each image represents the reef extent as defined by M. Rine (personal comm., 2020). Figure 12 A) two-way time (TWT) map of the horizon. The reef complex is a clear structural high compared to the off-reef areas, and there is slightly higher structure observed in the northern section of the reef complex compared to the southern. The slope is gentler on the western edge of the reef and steeper on the eastern edge. Figure 12 B) pre-stack time migrated (PSTM) amplitude data. There is a consistent negative amplitude that composes most of the reef top, followed by a ring of positive amplitude that contours the reef outline. Figure 12 C) energy ratio similarity (ERS). The yellow arrows filled with black are showing areas of lower similarity along the eastern side of the reef, as well as one spot in the southern portion. The yellow lines outline some sinuous features that surround the main reef body. Figure 12 D) negative curvature attribute. Outlined in yellow is a connected feature that runs throughout the reef body. There is also a broad trend of negative curvature that wraps around the reef outline itself everywhere except for the southern tip. The area that surrounds the reef complex is comprised of alternating carbonate and halite layers, which have a much greater acoustic impedance than the reef complex interior which is comprised of only carbonate. Figure 12 E) aberrancy. An interconnected feature is present here as well, but it takes up more of the reef. Within that feature there are small pockets of little to no aberrancy. At the bioherm level, these features could be associated with coral growth patterns within the reef. Figure 12 F) GLCM homogeneity. The yellow circle shows an area of high homogeneity that is concentrated in the northern section of the reef. There is then a low homogeneous zone surrounded by a tight ring of high homogeneity on the reef outline. The tight ring of homogeneity could be areas in which reef debris gathered as the reef died due to being drown. The yellow arrows filled with black are pointing to areas surrounding the reef that are high homogeneity concentrations. These could be areas where smaller bioherm mounds initially formed but were abandon/drown as sea level rose during the time of reef growth. Figure 13 shows a zoom in on the same Brown horizon with the frequency-based attributes extracted onto it. Figure 13 A) average frequency. The black shapes outline areas of particularly low

average frequency in the main reef body. The rest of the reef is a higher average frequency. The black arrows are pointing to areas of anomalously high or low average frequency which lie outside of the reef body. The varying frequencies found within the reef core could indicate a transition from a higher porosity and permeability to a lower porosity and permeability lithofacies. Figure 13 B) cosine of the instantaneous phase accentuates what the PSTM amplitude shows. There is a negative cosine value in the reef body, surrounds by a positive ring that hugs the reef body. The attribute also shows that there is another ring with a negative cosine value that tightly curves the inner features to the east and more broadly curves to the west. Outside of that ring is mostly positive values speckled with negatives. Figure 13 C), D), and E) display the CWT spectral decomposition at frequencies 29 Hz, 57 Hz, and 81 Hz, respectively. 29 Hz corresponds to approximately 107-foot thicknesses, 57 Hz to 55-foot thicknesses, and 81 Hz to 38-foot thicknesses. Figure 13 C) CWT spectral decomposition at 29 Hz shows the main reef body has a lower presence of 29 Hz relative to its surroundings everywhere except where the yellow circle is in the southern portion of the reef. The presence of 29 Hz in the southern portion of the reef could indicate that it is slightly thicker than the rest of the reef. Figure 13 D) is the CWT spectral decomposition at 57 Hz. Around the reef there is a ring of higher presence of 57 Hz. The southern half of the ring exhibits a higher presence than the northern half. Most of the reef body is near void of 57 Hz, except where the yellow lines are outlining. There appear to be small shapes or features that have some presence of 57 Hz within the reef itself. Going from 29 Hz to 57 Hz, we begin to pick up on thinner features. In this case we go from frequencies that are associated with 107-foot thicknesses to 55-foot thicknesses. Seeing more detail within the reef itself as the frequency increases could imply that the internal growth patterns of the reef happened on a smaller scale. The ring surrounding the reef seen with the 57 Hz spectral decomposition could be associated with an area of reef debris that can be found surrounding the reef core. Figure 13 E) is the CWT spectral decomposition at 81 Hz. Within the reef outline, there is a lot of variability in whether 81 Hz is present. Upon closer inspection, areas where the presence is similar are usually connected. The yellow lines outline the more drastic regions where the higher presence occurred within the reef. Looking out from the reef the same pattern can be seen. The highly interconnected areas seen with the 81 Hz spectral

decomposition could be associated with the more complex internal coral growth patterns found within the reef core. Each of these attributes brings something different to the table that will become more important when combining them into a SOM.

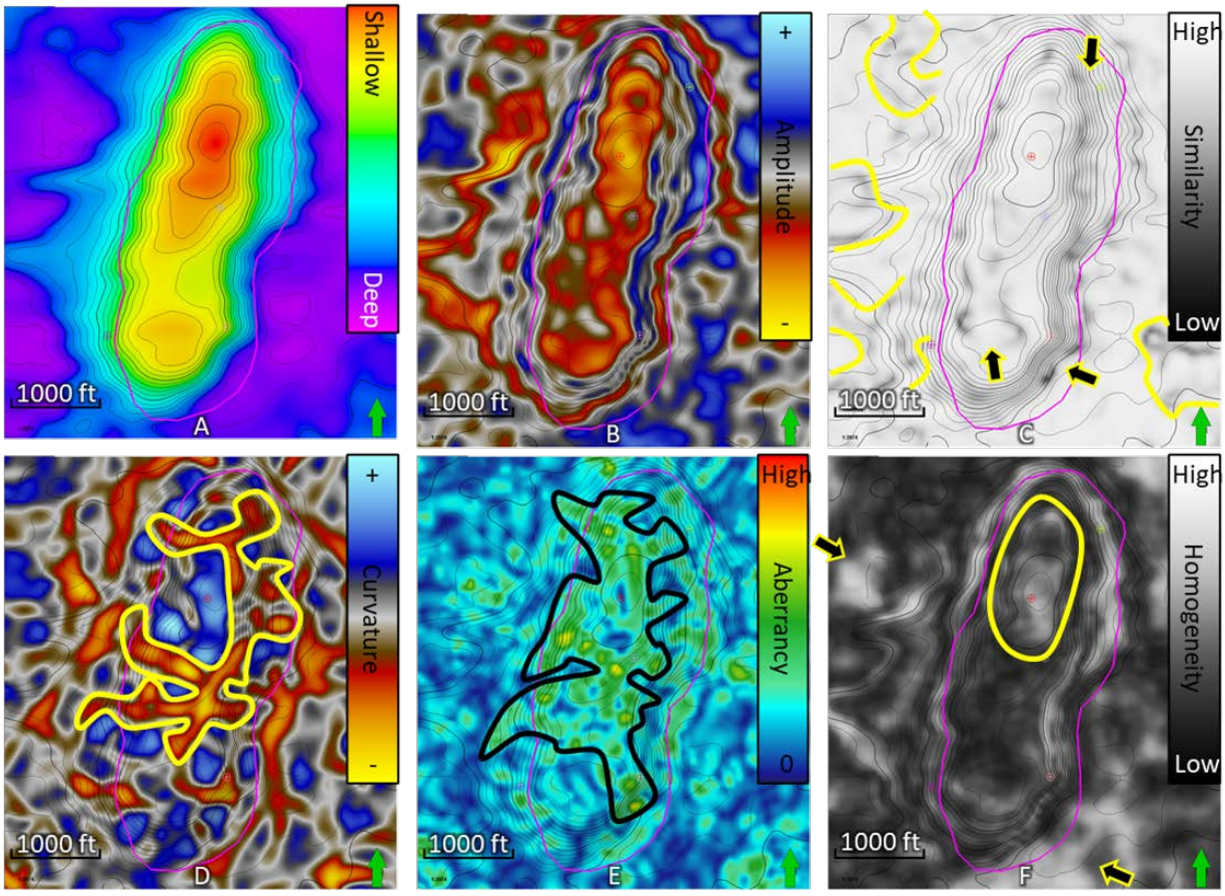


Figure 12: A) The two-way time map for the Brown horizon. B) The pre-stack time migrated (PSTM) amplitude data extracted onto the Brown horizon. C) Energy ratio similarity (ERS). D) Negative curvature. E) Aberrancy. F) Grey level co-occurrence matrix (GLCM) homogeneity. Pink outline marks the outer reef boundary as defined by the A-1 Carbonate horizon.

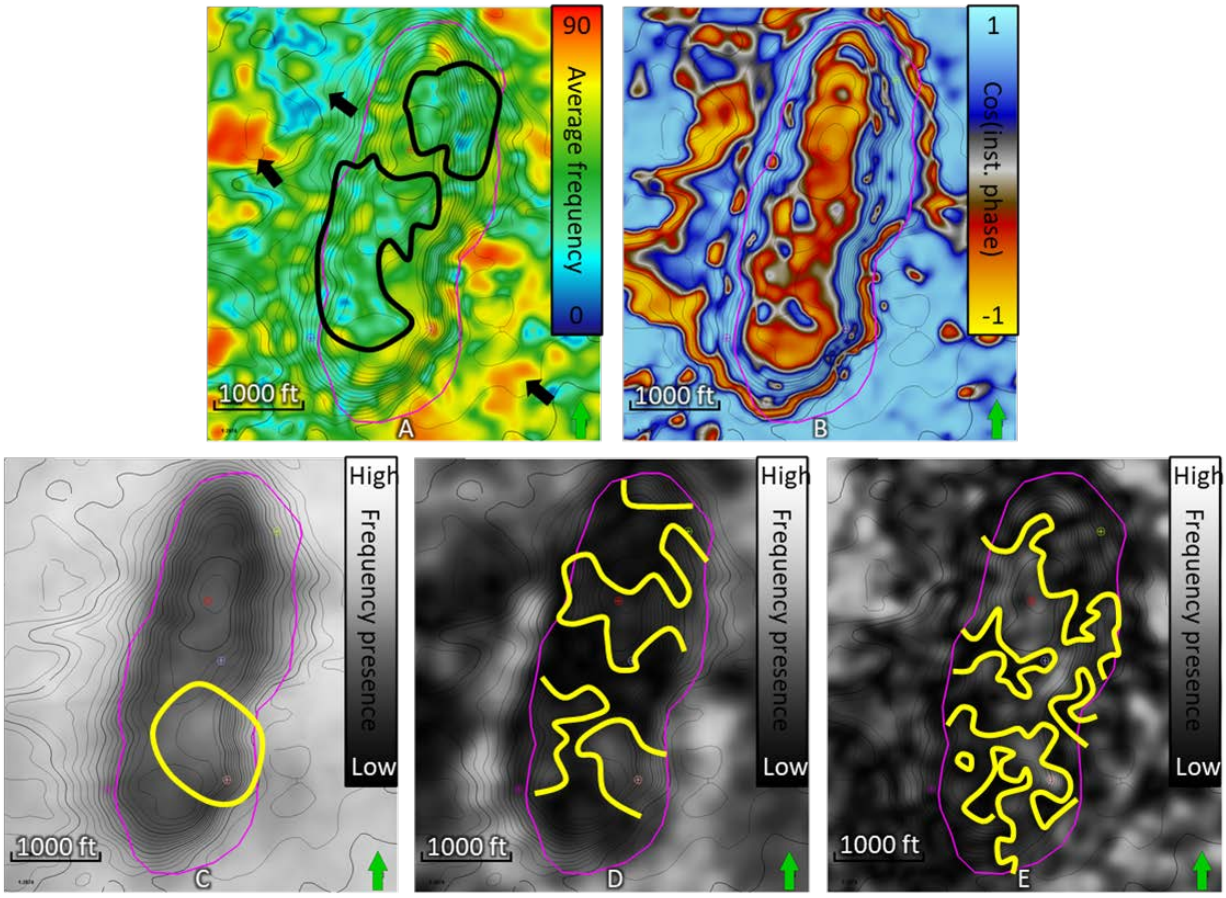


Figure 13: A) Average frequency. B) Cosine of the instantaneous phase. C) Continuous wavelet transform (CWT) spectral decomposition at 29 Hz. D) CWT spectral decomposition at 57 Hz. E) CWT spectral decomposition at 81 Hz. Pink outline marks the outer reef boundary as defined by the A-1 Carbonate horizon.

SOMs on Brown

This section shows the results of the final two SOM runs extracted onto the Brown horizon. The Brown horizon is the top of the Guelph reef complex (the top of the Reef Core, Reef Apron, and Reef Talus geobodies), which made it the most important horizon for displaying the attribute maps because it is the most representative of the morphology of the Guelph reef complex. Appendix B has additional SOM extractions on the other horizons of interest. Also, the third SOM run that was vertically constrained between the A-1 Carbonate and the Gray horizons only has the Brown horizon between them. The SOM result cannot be

extracted onto the A-1 Carbonate or Gray horizons for the third SOM run as they are the boundary for that SOM and any results at the boundary are potentially compromised. The white dots in Figure 14 and Figure 15 denote the locations of four wells that penetrate the reef. From north to south the wells are, P-106, P-201, P-103, P-102. When comparing different SOMs in general, it must be noted that the colors and the neuron number are only place holders. The resultant distribution of attributes within each neuron is unique to each individual SOM run based on the input data and calculation parameters. Figure 14, for example, shows the second and third SOM runs using the structure-based attributes. We see a connected feature that is present in both SOM runs and is visually similar when extracted on the Brown horizon, outlined by the white dashed line. Neurons 22 and 23 compose this feature for the second SOM (left) while neurons 19 and 23 comprise it in the third SOM (right). Table 4 contains a detailed list of how much each attribute in the SOM contributed to that specific neuron. The first thing to note is that neuron 23 is present for both SOM runs, this is just coincidence. The attribute blend for each neuron 23 is different. The 23rd neuron for the second SOM run has the attributes of PSTM amplitude, ERS, and GLCM homogeneity contributing over 20% each. The 23rd neuron for the third SOM run has PSTM amplitude, negative curvature, and GLCM homogeneity contributing over 20%. Moving forward, it is important to keep in mind that features that are similar between these two SOMs may not be characterized by the same combination and blending of attribute, even though the same attribute set was used. The factor causing the changes is the amount of initial data that was given when creating the SOMs in the first place. The second SOM run used the data between the A-2 Carbonate and the Clinton Formations while the third SOM run was between the A-1 Carbonate and the Gray Formations. Removing just that amount of data from the top and bottom can cause significant changes to the results for SOMs. The connected feature is not the only thing that is similar between the two SOMs in Figure 14. The white arrows in Figure 14 point to another group of neurons that characterize some feature the is more concentrated or mounded near the center of the reef. Moving off and away from the reef there are some linear features seen outlining the base of the reef that are composed of the same neurons that made up the sinuous feature within the reef itself. In general, there are a set of neurons that are classifying more sinuous or linear features and another set that classify

more condensed or mounded features. Figure 15 shows the frequency SOMs displayed with a random color bar. Along the reef body, there is a distribution of three to four different neurons. The white arrows are pointing to areas where one or two neuron clusters are consistently located near the well locations. Moving off the main reef body the neurons that are present change completely. There is little to no connection between the neurons on the reef and those that are off the reef. These areas that are concentrated on the reef body could be related to changes in rock properties associated with permeability and porosity. These neurons are also tending to cluster near areas where there is well penetration. The clustering occurring at the well locations could be an indicator of similar and desirable rock properties.

Neuron	PSTM amplitude	Aberrancy	Negative Curvature	ERS	GLCM homogeneity
Left SOM: 22	23%	4.6%	7.5%	29%	35.9%
Left SOM: 23	22.9%	8.6%	9.5%	21.6%	37.5%
Right SOM: 19	0.1%	35.7%	36.6%	25.8%	1.7%
Right SOM: 23	24%	9.3%	21.6%	16.4%	28.6%

Table 4: Two neurons from each SOM run from Figure 14 were chosen that characterized an interesting structural feature (which is outlined in a white dashed line). The table shows the percentages of each attribute that was used to create each neuron. Notice that there is neuron 23 listed twice but that it has different distributions of the attributes. Neuron 23 having different distributions was because each SOM had different input parameters, which caused the final results to differ.

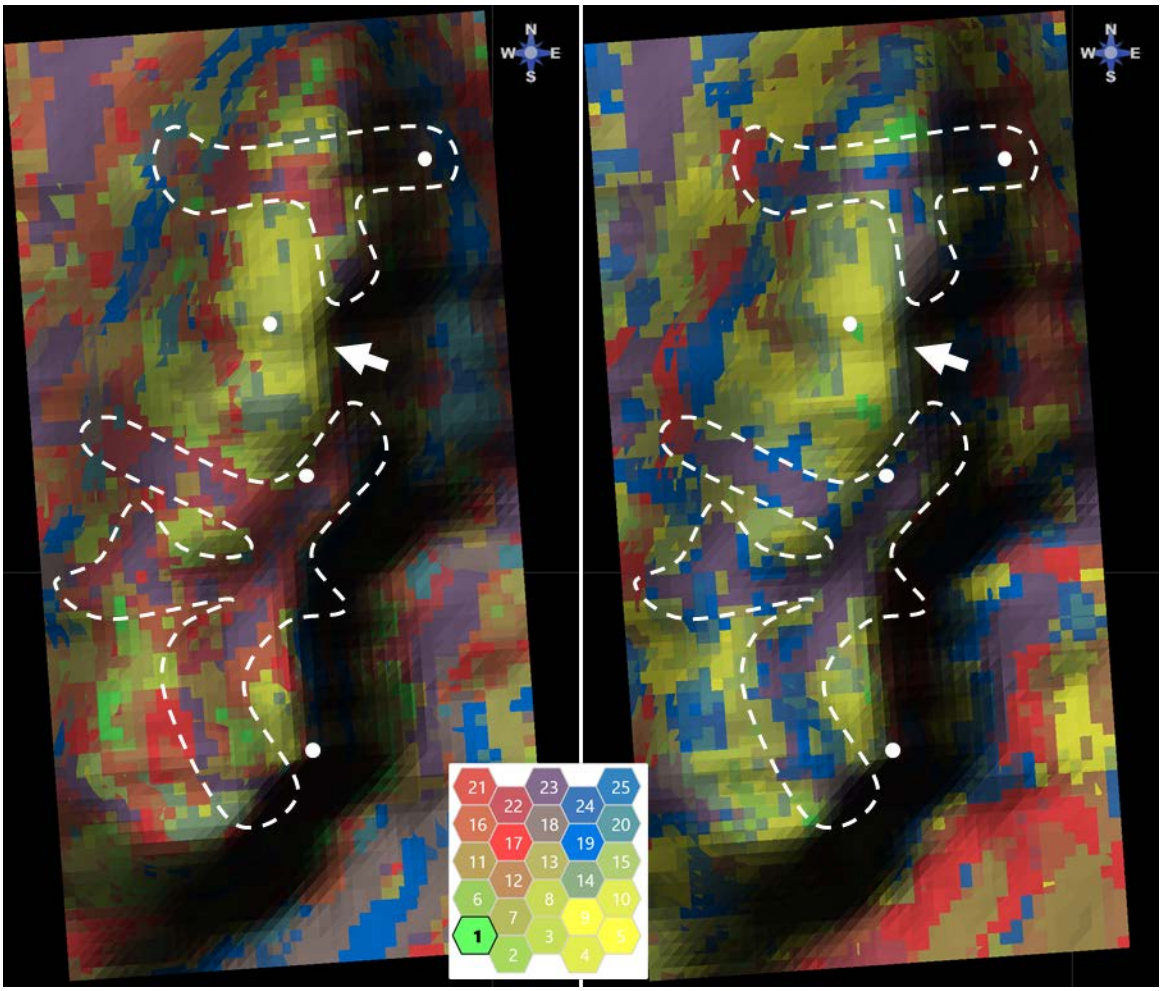


Figure 14: Structure SOMs with a more gradational color bar. Left image was created between A-2 Carbonate and Clinton horizons. Right image is a SOM created between the A-1 Carbonate and the Gray horizons. Both SOMs are shown on the Brown horizon. Both SOMs were created with the cropped inline and crossline extent discussed in Figure 11. The white dots represent four wells that penetrate the reef. From north the south they are: P-106, P-201, P-102, P-103. Refer to text for description of white-dashed area and white arrows. The black area surrounding the SOMs is the background color for the software where there is no information being shown.

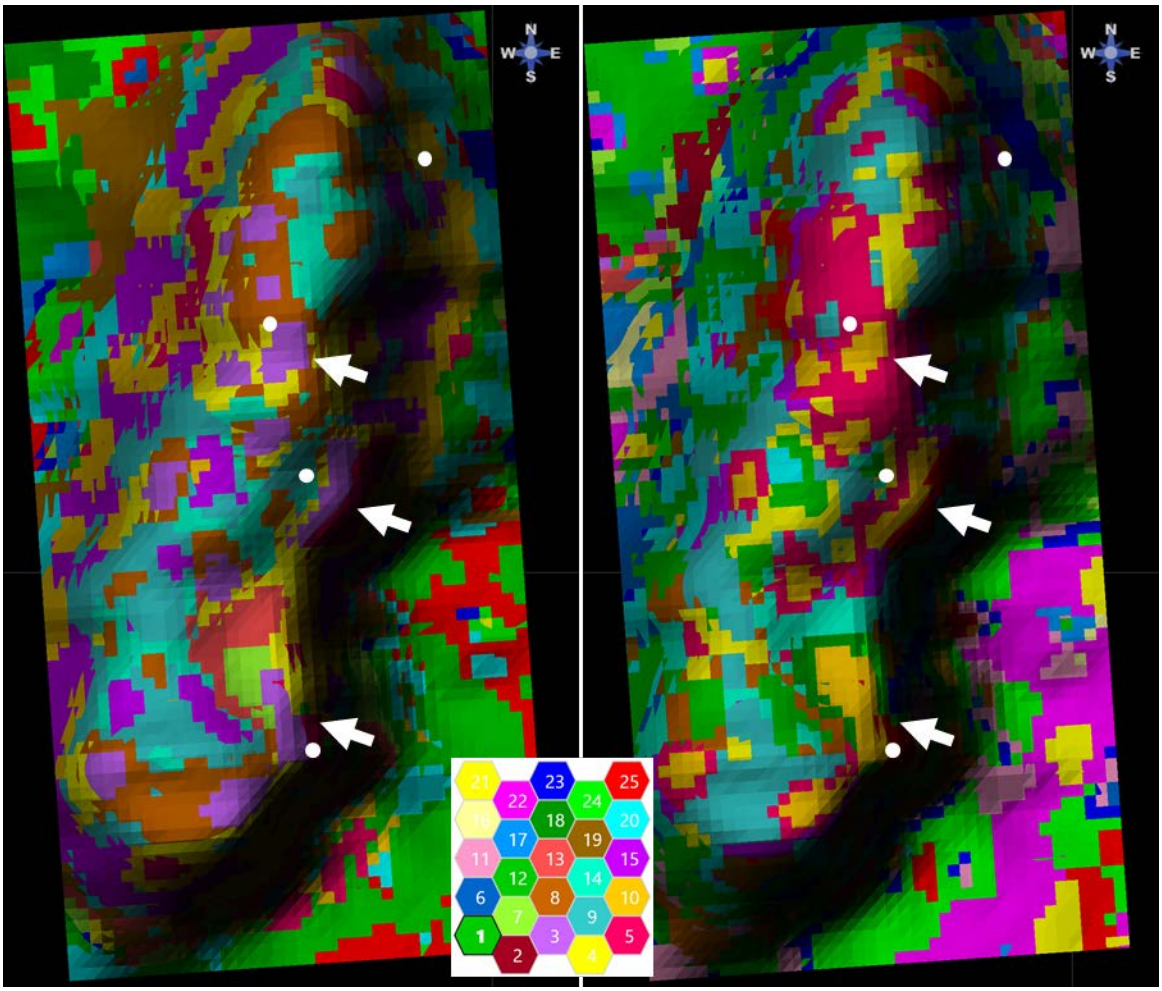


Figure 15: Frequency SOMs with random color bar. Left image was created between A-2 Carbonate and Clinton horizons. Right image is a SOM created between the A-1 Carbonate and the Gray horizons. Both SOMs are shown on the Brown horizon. Both SOMs were created with the cropped inline and crossline extent discussed in Figure 11. The white dots represent four wells that penetrate the reef. From north the south they are: P-106, P-201, P-102, P-103. The black area surrounding the SOMs is the background color for the software where there is no information being shown.

SOMs in vertical seismic displays

The next step is to look at the SOMs in vertical section to better understand and compare the lateral extent of the revealed features. Figure 16, Figure 17, and Figure 18 show the second and third SOM runs side by side. All images were taken at Inline 92 in the survey, which crosscuts well P-201, indicated by the white line (approximately Crossline 66). The width of the images is from Crossline 45 to 85. The dashed white line represents the time of 417 ms in

the subsurface and where it meets the vertical white line representing the P-201 well is where the top of the Brown Formation is located at that well. Figure 16 only shows one feature of interest which looks like a hollow mound. The feature is mostly blue (neurons 18, 19, 20, 24, and 25) in the left image (the second SOM run) and mostly red and yellow (neurons 5, 10, 11, 12, 16, 17, 21, and 22) in the right image (the third SOM run). Figure 17 displays this feature with only the neurons that compose it turned on. The feature peaks below the top of the Brown Formation and rest entirely within the bioherm section. Expanding out from this inline into the rest of the survey revealed that this feature consistently remained under the Brown Formation top and rested within the bioherm. One possible explanation for the mound feature is that it is the remnant of the bioherm mound that the reef eventually grew on.

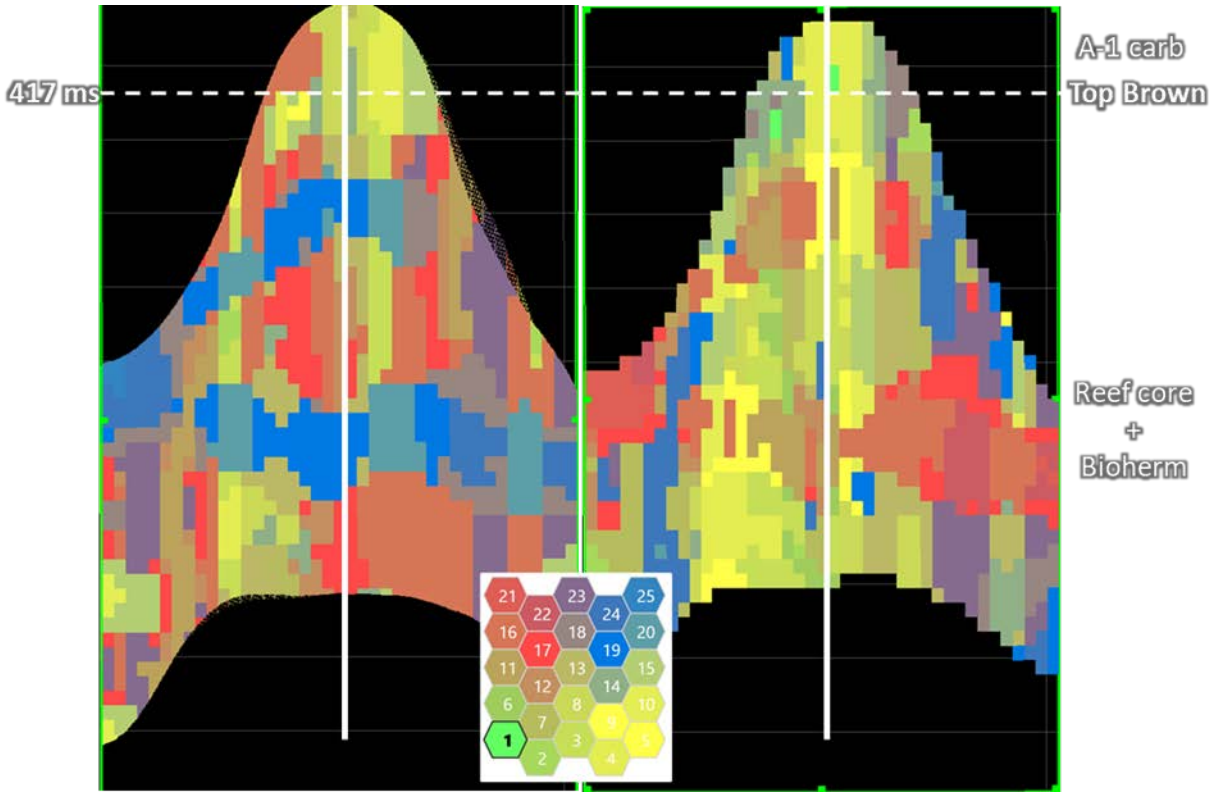


Figure 16: Structure SOMs with a more gradational color bar. Left image was created between A-2 Carbonate and Clinton horizons but visually cropped between the A-1 Carbonate and the Gray horizons. Right image is a SOM created between the A-1 Carbonate and the Gray horizons. Both VSDs are Inline 92 through well P-201, which is marked by the white vertical line. Both SOMs were created with the cropped inline and crossline extent discussed in Figure 11. The black area surrounding the SOMs is the background color for the software where there is no information being shown.

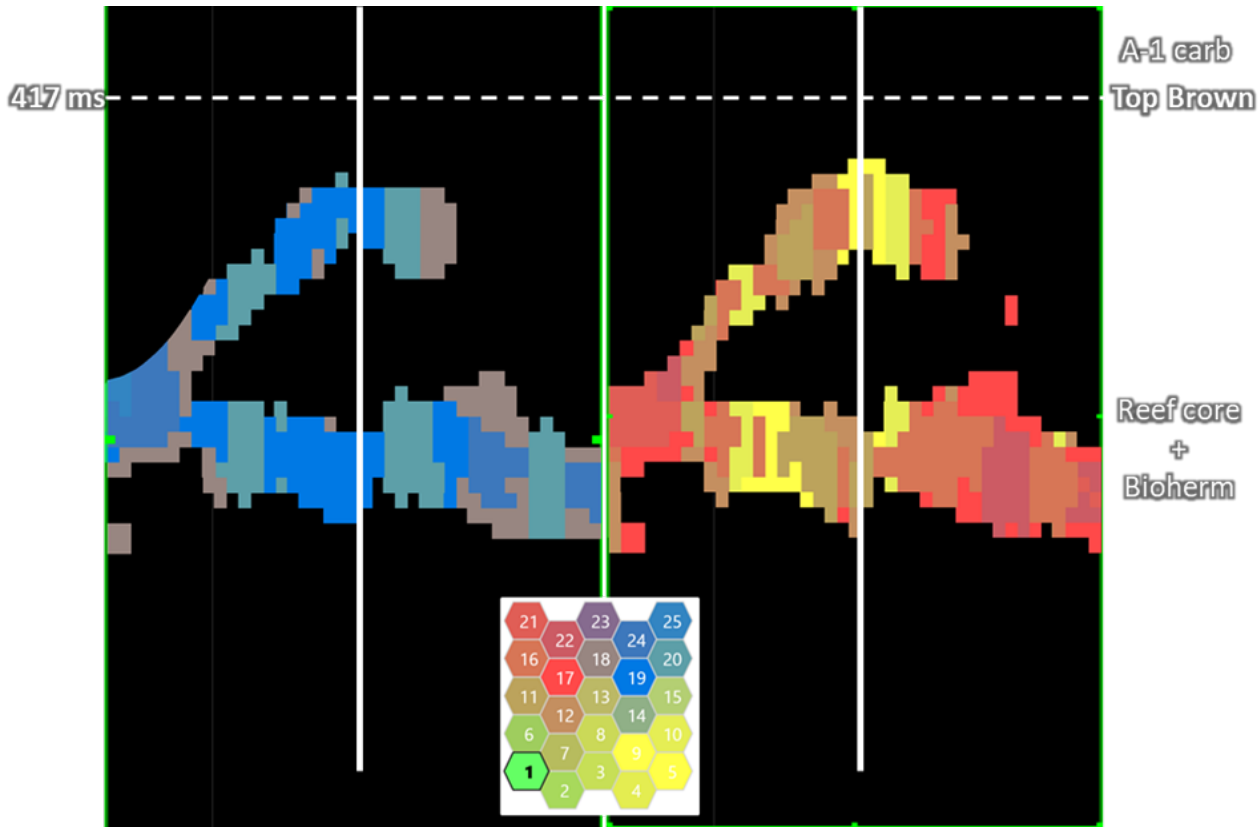


Figure 17: The mound feature with only relevant neurons turned on. The left SOM created the feature using five neurons while the right SOM produced it with eight neurons. The black area surrounding the SOMs is the background color for the software where there is no information being shown.

Figure 18 uses a different color bar with random colors to help increase the contrast between areas that differ slightly. Around the well location there are a few different pockets of individual neurons. Some glaring similarities can be seen by the gold color in the left SOM and the brown color in the right SOM. They seem to represent similar areas and are only found in the bioherm section. Those neurons could potentially indicate areas within the reef that have similar porosity or permeability properties. Yet, the right SOM image seems to have more variability overall. One example of this can be seen when looking on the right of each SOM. The large purple section in the left SOM is divided up into two or three different neurons in the right SOM. The increase in variation is due to the differing amount of initial data given when creating the SOM but keeping the number of classifications (neurons) the same. Since less data were

given to the third SOM at the start and there were still 25 neurons to utilize it was able to divide up more of the reef interior when compared to the previous SOM runs where more data were initially provided.

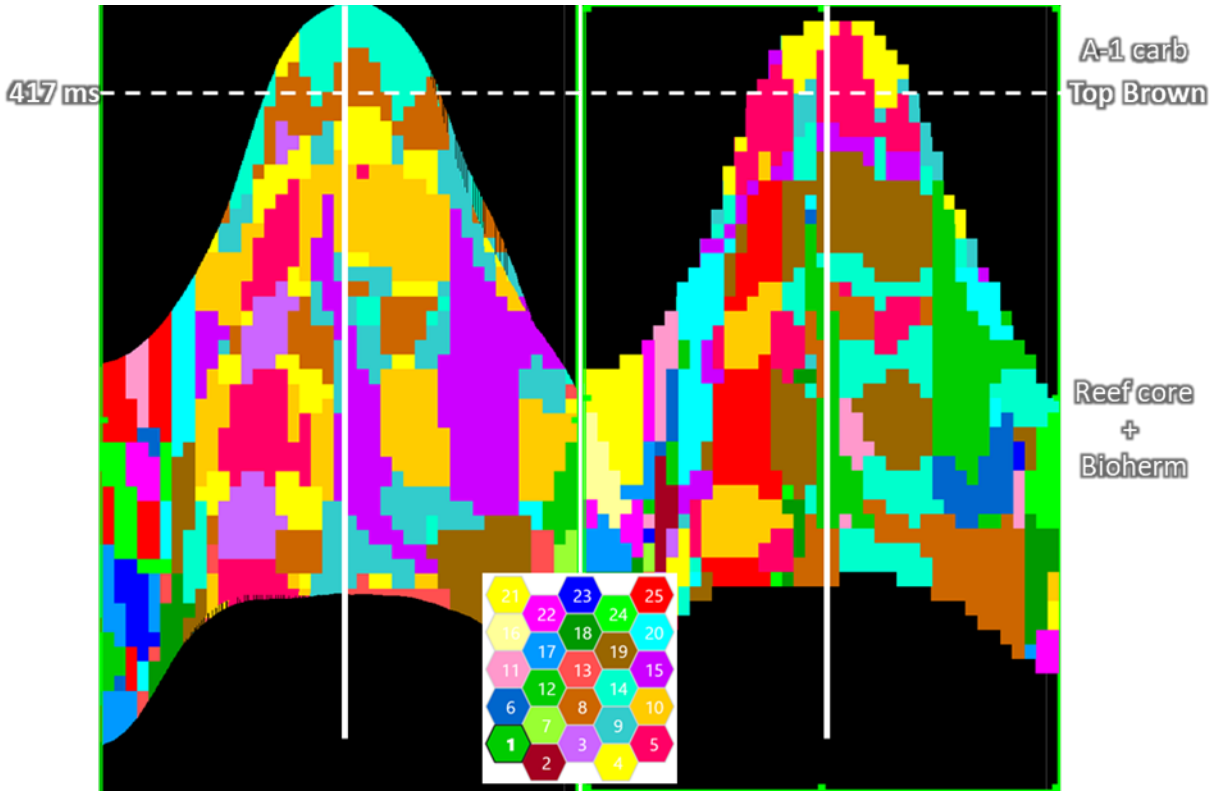


Figure 18: Frequency SOMs with a random color bar. Left image was created between A-2 Carbonate and Clinton horizons but visually cropped between the A-1 Carbonate and the Gray horizons. Right image is a SOM created between the A-1 Carbonate and the Gray horizons. Both VSDs are Inline 92 through well P-201, which is marked by the white vertical line. Both SOMs were created with the cropped inline and crossline extent discussed in Figure 11. The black area surrounding the SOMs is the background color for the software where there is no information being shown.

Discussion

In the end, the third SOM run with the frequency attributes was chosen to explore the reef further. The input data and parameters for the third SOM were best suited to achieve the goal of identifying areas of poor to great permeability and porosity. The ranges for these classifications for porosity are: 0% - 3% is poor, 3% - 6% is intermediate, 6% - 10% is good, and

greater than 10% is great. The ranges for permeability are: 0 - 1 mD is poor, 1 - 10 mD is intermediate, 10 - 50 mD is good, and greater than 50 mD is great. Horizons with high levels of confidence were used to bridge the gap between the well logs and the time volumes. A qualitative interpretation on the efficacy of the frequency SOM runs to identify sub-seismic areas of varying permeability and porosity was conducted using the available data. In order to create Figure 19, SOM vertical display images were taken at each inline where a well was located. The well crossline location was marked by a vertical white line. Then the permeability and porosity logs were taken from Petrel and overlain on these VSDs. The logs were then stretched and squeezed between the A-1 Carbonate, the Brown, and the Gray Formations.

Areas of varying permeability and porosity were located on the well logs and then the neurons associated with those locations were noted, see Table 5. At well P-106 the best case scenario was found with great permeability and porosity on average, denoted by the blue box in Figure 19. Neurons associated with this box are numbers 19 and 23. Two areas of good to great porosity were found with widely varying permeability at wells P-201 and P-102. They are marked with the green squares. Neuron 19 is associated with the green boxes. Areas of poor permeability and at best intermediate porosity are marked with the red boxes at wells P-106 and P-102. The neurons found within the red boxes are 18 and 20. Finally, the yellow boxes at well P-103 mark two locations where the porosity is roughly the same, with values ranging from good to great, but with vastly different permeability. The two neurons within the yellow boxes are 10 and 25. Neuron 23 is only present at the one location where there is the highest values of permeability and porosity. Neuron 23 is also the only neuron with a high percentage of CWT spectral decomposition at 81 Hz at 40.6% contribution. The other top contributors for this neuron are the average frequency at 35.3% and CWT spectral decomposition at 29 Hz with a 22.4% contribution. Neuron 19 can be found where there was a wide range of permeability but intermediate to great porosity. Neuron 19 is also found next to neuron 23 at well P-106 where the best properties were found. The top three attribute contribution percentages for neuron 19 are CWT spectral decomposition at 29 Hz with 39.3%, average frequency with 29.9%, and CWT spectral decomposition at 57 Hz with 24.3%. The yellow boxes at well P-103 seem confusing at first, but upon closer inspection the attribute contribution percentages for neurons 10 and 25

are almost identical. The porosity in this well has slight variations from good to great through the whole section while the permeability is more highly varied and does not seem to follow any specific trend. That information implies that these two neurons are mostly driven by the porosity and not as affected by the permeability. The blends of neurons 10 and 25 have attribute contribution percentages of ~38% for CWT spectral decomposition at 29 Hz, ~31-35% for CWT spectral decomposition at 57 Hz, ~14-15% for average frequency, and ~11% for CWT spectral decomposition at 81 Hz. The banding seems to come from the 3.2% difference in the cosine of instantaneous phase attribute contribution. The undesirable rock properties are associated with neurons 18 and 20. These two neurons only appear at well locations associated with poor porosity and permeability conditions. These two neurons are dominated by two attributes. Neuron 18 has a 51.2% contribution from CWT spectral decomposition at 29 Hz and a 30.5% contribution from average frequency. Neuron 20 has a 44.5% contribution from average frequency and a 39.3% contribution from CWT spectral decomposition at 29 Hz.

Table 5 numerically summarizes the attribute contributions for each neuron. Essentially, areas of high permeability and porosity are found where CWT spectral decomposition at 81 Hz, average frequency, and CWT spectral decomposition at 29 Hz are the highest contributing attributes. Areas that have high porosity, but widely varying permeability, were found to be characterized by two sets of attributes: 1) CWT spectral decomposition at 29 Hz, average frequency, and CWT spectral decomposition at 57 Hz. 2) CWT spectral decomposition at 29 Hz, CWT spectral decomposition at 57 Hz, average frequency, CWT spectral decomposition at 81 Hz. Finally, areas of poor porosity and permeability were characterized by attribute combinations dominated by average frequency CWT spectral decomposition at 29 Hz.

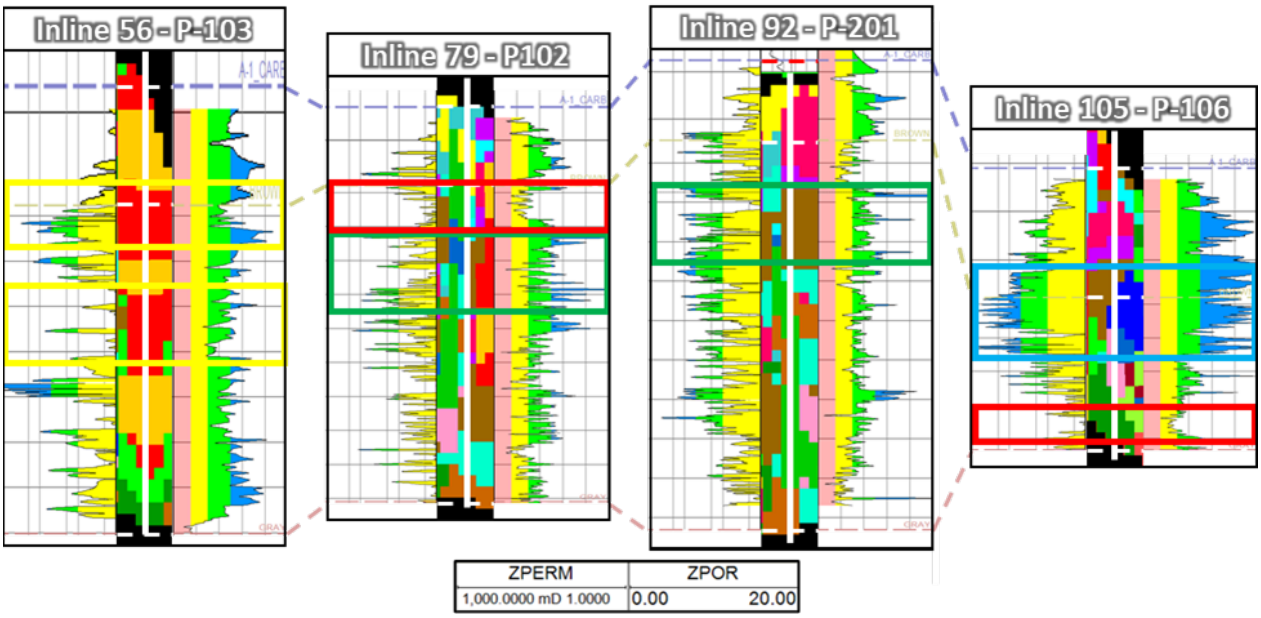


Figure 19: Qualitative well/SOM correlation. Porosity (right log) and permeability (left log) logs were stretched and squeezed between SOMs at inlines that the wells are located. The blue box on well P-106 indicates an area with great permeability and porosity. The red boxes on wells P-106 and P-102 indicate areas of poor permeability and poor to intermediate porosity. The green boxes on wells P-201 and P-102 are areas of widely varying permeability but good to great porosity. The yellow boxes on well P-103 show two areas. Both with good to great porosity but with opposite permeabilities.

Neuron	cos(inst. phase)	Average frequency	CWT spec decomp 29Hz	CWT spec decomp 57Hz	CWT spec decomp 81Hz
10	3.8%	15.1%	38.2%	31%	11.8%
18	6.4%	30.5%	51.2%	4%	7.9%
19	0%	29.9%	39.3%	24.3%	6.5%
20	0.6%	44.5%	39.5%	5.2%	10.2%
23	0.2%	35.3%	22.4%	1.5%	40.6%
25	0.6%	13.8%	38%	35.8%	11.9%

Table 5: List of relevant neurons along the four wells in Figure 19.

Conclusions

There are two main conclusions to this investigation. The first is that confining the data closer to the reef boundary allowed for the SOMs to create more variability in the areas of interest. Figure 17 showed this with the two structural SOMs characterizing a similar mounded feature. The more confined SOM (right image) required more neurons to fully characterize that feature while the less confined SOM (left image) required less. Figure 18 also showed this concept with the different zones within the reef being characterized by more neurons in the more confined SOM. For this case, we want to have more classifications within the reef because we are looking for smaller changes in the rock properties. Removing the overlying A-2 Carbonate and the underlying Clinton Formation from the input data to the SOM, which are outside of the reservoir and therefore not important for mapping, allowed for more of the internal variability within the reef to be captured by the neurons that were characterizing features external to the reef before.

The second is that there does seem to be a trend or relationship between porosity and permeability in the seismic/well data and the third SOM run. When comparing the well logs to the SOM results, areas where there is great permeability and great porosity present coincide with attribute blends with high percentages of CWT spectral decomposition at 81 Hz, average frequency, and CWT spectral decomposition at 29 Hz. The core profile for well P-106 associates this depth with a heavily karsted reservoir zone. Other attribute combinations were also found that were mainly affected by porosity and not so much by permeability. Areas of good to great porosity were associated with attribute blends of CWT spectral decomposition at 29 and 57 Hz in higher percentages and average frequency and CWT spectral decomposition at 81 Hz in lower, but still significant, percentages. The relationship between those four attributes and the porosity was discovered at well P-103 and stretched from the A-1 Carbonate down almost to the base of the bioherm layer. These two neurons exhibit a similar vertical extent in multiple locations throughout the reef, creating pillars of desirable porosity. Finally, areas with a wider range of porosity, from intermediate to great, had attribute blends in decreasing percentages of CWT spectral decomposition 29, average frequency, and CWT spectral decomposition at 57

Hz. These locations were near the upper section of the bioherm. Areas with attribute blends dominated with only CWT spectral decomposition at 29 Hz and average frequency should be avoided as they were associated with areas of lower porosity and permeability.

Figure 20 illustrates a Puttygut reef model created by Garrett (2016) compared to the four best porosity and permeability case neurons from the final SOM run over Puttygut from this study. It is possible to make a qualitative comparison between the chosen neurons and the geology of the reef. The attributes associated with neuron 23 seem to correspond to areas where the reef talus is present. Neuron 19 corresponds to areas where the reef core is located. Neurons 10 and 25 correspond to areas where the reef core and bioherm are located. Appendix C shows multiple inlines stepping through the reef. From those images we can see that the neurons are consistently located at approximately the same depths as the geologic features they represent. Figure 21 shows that same model from Garret (2016) populated with calculated porosity and permeability values for the reef model. The hotter colors on those models indicate areas of higher porosity and permeability. The hot colored areas also correlate well with the chosen neurons from the SOM created from this workflow.

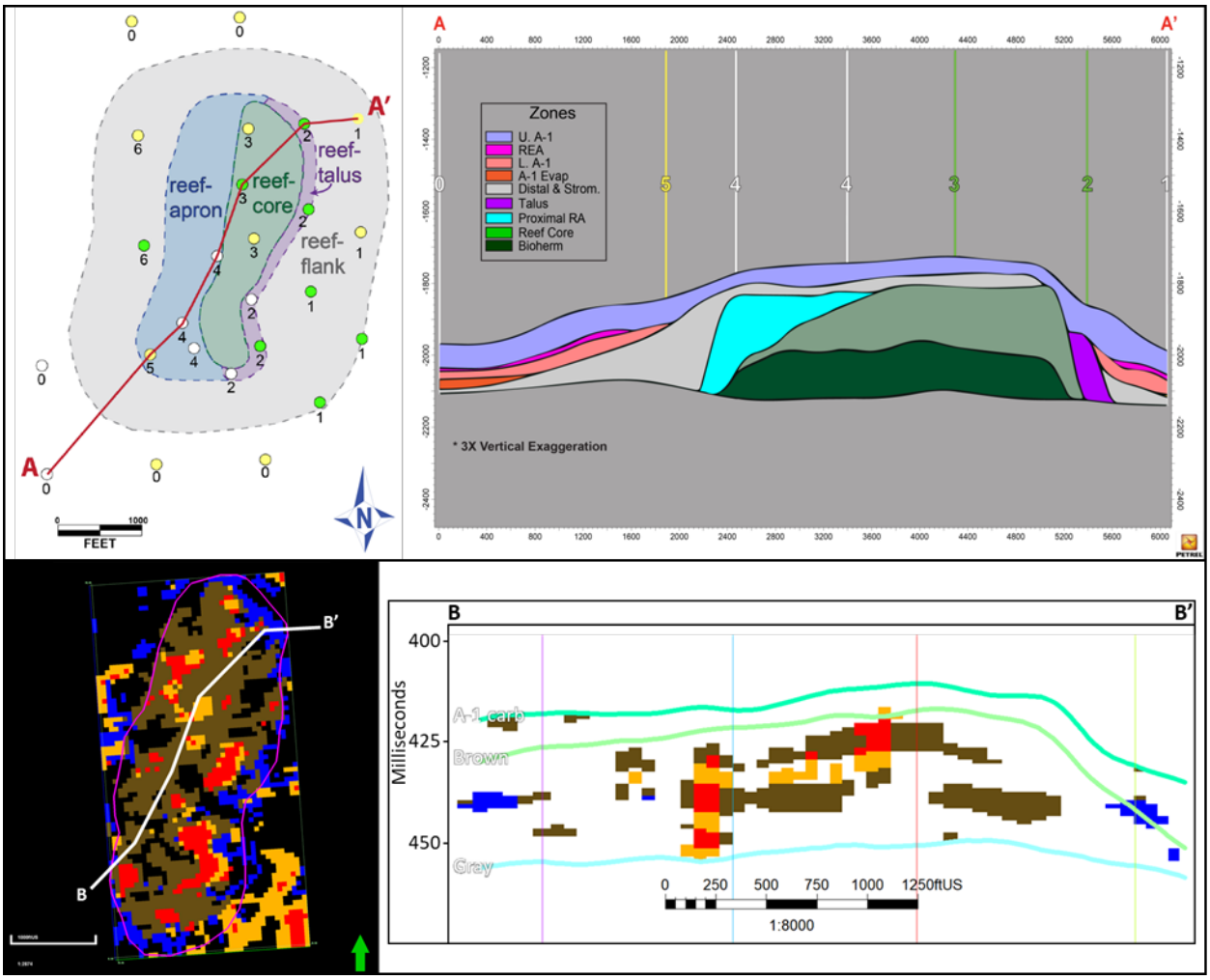


Figure 20: Relating the SOM neurons to the geology. Top image from Garrett (2016) shows a facies distribution on cross section line A-A' within the Puttygut reef and in 2D map view. Bottom shows the results from the Puttygut SOM in both map view and on cross section line B-B'. B-B' goes from "2" to "5" on the A-A' line. Black dashed lines show where the edges of the model meets the edge of the SOM.

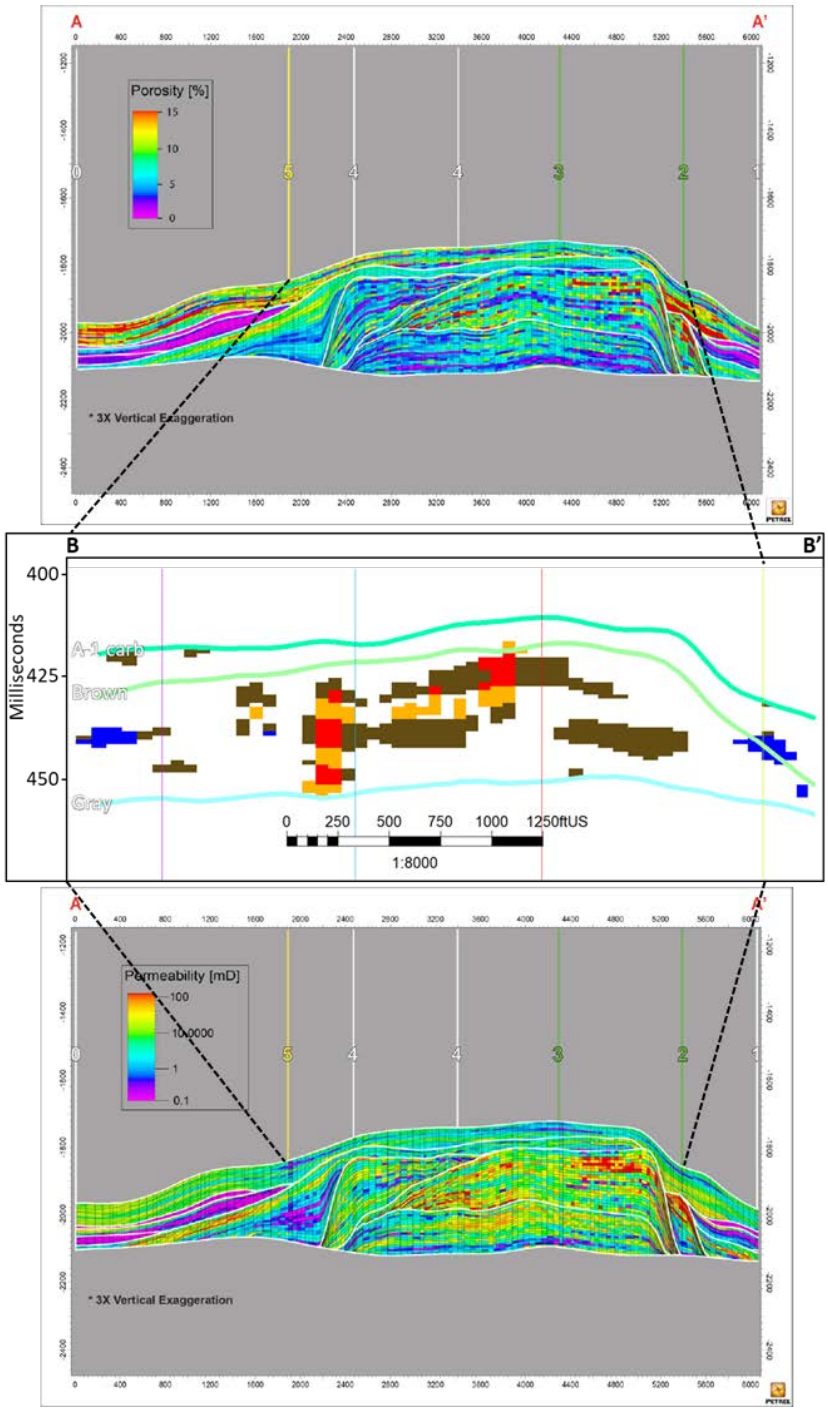


Figure 21: Top and bottom images from Garrett (2016) showing the calculated porosity (top image) and permeability (bottom image) for a reef model. Black dashed lines show where the edges of the model meet the edge of the SOM. Hotter colors indicate more porosity or permeability. When comparing those models to the SOM we see a good correlation between the two. The reef talus, reef core, and bioherm all have higher values of porosity and permeability when compared to the rest of the model. These are also the areas where the SOM neurons are focused.

Chapter 3: Applications of workflow to different areas

This chapter focuses on taking the workflow developed over the Puttygut reef and applying it to other nearby reef complexes to test the repeatability and robustness of the method. These reefs have less porosity and permeability control, so this is a qualitative study in the end. Figure 22 shows the locations of the reef complexes in relation to each other.

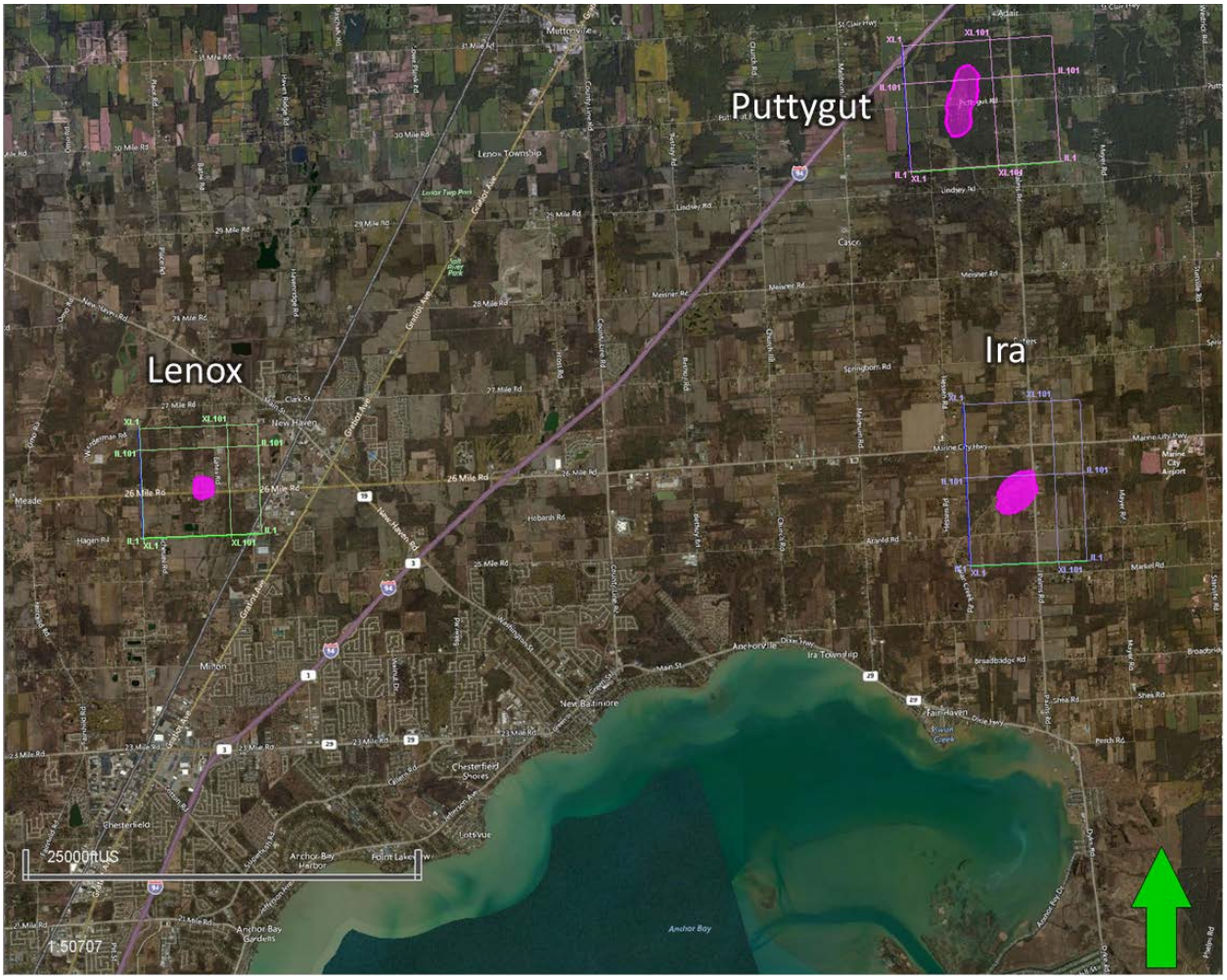


Figure 22: Locations of the two reef complexes used to test the developed workflow. Ira lies to the south and slightly east of Puttygut while Lenox lies to the southwest. Bing Maps Hybrid Imagery overlay is displaying satellite imagery.

The input data for the Ira and Lenox SOMs was the 3D PSTM amplitude volume and the following frequency attributes: average frequency, cosine of instantaneous phase, CWT spectral

decomposition at 29 Hz, 57 Hz, and 81 Hz. These attributes were calculated in AASPI. Horizons for each reef were also provided from the A-2 Carbonate down to the Clinton. Only the A-1 Carbonate, the Brown, and the Gray horizons were used for this exercise. These attributes and horizons were imported into Paradise and the SOMs were created. The boundaries for each SOM were slightly different but followed the same principles as with the third Puttygut SOM run. They were vertically confined between the A-1 Carbonate and Gray horizons and confined laterally by a set of inlines and crosslines.

Once each SOM was completed, the resultant neurons were filtered based on their attribute contribution percentages. If there were any blends like the successful blends developed from the Puttygut trials then they were kept, if not they were discarded. There were no exact matches with the attribute percentages in neurons calculated at Ira, but there were three results that were very close. Lenox was primarily composed of three neurons within the reef body, so the filtering and selection process was very short. Again, there were no exact matches at this reef either, but two of the three neurons that were found within the reef were very close. The three blends of attributes that were developed at Puttygut and that were looked for in the Ira and Lenox reefs were: 1) Areas of great permeability and porosity had a blend of CWT spectral decomposition at 81 Hz, average frequency, and CWT spectral decomposition at 29 Hz in order from highest contribution to lowest. 2) Areas with good to great porosity had a blend of CWT spectral decomposition at 29 and 57 Hz in higher percentages and average frequency and CWT spectral decomposition at 81 Hz in lower, but still significant, percentages. 3) Areas with porosity ranging from intermediate to great had a blend of CWT spectral decomposition 29, average frequency, and CWT spectral decomposition at 57 Hz in order from highest contribution to lowest. A close proxy to each of these cases was found at the Ira reef while proxies to cases one and two were found at the Lenox reef. The attribute blends were surprisingly similar and can be seen compared on Table 8.

Ira 3D

Ira 3D is located to the south of Puttygut. The reef has an area of 100 acres and is approximately 190 feet tall with a capacity of 6.3 BCFG. The seismic data that were used as the

base for all the attribute and SOM analysis was the PSTM amplitude data shot in 2018. The inline and crossline spacing was 440 feet, the shot and receiver spacing was 110 feet, and bin size was 55 by 55 feet, and the sample rate was 1 millisecond. All the frequency-based attributes were calculated from the PSTM amplitude in AASPI and then imported into Paradise. These attributes are the cosine of the instantaneous phase, the average frequency, and the CWT spectral decomposition at 29 Hz, 57 HZ and 81 Hz. Figure 23 shows the survey and SOM boundary extent. The pink outline represents the reef extent. The blue box is a range of inlines from 58 to 106 and of crosslines from 33 to 81. Figure 24 shows the approximate reef location with all the wells label and the associated well flow rankings. Figure 25 is a VSD of Inline 82 which cut through the center of the reef. The given horizons are shown as well as the reef extent. The upper and lower limit for the SOM was the A-1 Carbonate and the Gray Formations, like Puttygut. After filtering through the results of the SOMs, three neurons were found that had attribute contribution percentages very similar to those found at Puttygut when looking for areas of varying permeability and porosity. Those neurons and their respective attribute percentages can be found at Table 6.

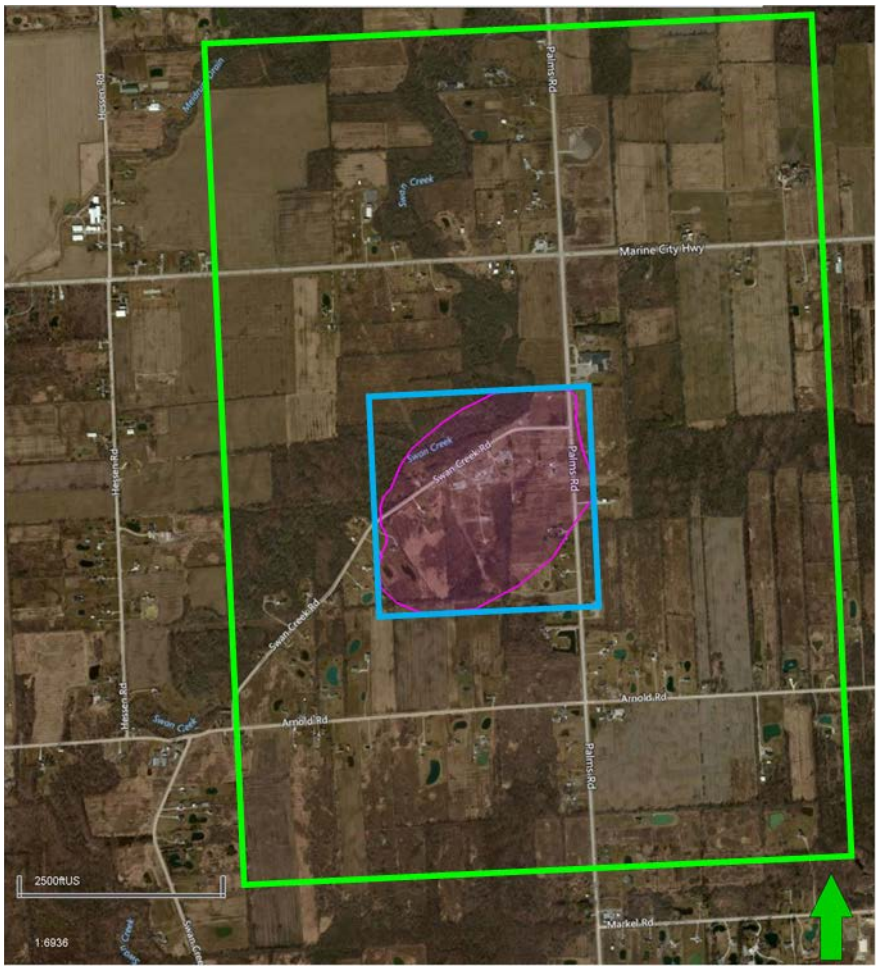


Figure 23: Ira reef in map view. Refer to Figure 22 for location or reef in relation to other reefs. The survey boundary is seen in the green box. The pink line represents the boundary of the reef. The blue box represents the boundary of the SOM survey. The inline range is from 58 to 106 and the crossline range is from 33 to 81. Bing Maps Hybrid Imagery overlay is displaying satellite imagery.

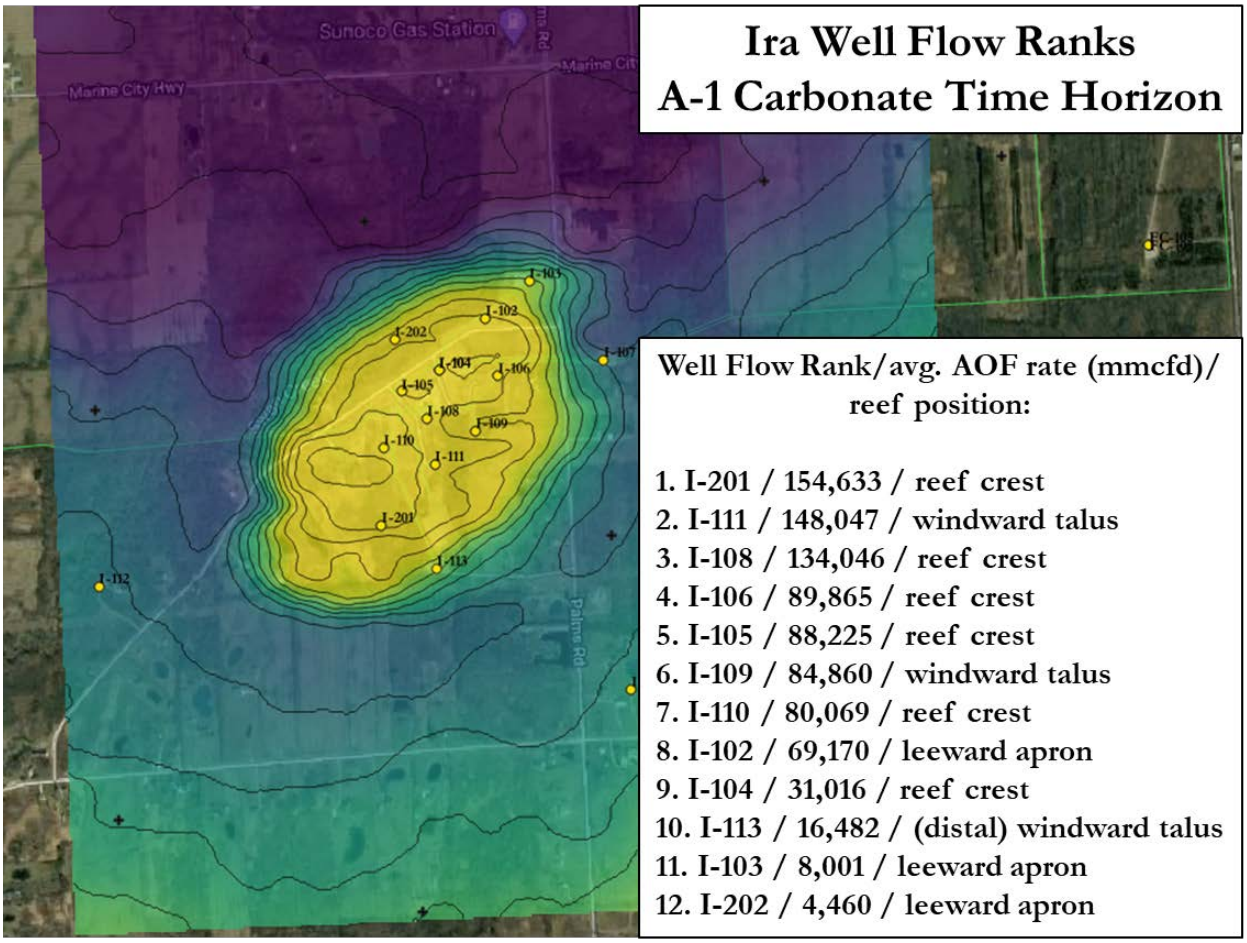


Figure 24:Ira reef approximate location with all wells labeled with well flow rankings. Map from M. Rine (personal comm., 2020).

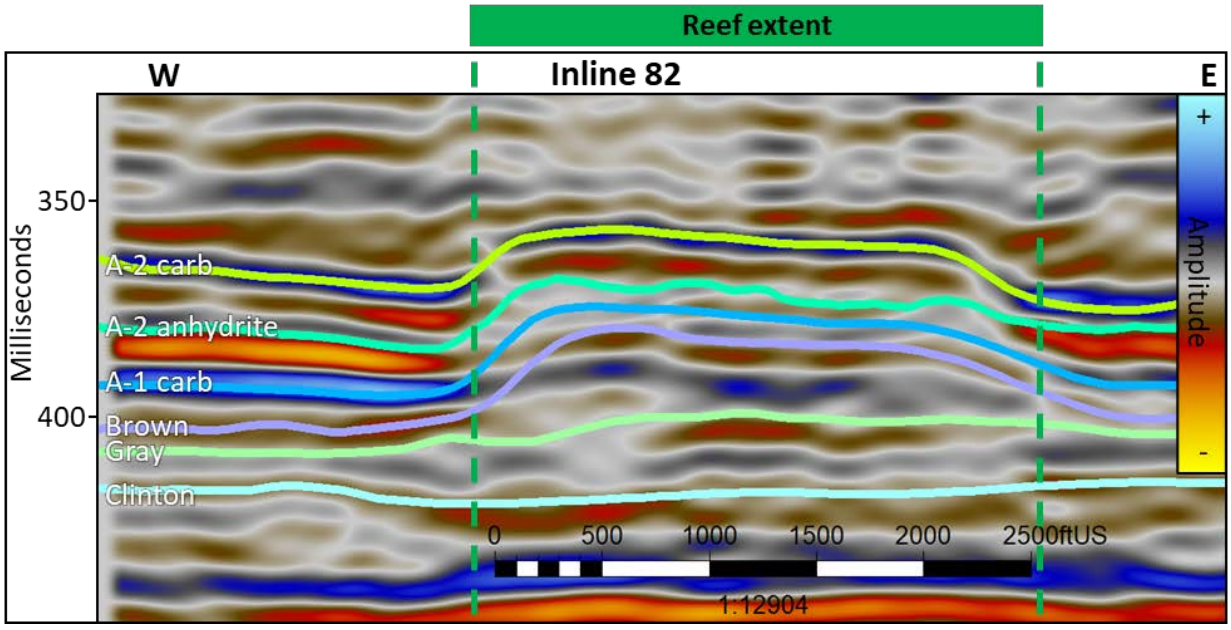


Figure 25: Ira 3D seismic survey: Inline 82 at 20 times vertical exaggeration through the center of the reef with the horizons on.

Neuron	cos(inst. phase)	Average frequency	CWT spec decomp 29Hz	CWT spec decomp 57Hz	CWT spec decomp 81Hz
6	0.3%	33.9%	17%	48.6%	0.2%
16	0.8%	23.4%	13.4%	36.2%	26.2%
23	0.5%	35.3%	34.9%	0.9%	28.4%

Table 6: The filtered neurons for the Ira frequency SOM. While the exact percentages and attribute ratios are not exactly the same, the presence of the dominant attributes in the blends is the same. Neuron 6 is like case three from Puttygut. Neuron 16 is like case two from Puttygut. Neuron 23 is like case one from Puttygut.

Frequency SOMs from Ira 3D

Figure 26 shows the results of the SOM in map view extracted onto the Brown horizon. The left image shows the SOM with all the neurons turned on while the right image only has the filtered neurons from Table 6 turned on. When comparing the neuron attribute blends of Ira to Puttygut, it is observed that neuron 6 from Ira is most like the third case at Puttygut where

there is a wider range of porosities from intermediate to great but changes in permeability are not captured. Neuron 16 is most like case two from Puttygut where there are areas of good to great porosity, but again changes in permeability is not well captured. Finally, neuron 23 is most like case one at Puttygut where there are areas of great permeability and porosity present. When looking from above, there is some variability on the horizon surface, but when only the filter neurons are activated there is a separation that can be seen that breaks the reef into smaller clusters with higher porosity and permeability. Figure 27 shows this in vertical section. The top left image is Inline 82 through the center of the reef and the top right image is Crossline 58, both have all the neurons turned on. The images directly below them have only the filtered neurons turned on. Neuron 6 had a similar attribute contribution percentage as case three from Puttygut but was not very abundant overall. There is a higher concentration of neurons 16 and 23 within the Ira reef. Neuron 16 is localized near the center of the reef while neuron 23 is seen more in larger clumps on the outskirts of the reef, as well as in a single location in the center of the reef, in between a section of neuron 16. The vertical white lines on the crossline image represent the locations of wells that penetrate the reef. Three of the five wells land within areas of higher porosity and permeability, with the other two wells to the north coming close to areas of high permeability and porosity. Those three wells, I-201, I-111, and I-108 also happened to be the three highest ranked wells in the field according to Figure 24. The other two wells in Figure 27 that did not penetrate the neurons but only came close were I-104 and I-202, which were ranked ninth and twelfth out of twelve in the field.

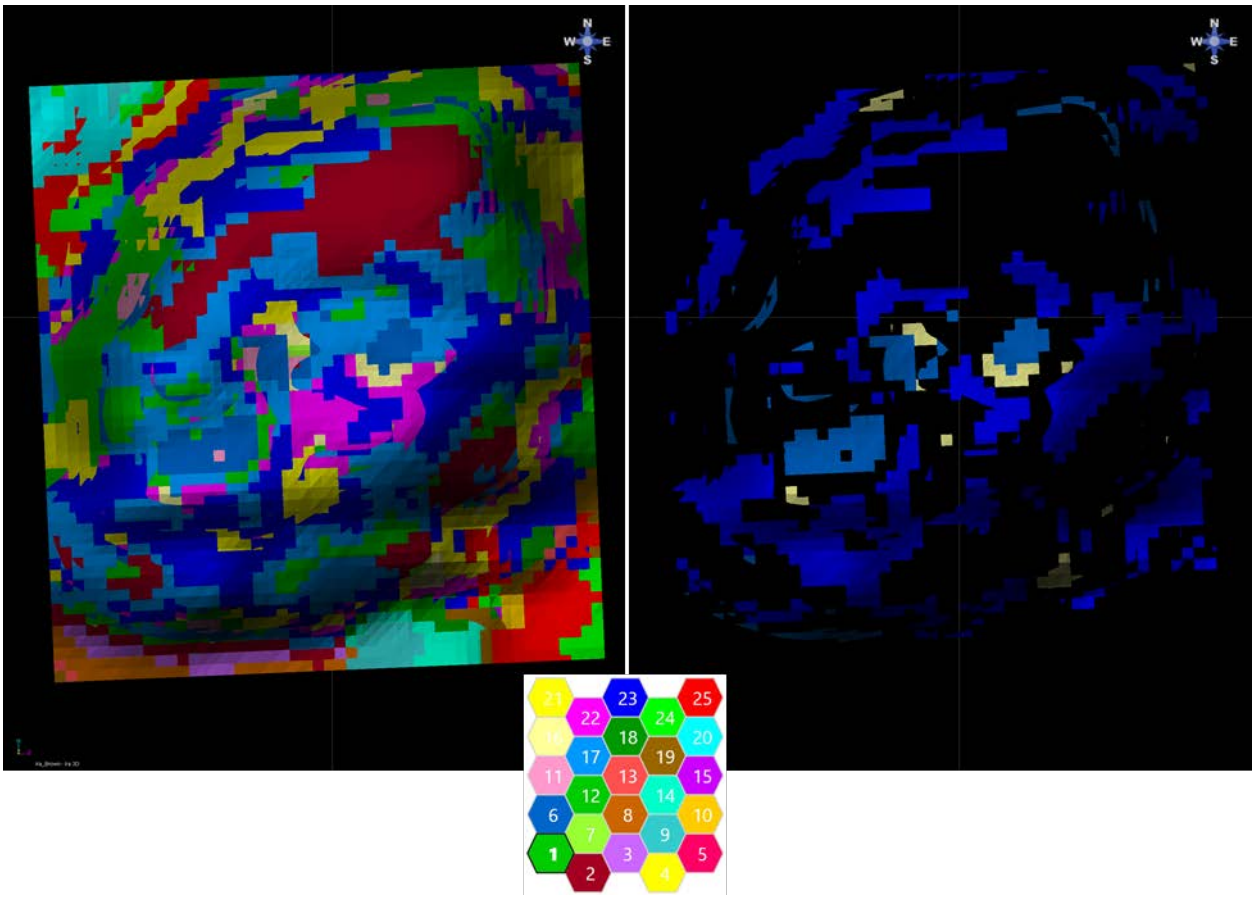


Figure 26: Ira frequency SOM on the Brown horizon. The left image is with all neurons active while the right image only has neurons 6, 16, and 23 turned on.

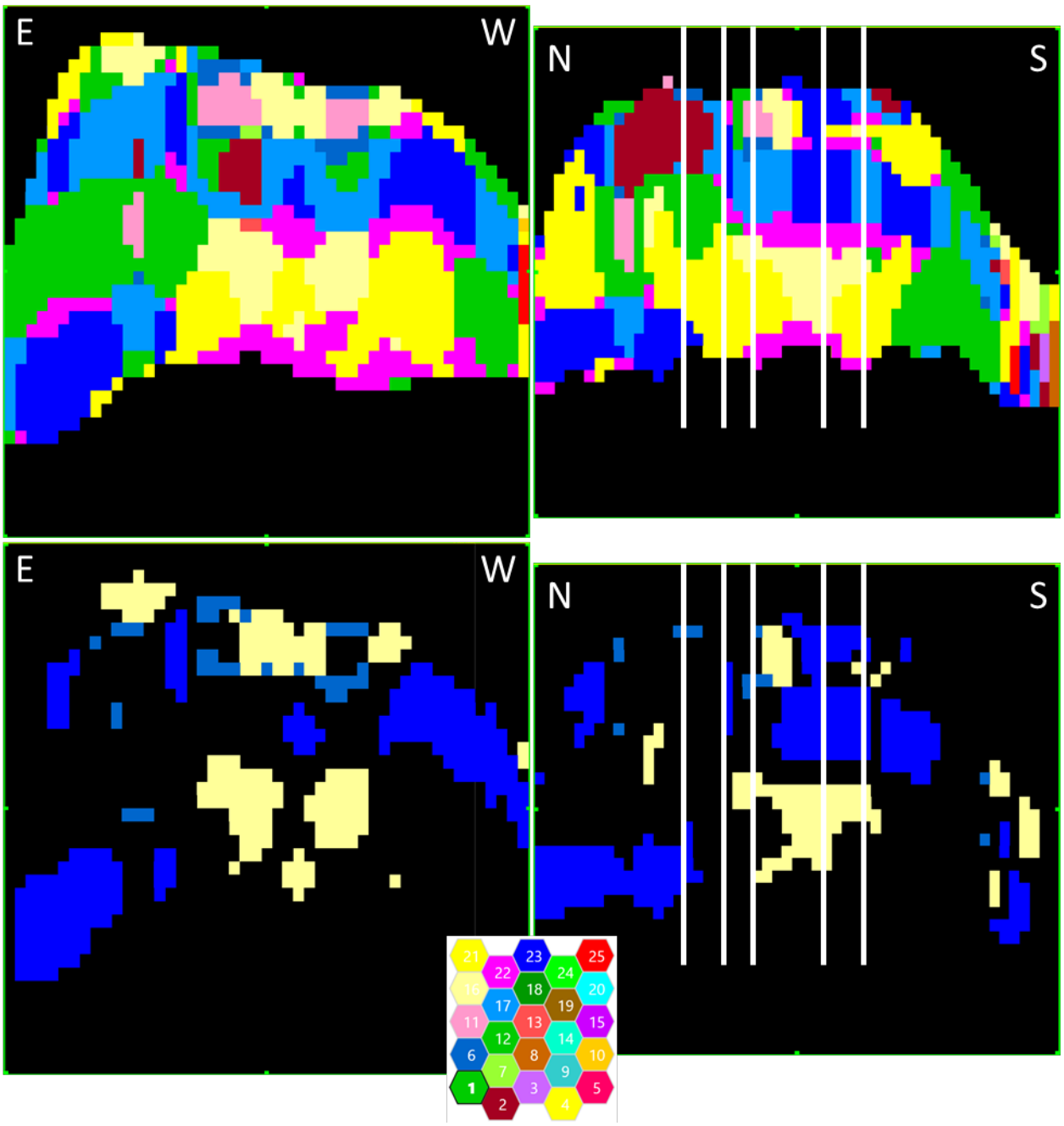


Figure 27: Ira frequency SOM in VSD. Top let is Inline 82 and top right is Crossline 58. The vertical white lines are five wells that are located on Crossline 58. From left to right they are I-104, I-202, I-201, I-111, I-108. Below each of those is the same inline and crossline with only neurons 6, 16, and 23 turned on.

Lenox 3D

Lenox 3D is located to the west and slightly south of Puttygut. The reef has an area of 35 acres and is approximately 260 feet tall with a capacity of 3.2 BCFG. The seismic data that were used as the base for all the attribute and SOM analysis was the PSTM amplitude data shot in 2018. The inline and crossline spacing was 660 feet, the shot and receiver spacing was 110 feet, and bin size was 55 by 55 feet, and the sample rate was 1 millisecond. All the frequency-based attributes were calculated from the PSTM amplitude in AASPI and then imported into Paradise. These attributes are the cosine of the instantaneous phase, the average frequency, and the CWT spectral decomposition at 29 Hz, 57 HZ and 81 Hz. Figure 28 shows the survey and SOM boundary extent. The pink outline represents the reef extent. The blue box is a range of inlines from 43 to 68 and of crosslines from 60 to 84. Figure 29 shows the approximate reef location with all the wells label and the associated well flow rankings. Figure 30 is a VSD of Inline 56 which cuts through the center of the reef. The given horizons are show as well as the reef extent. The upper and lower limit for the SOM was the A-1 Carbonate and the Gray Formations, just like for Puttygut. The filtering process for the Lenox reef was much easier, as there were only three neurons that were within the reef body, one of which did not match any of the attribute trends or relationships from Puttygut. That left two that were relatively similar to the cases discovered at Puttygut. The neurons and their attribute contribution percentages can be seen in Table 7.

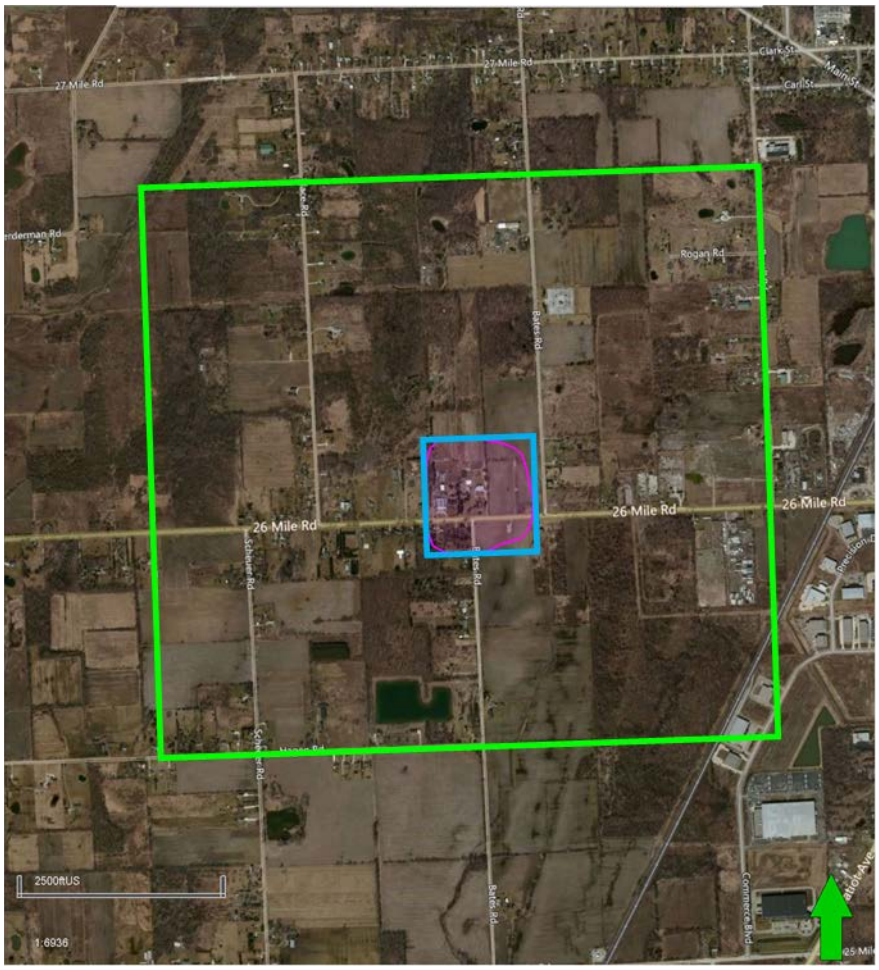


Figure 28: Lenox reef in map view. Refer to Figure 22 for location or reef in relation to other reefs. The survey boundary is seen in the green box. The pink line represents the boundary of the reef. The blue box represents the boundary of the SOM survey. The inline range is from 43 to 68 and the crossline range is from 60 to 84. Bing Maps Hybrid Imagery overlay is displaying satellite imagery.

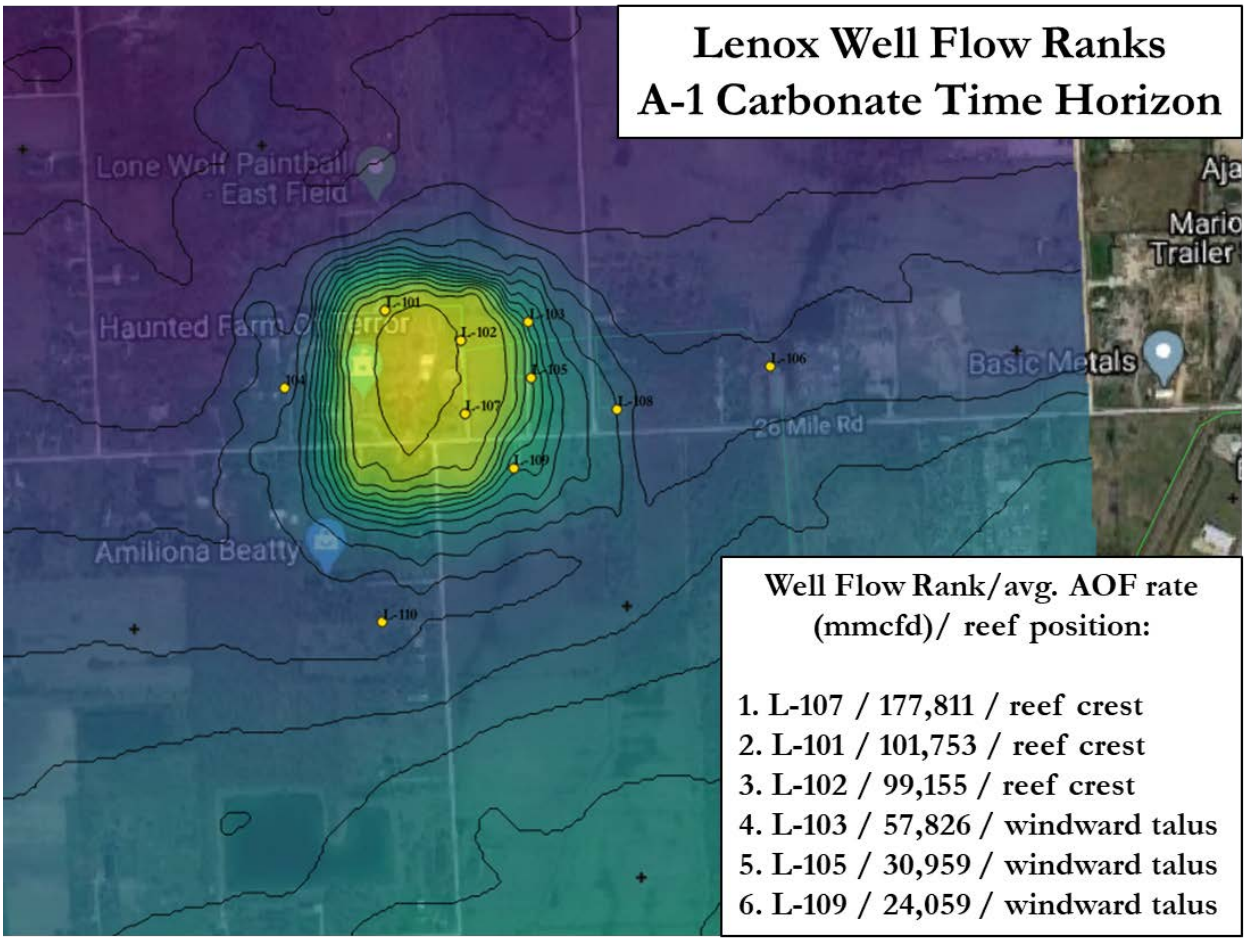


Figure 29: Lenox reef approximate location with all wells labeled with well flow rankings. Map from M. Rine (personal comm., 2020).

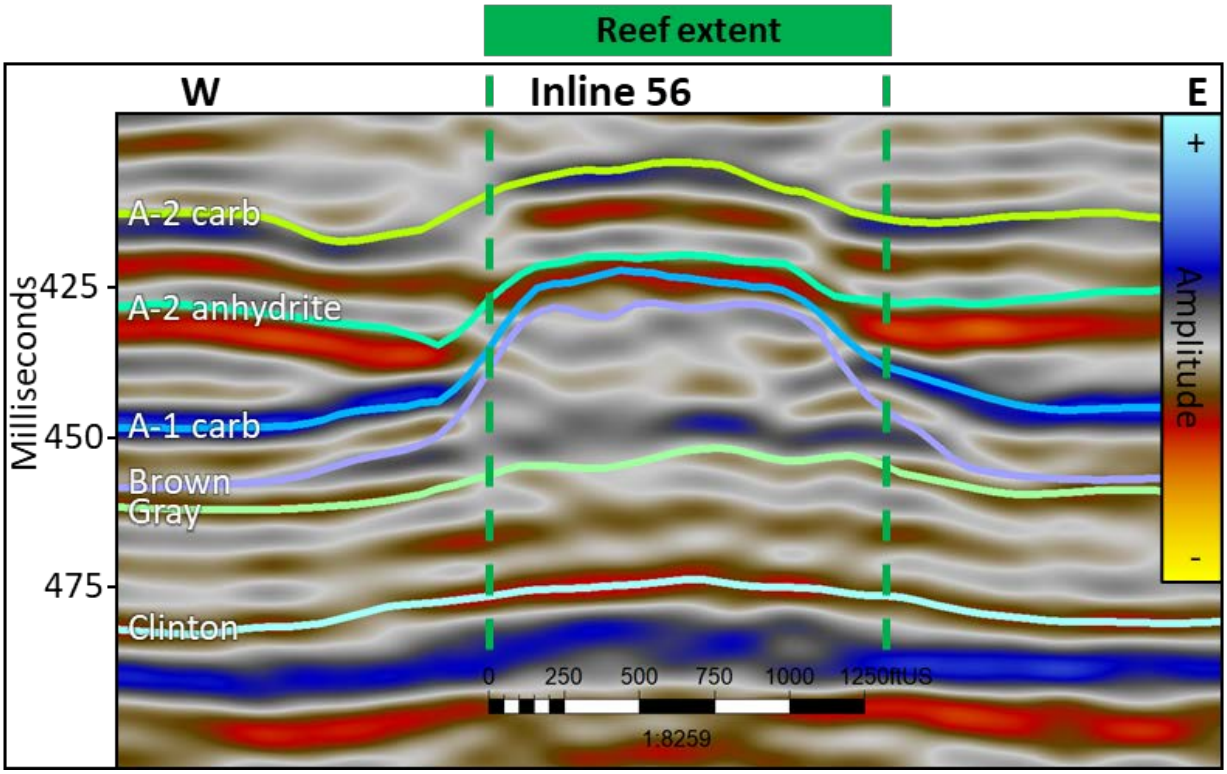


Figure 30: Lenox 3D seismic survey: Inline 56 at 20 times vertical exaggeration through the center of the reef with the horizons on.

Neuron	cos(inst. phase)	Average frequency	CWT spec decomp 29Hz	CWT spec decomp 57Hz	CWT spec decomp 81Hz
23	4.4	25.3	30	6.3	34.1
24	8.4	23.4	23.5	29.1	15.7

Table 7: The filtered neurons for the Lenox frequency SOM. While the exact percentages and attribute ratios are not exactly the same, the presence of the dominant attributes in the blends is the same. Neuron 23 is like case one from Puttygut. Neuron 24 is like case two from Puttygut.

Frequency SOMs from Lenox 3D

Figure 31 shows the results of the SOM in map view extracted onto the Brown horizon. It is very clear that the dominant neurons for this reef are numbers 23 and 24. From above those are the only neurons that are present within the reef itself, with the remaining neurons

composing the outline and boundary of the reef. Comparing the neuron attribute blends of Lenox to Puttygut it can be seen that: Neuron 23 from Lenox is most like case one at Puttygut where there are areas of great permeability and porosity present. Neuron 24 at Lenox is most like case two from Puttygut where there are areas of good to great porosity, but changes in permeability are not well captured. Figure 32 shows the frequency SOM in vertical sectionfis very clear that neuron 24 is most of the reef interior while neuron 23 makes up more of the reef boundary. There is some slight intrusion of another neuron, number 9, in the reef core, but its attribute contribution percentages did not closely resemble anything from the three Puttygut cases, so it was excluded from further analysis.

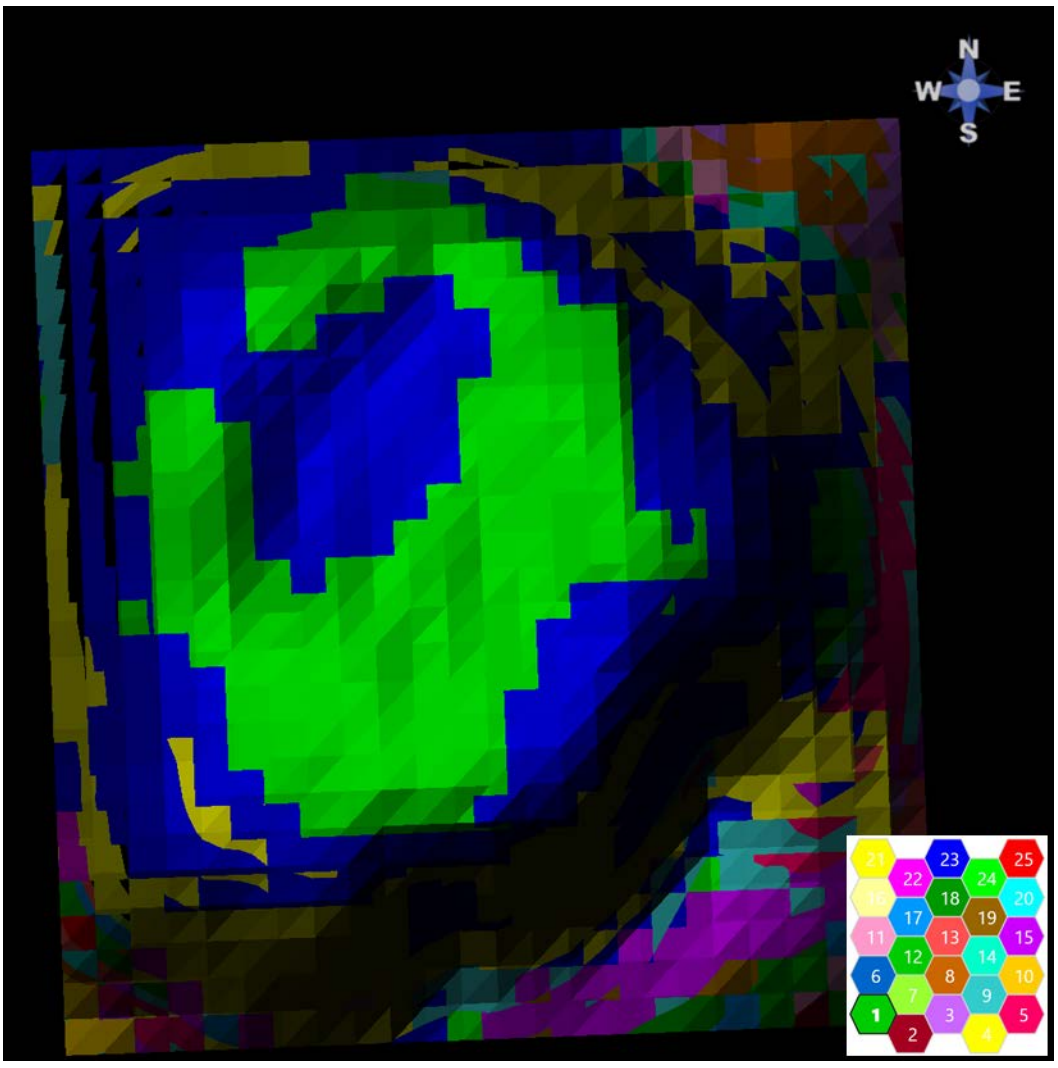


Figure 31: Lenox frequency SOM on the Brown horizon. The dominant neurons for the reef can clearly be seen as neurons 23 and 24.

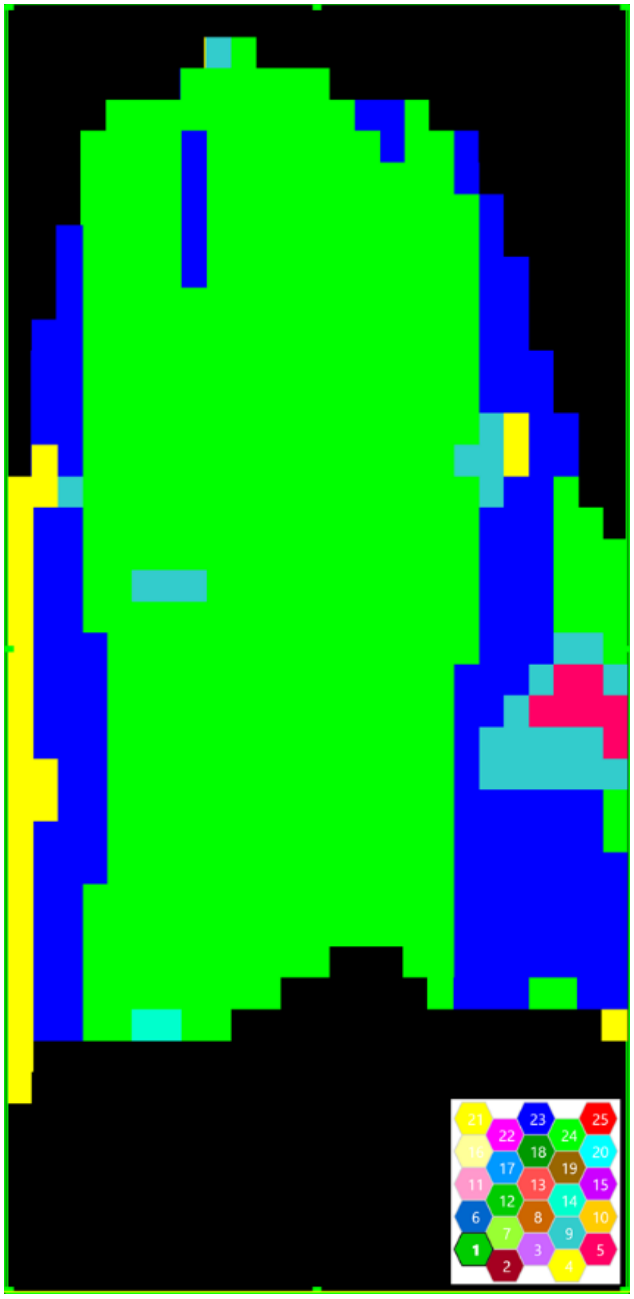


Figure 32: Lenox frequency SOM in VSD through the center of the reef at Inline 56. There is a clear dominance of neuron 24 in the reef core at this inline with neuron 23 making up more of the outer reef.

Chapter 4: Conclusions and future work

Overall, the presence of certain attribute contribution percentages was consistent among the three reefs in this study. Table 8 shows the three desirable cases that were developed at Puttygut with the percentage contribution from each attribute that composed the neurons at each reef location. Attribute contribution percentages are highlight based on their ranking for each neuron. Blue indicates the number one contributor, followed but green, then yellow, and finally orange where applicable. There is no case where every ranking is exactly honored when looking for similarities at different reefs, however, there is most definitely a consistent trend/relationship when looking solely at the highest contributing attribute combinations. For the case of great porosity and permeability, CWT spectral decomposition at 81 Hz, average frequency, and CWT spectral decomposition at 29 Hz were always the highest contributors by a significant margin. In the second case where there is a range of good to great porosity but no noticeable effect on permeability, every attribute significantly contributes except for the cosine of the instantaneous phase. Finally, In the case where a range of intermediate to great porosities are found, CWT spectral decomposition at 29 Hz, average frequency, and CWT spectral decomposition at 57 Hz are found to be the most prevalent contributors. From the results shown, it seems that the workflow created at Puttygut was able to translate over Ira and Lenox well. The similar attribute blends being found at similar geological locations within each reef increase the confidence that this workflow was able to accurately distinguish areas of higher porosity and potentially permeability.

Case one from Puttygut: great porosity and permeability					
Reef	**cos(inst. phase)**	**Average frequency**	**CWT spec decomp 29Hz**	**CWT spec decomp 57Hz**	**CWT spec decomp 81Hz**
Puttygut	0.2%	35.3%	22.4%	1.5%	40.6%
Ira	0.5%	35.3%	34.9%	0.9%	28.4%
Lenox	4.4	25.3	30	6.3	34.1
Case two from Puttygut: good to great porosity with no permeability affect					
Reef	**cos(inst. phase)**	**Average frequency**	**CWT spec decomp 29Hz**	**CWT spec decomp 57Hz**	**CWT spec decomp 81Hz**
Puttygut	~0-4%	~14-15%	~38%	~31-35%	~11%
Ira	0.8%	23.4%	13.4%	36.2%	26.2%
Lenox	8.4	23.4	23.5	29.1	15.7
Case three from Puttygut: intermediate to great porosity with no permeability affect					
Reef	**cos(inst. phase)**	**Average frequency**	**CWT spec decomp 29Hz**	**CWT spec decomp 57Hz**	**CWT spec decomp 81Hz**
Puttygut	0%	29.9%	39.3%	24.3%	6.5%
Ira	0.3%	33.9%	17%	48.6%	0.2%

Table 8: Comparative table showing the attribute contribution percentages for each case at each different reef. The blue highlighting represents the attribute with the highest contribution for each SOM at each reef. The green represents the second most contributing attribute, the yellow represents the third highest contributor, and finally the orange represents the fourth highest contributor.

When looking for areas of great permeability and porosity, it is recommended to use this SOM set up and search for neurons where the attribute contributions are heavily skewed towards

CWT spectral decomposition at 81 Hz, average frequency, and CWT spectral decomposition at 29 Hz, ideally in this order from most to least contributing.

This workflow has only been tested in a localized area and would benefit from testing further away from the area it was created. The first logical location would be to move out to the other reefs in the Michigan Basin, where there is a significant amount of permeability and porosity data. If results like this study are found again, then it would be recommended to move to another basin and rerun these SOMs to see if basin locations have any sway on the results. As this workflow is tested further and further away from the reef it was created at, more and more variables begin to arise. Different parts of the basin could have been altered slightly different through time. Different basin in the world were created by varying geological processes under different physical conditions. These variations in the reefs and in the rocks cause variations in the rock properties that are present today. Attributes can detect these changes, sometimes wholly and sometimes partially, and when those attributes are input into a SOM then those changes become additive. After enough changes, a SOM could cluster together data points using attribute blends that in one area of the world indicate high permeability and porosity, but in another part of the world could indicate the opposite. Testing this workflow in different parts of the world is key for determining its repeatability and robustness.

Appendix A: Attributes on Puttygut pre-stack time migrated data

Extracted single attributes onto other expert picked horizons

In this appendix, the single structural and frequency based attributes that were previously shown on the Brown Formation are also extracted and shown on the remaining five formations, the A-2 Carbonate, the A-2 Anhydrite, and A-1 Carbonate, and Gray, and the Clinton. In addition to these horizons, two stratal slices were created between the Brown horizon and the Gray horizon. Stratal slice one (representative of the Mid-Reef) was created to be one fourth of the distance between the Brown horizon and the Gray horizon. Stratal slice two (representative of the bioherm) was created to be three fourths of the distance between the Brown horizon and the Gray horizon.

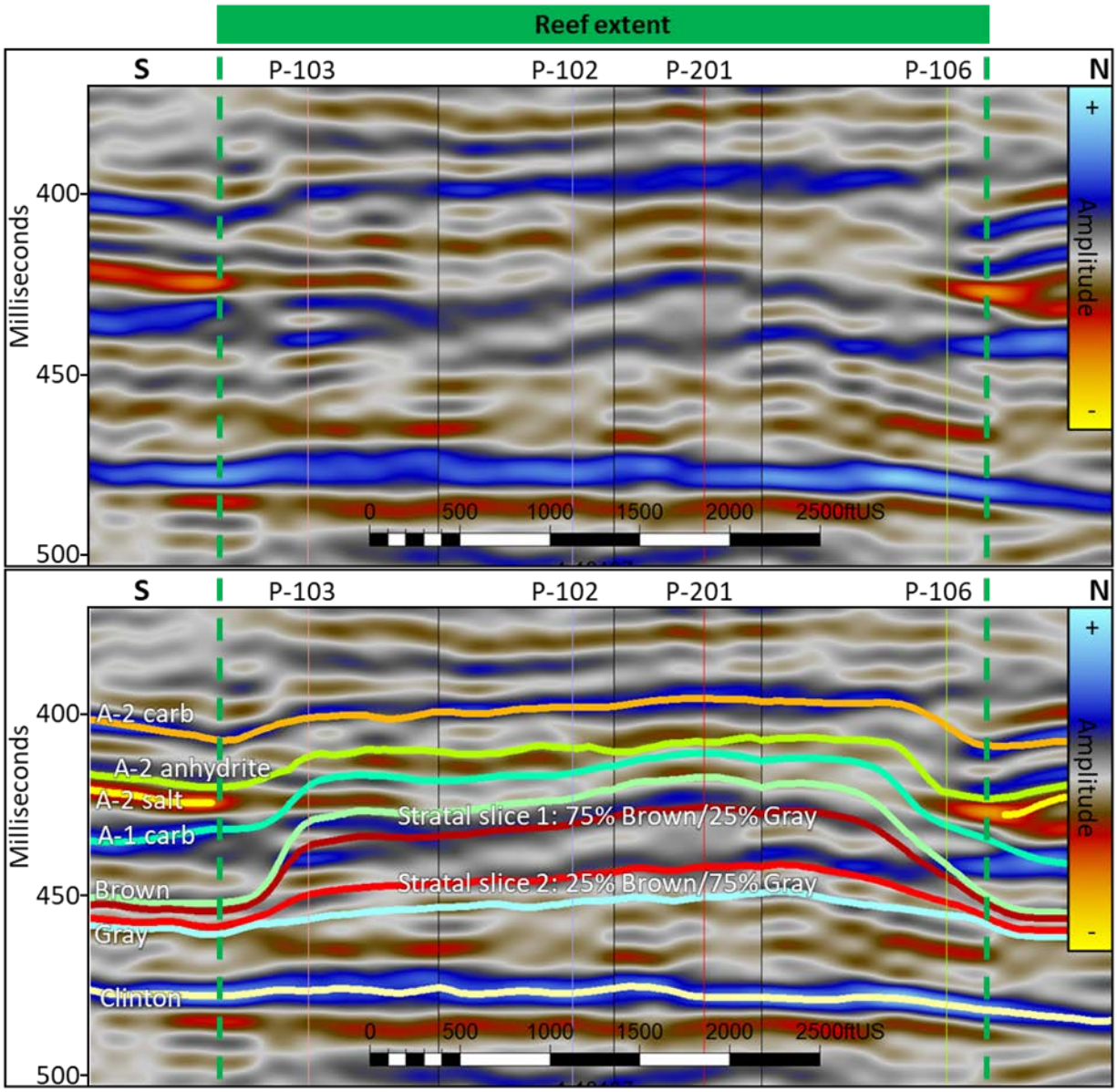


Figure 33: Cross section through the reef at 20 times vertical exaggeration showing the horizons that constitute the reef and the four key wells, P-103, P-102, P-201, and P-106. The path can be seen on the TWT map in Figure 2. The top image is the arbitrary line without interpretation, the bottom is with horizon interpretation.

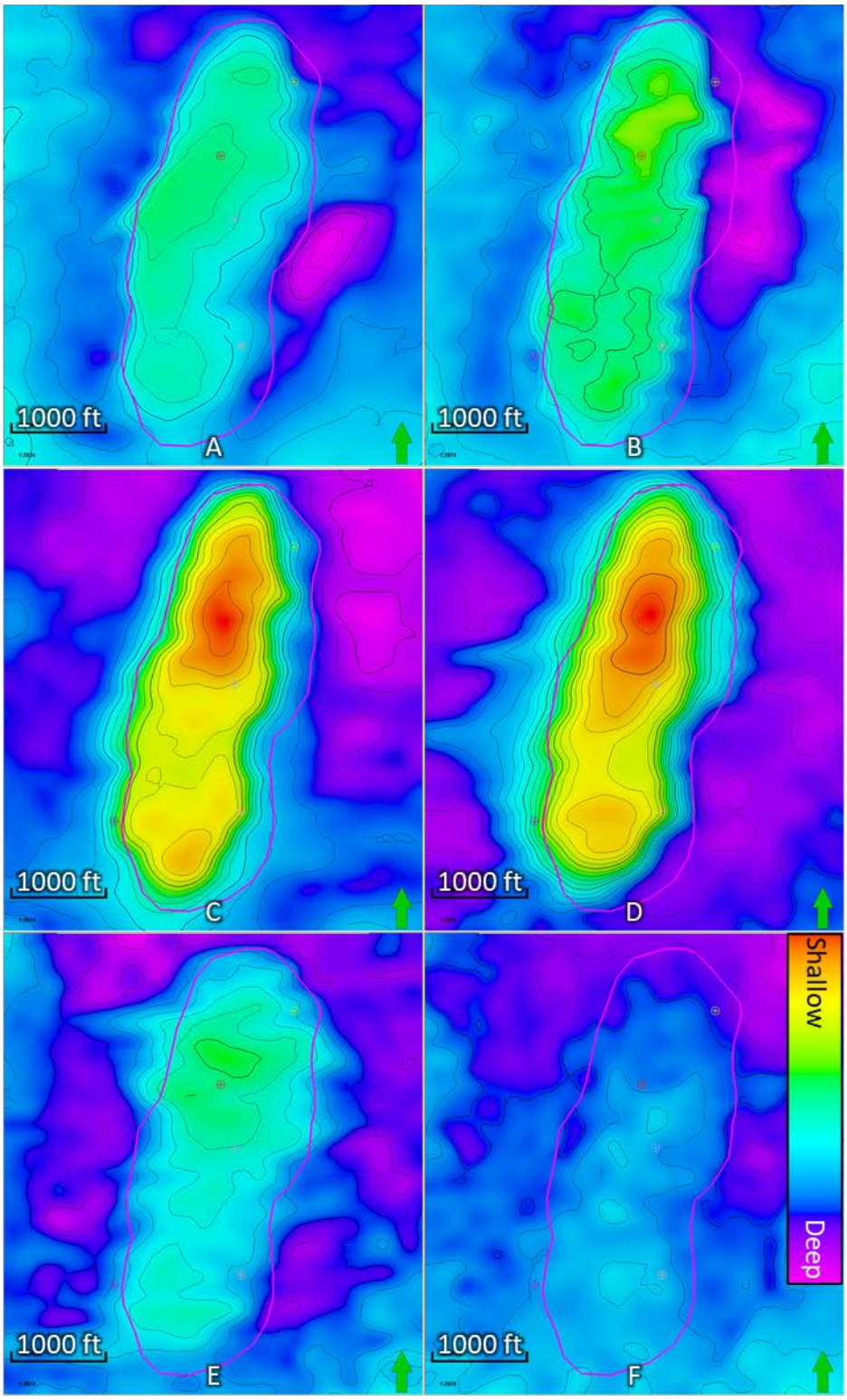


Figure 34: TWT maps for the expert picked horizons. Contour lines are 2 ms. A) A-2 Carbonate B) A-2 Anhydrite C) A-1 Carbonate D) Brown E) Gray F) Clinton

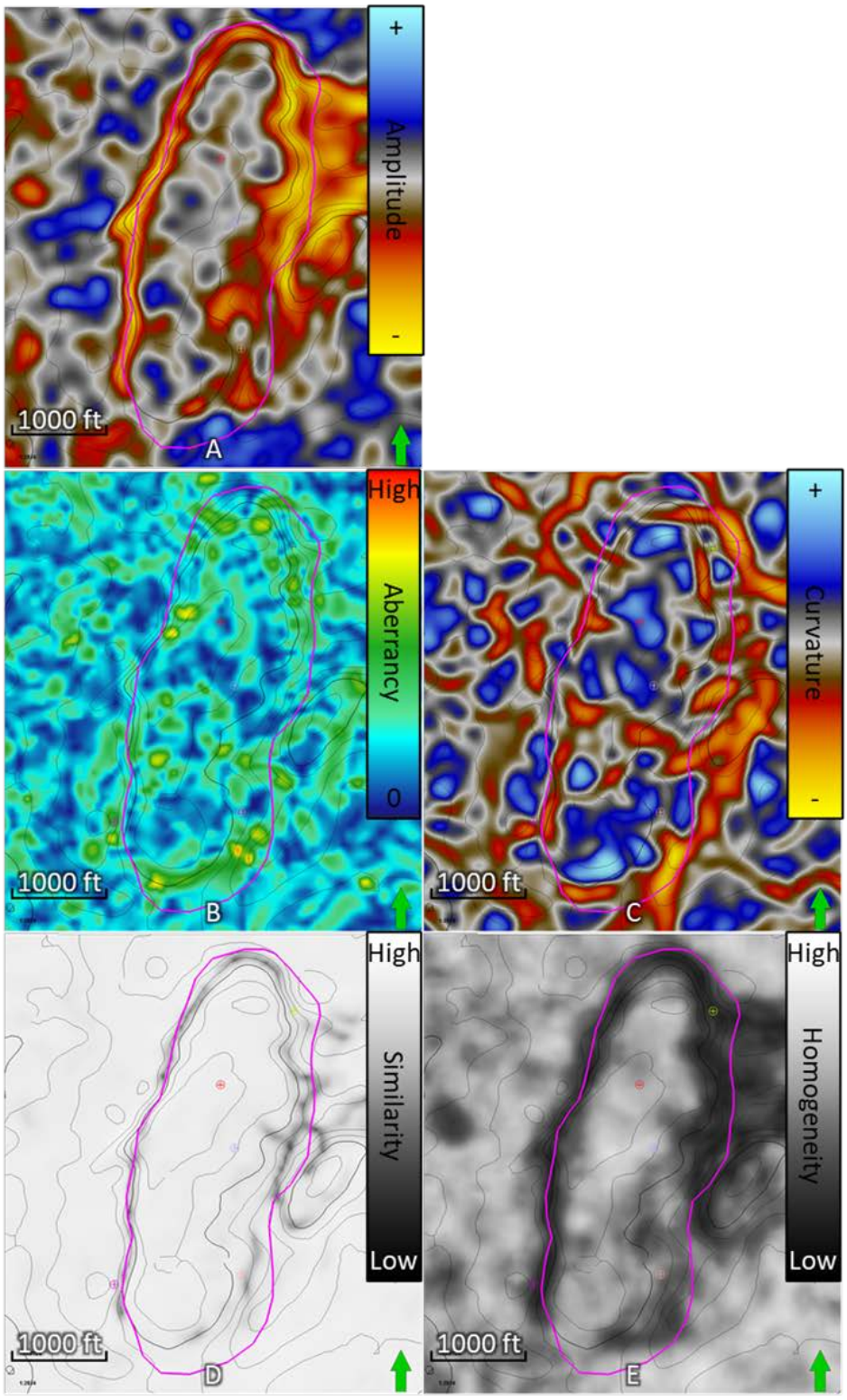


Figure 35: A-2 Carbonate horizon with extracted single structural attributes. A) PSTM amplitude B) Aberrancy C) Negative curvature D) ERS E) GLCM homogeneity Pink outline marks the outer reef boundary as defined by the A-1 Carbonate horizon.

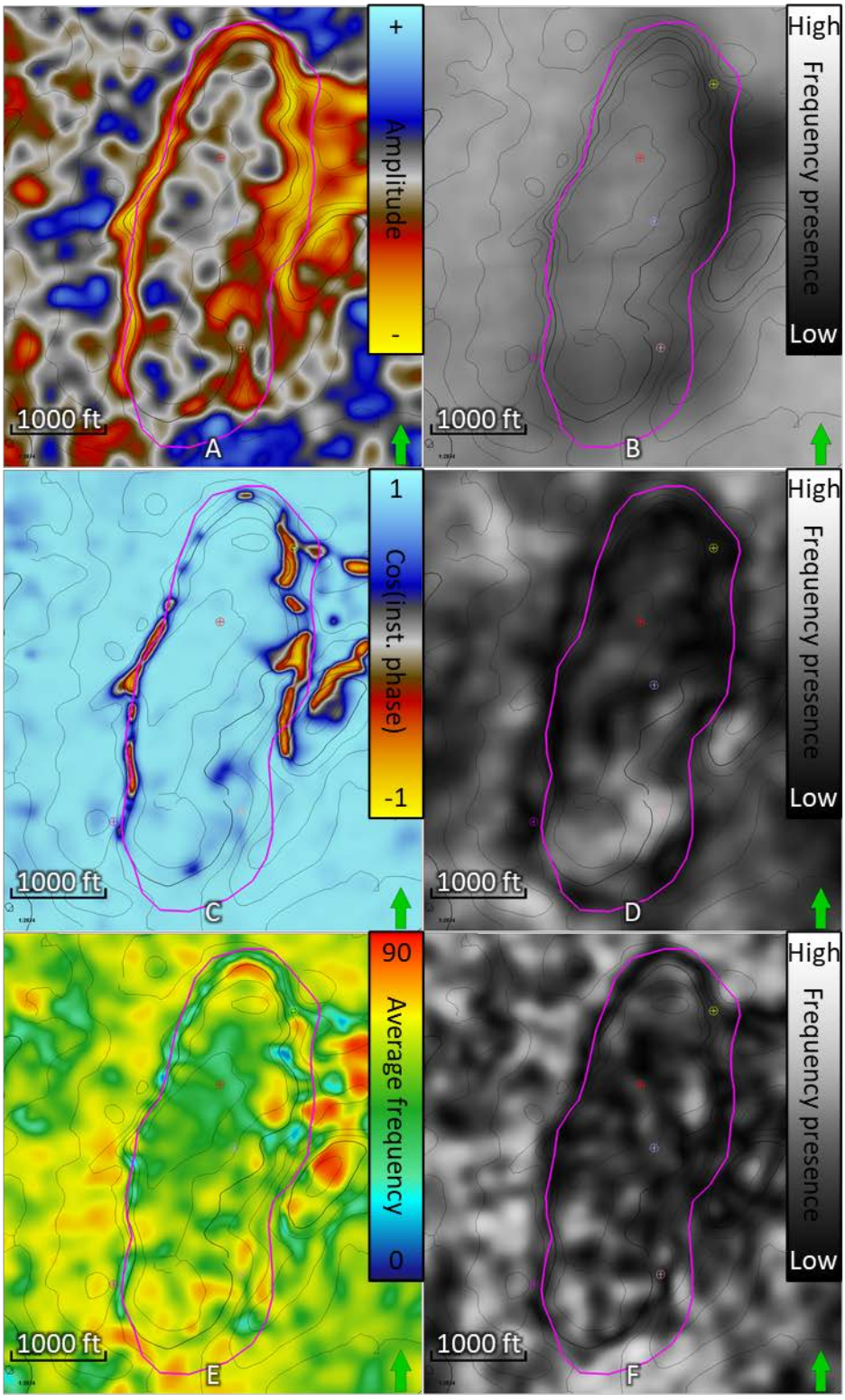


Figure 36: A-2 Carbonate horizon with extracted single frequency attributes. A) PSTM amplitude B) CWT 29 Hz C) Cosine of the instantaneous phase D) CWT 57 Hz E) Average frequency F) CWT 81 Hz Pink outline marks the outer reef boundary as defined by the A-1 Carbonate horizon.

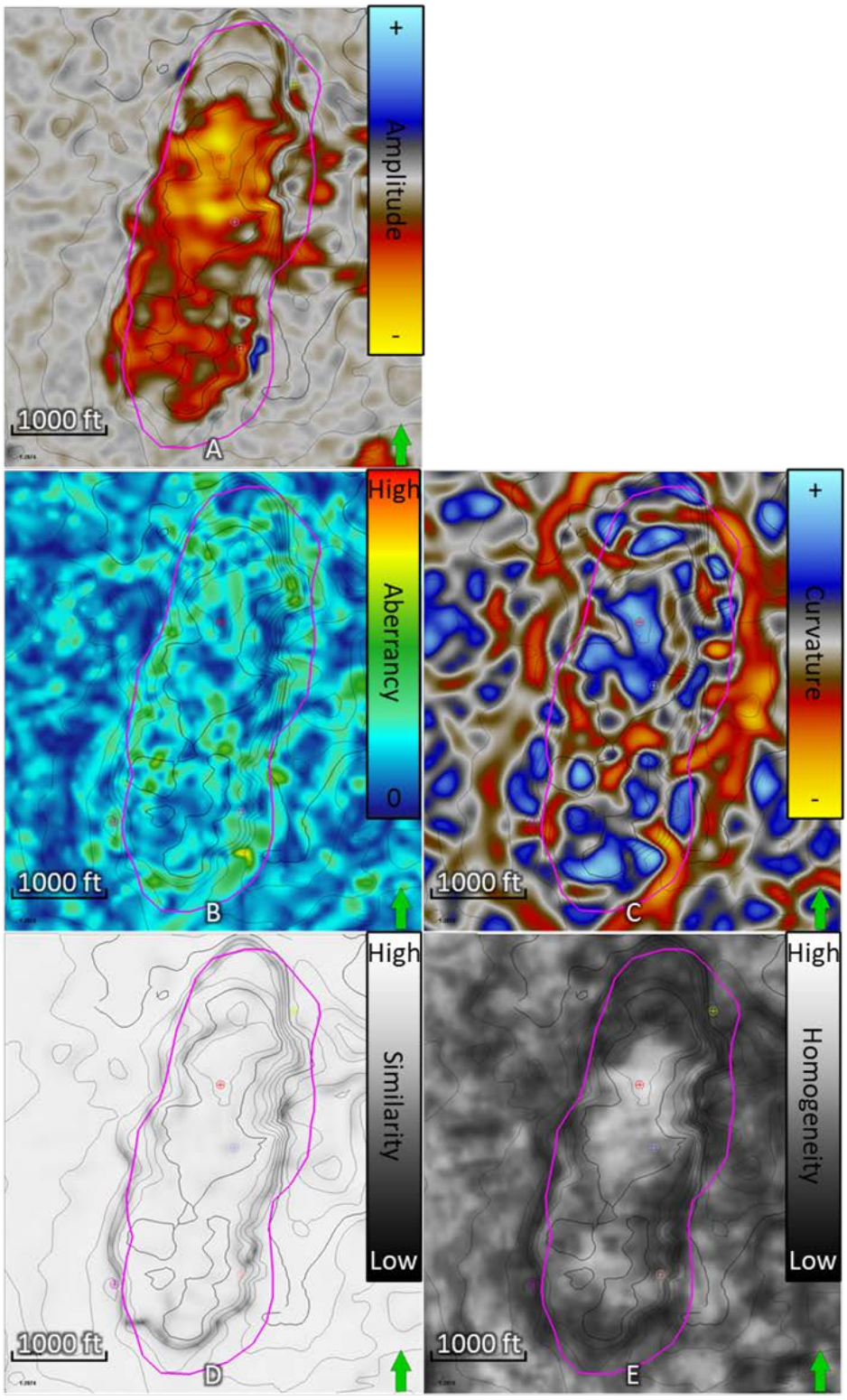


Figure 37: A-2 Anhydrite horizon with extracted single structural attributes. A) PSTM amplitude B) Aberrancy C) Negative curvature D) ERS E) GLCM homogeneity Pink outline marks the outer reef boundary as defined by the A-1 Carbonate horizon.

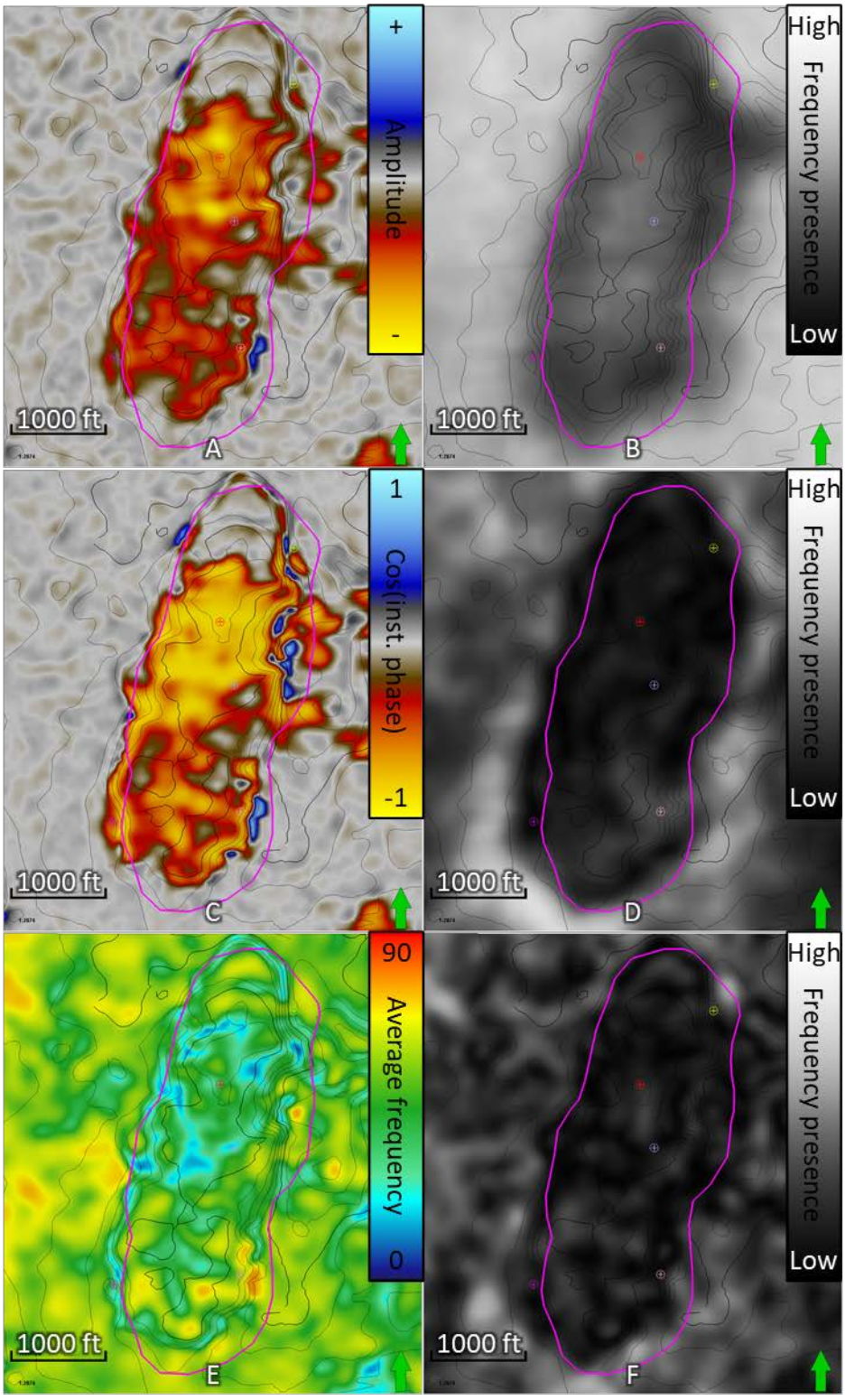


Figure 38: A-2 Anhydrite horizon with extracted single frequency attributes. A) PSTM amplitude B) CWT 29 Hz C) Cosine of the instantaneous phase D) CWT 57 Hz E) Average frequency F) CWT 81 Hz Pink outline marks the outer reef boundary as defined by the A-1 Carbonate horizon.

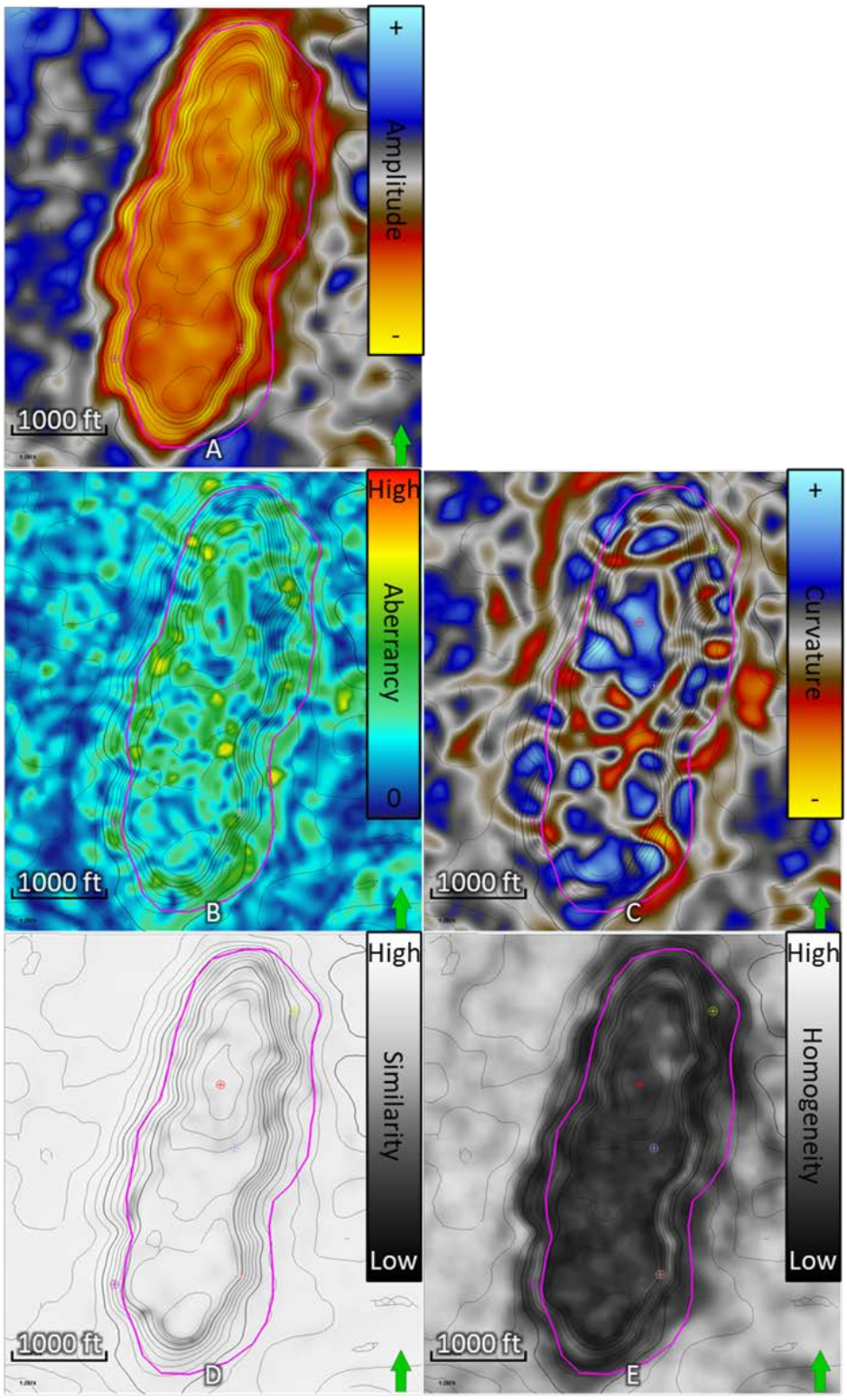


Figure 39: A-1 Carbonate horizon with extracted single structural attributes. A) PSTM amplitude B) Aberrancy C) Negative curvature D) ERS E) GLCM homogeneity Pink outline marks the outer reef boundary as defined by the A-1 Carbonate horizon.

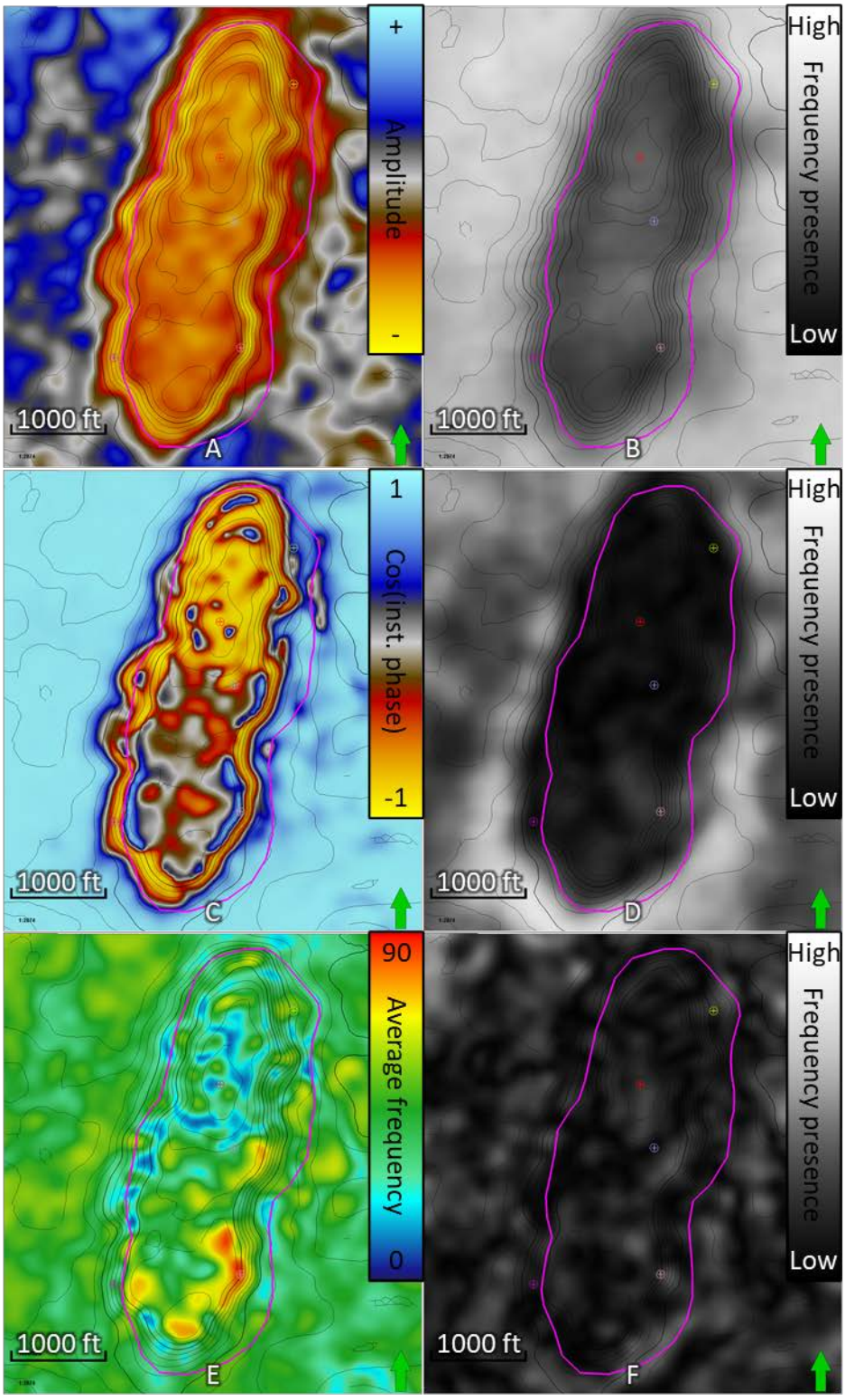


Figure 40: A-1 Carbonate horizon with extracted single frequency attributes. A) PSTM amplitude B) CWT 29 Hz C) Cosine of the instantaneous phase D) CWT 57 Hz E) Average frequency F) CWT 81 Hz Pink outline marks the outer reef boundary as defined by the A-1 Carbonate horizon.

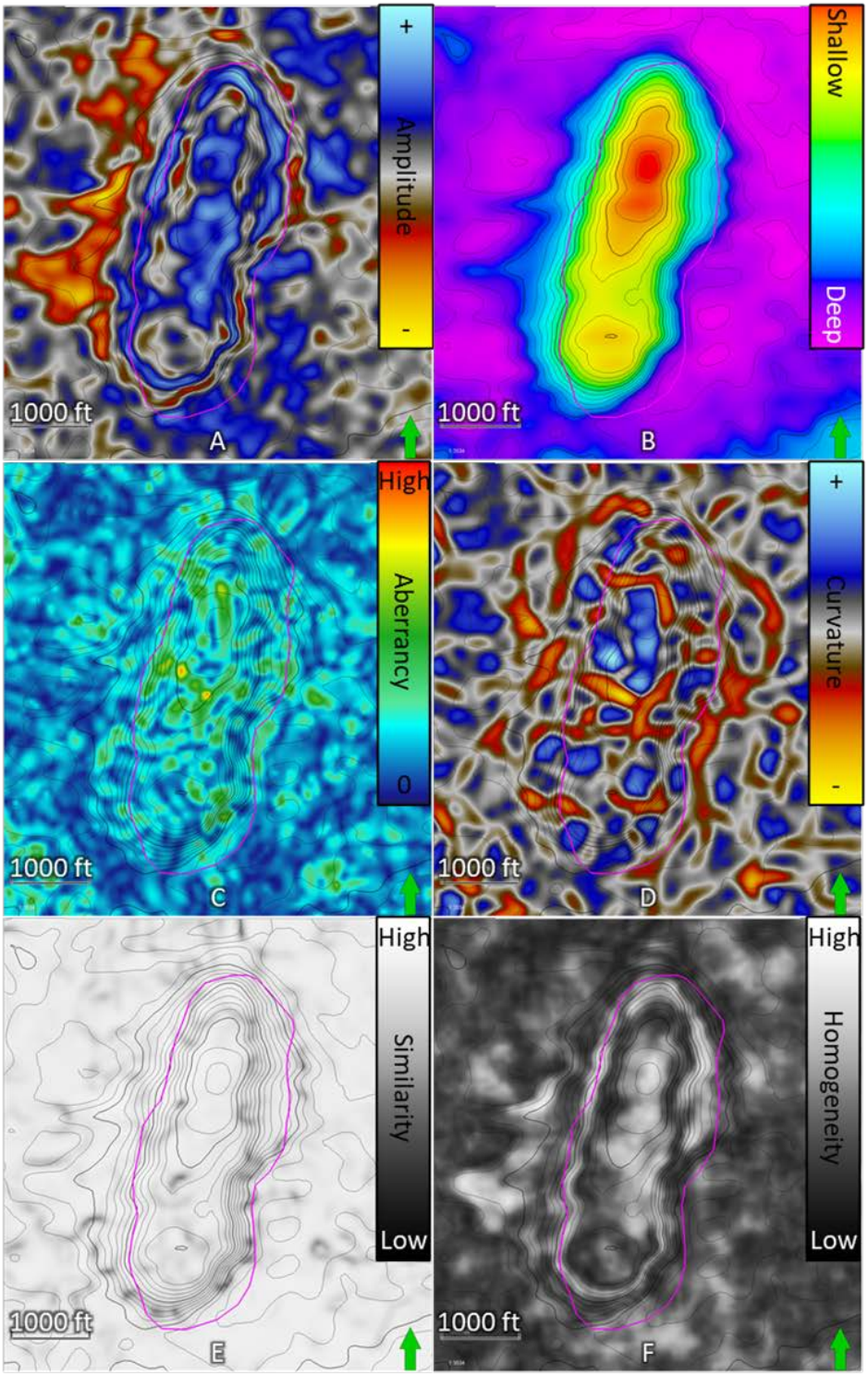


Figure 41: Stratal slice one (Mid-Reef) with extracted single structural attributes. A) PSTM amplitude B) TWT map C) Aberrancy D) Negative curvature E) ERS F) GLCM homogeneity Pink outline marks the outer reef boundary as defined by the A-1 Carbonate horizon.

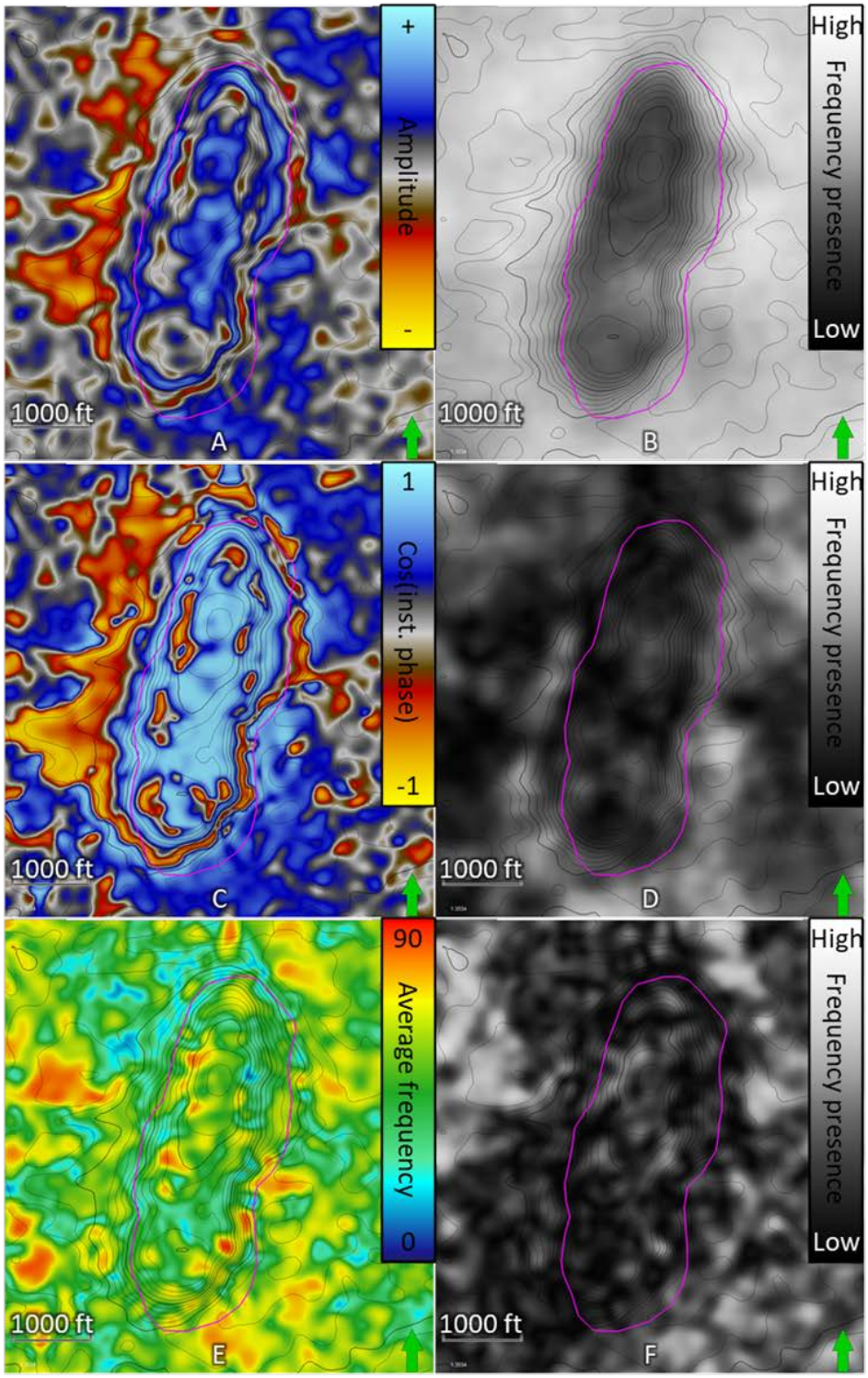


Figure 42: Stratal slice one (Mid-Reef) with extracted single frequency attributes. A) PSTM amplitude B) CWT 29 Hz C) Cosine of the instantaneous phase D) CWT 57 Hz E) Average frequency F) CWT 81 Hz Pink outline marks the outer reef boundary as defined by the A-1 Carbonate horizon.

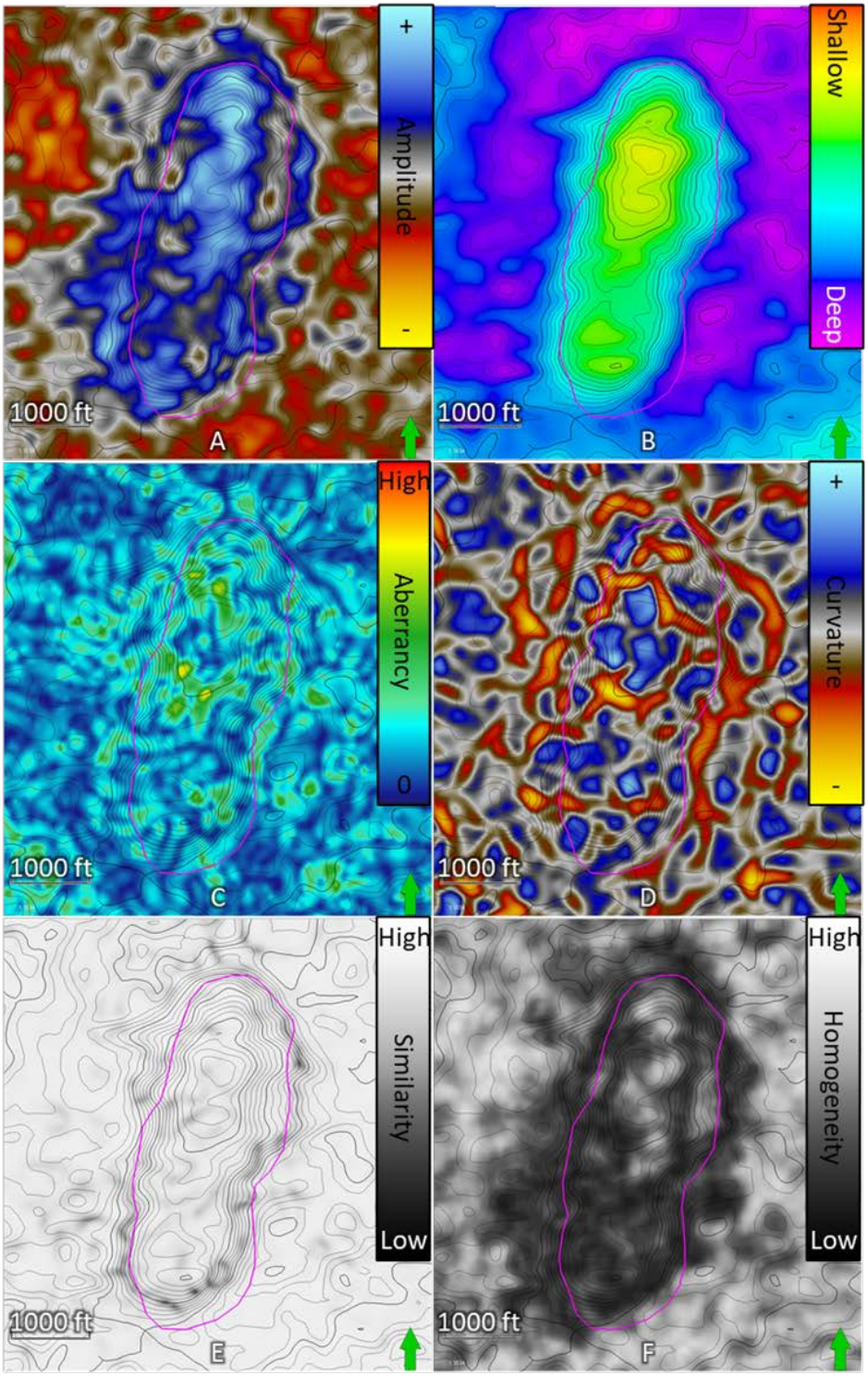


Figure 43: Stratal slice two (Bioherm) with extracted single structural attributes. A) PSTM amplitude B) TWT map C) Aberrancy D) Negative curvature E) ERS F) GLCM homogeneity Pink outline marks the outer reef boundary as defined by the A-1 Carbonate horizon.

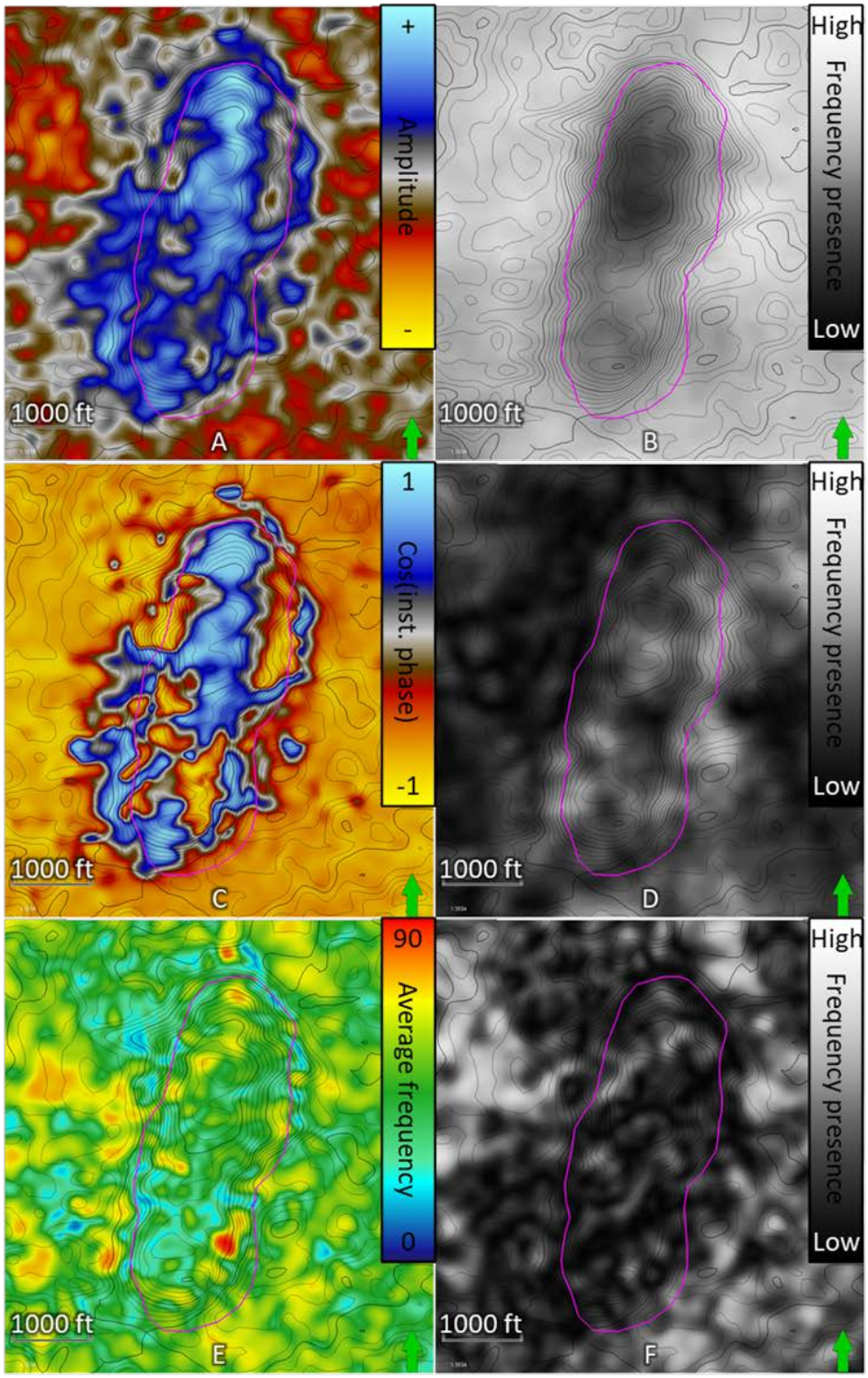


Figure 44: Stratal slice two (Bioherm) with extracted single frequency attributes. A) PSTM amplitude B) CWT 29 Hz C) Cosine of the instantaneous phase D) CWT 57 Hz E) Average frequency F) CWT 81 Hz Pink outline marks the outer reef boundary as defined by the A-1 Carbonate horizon.

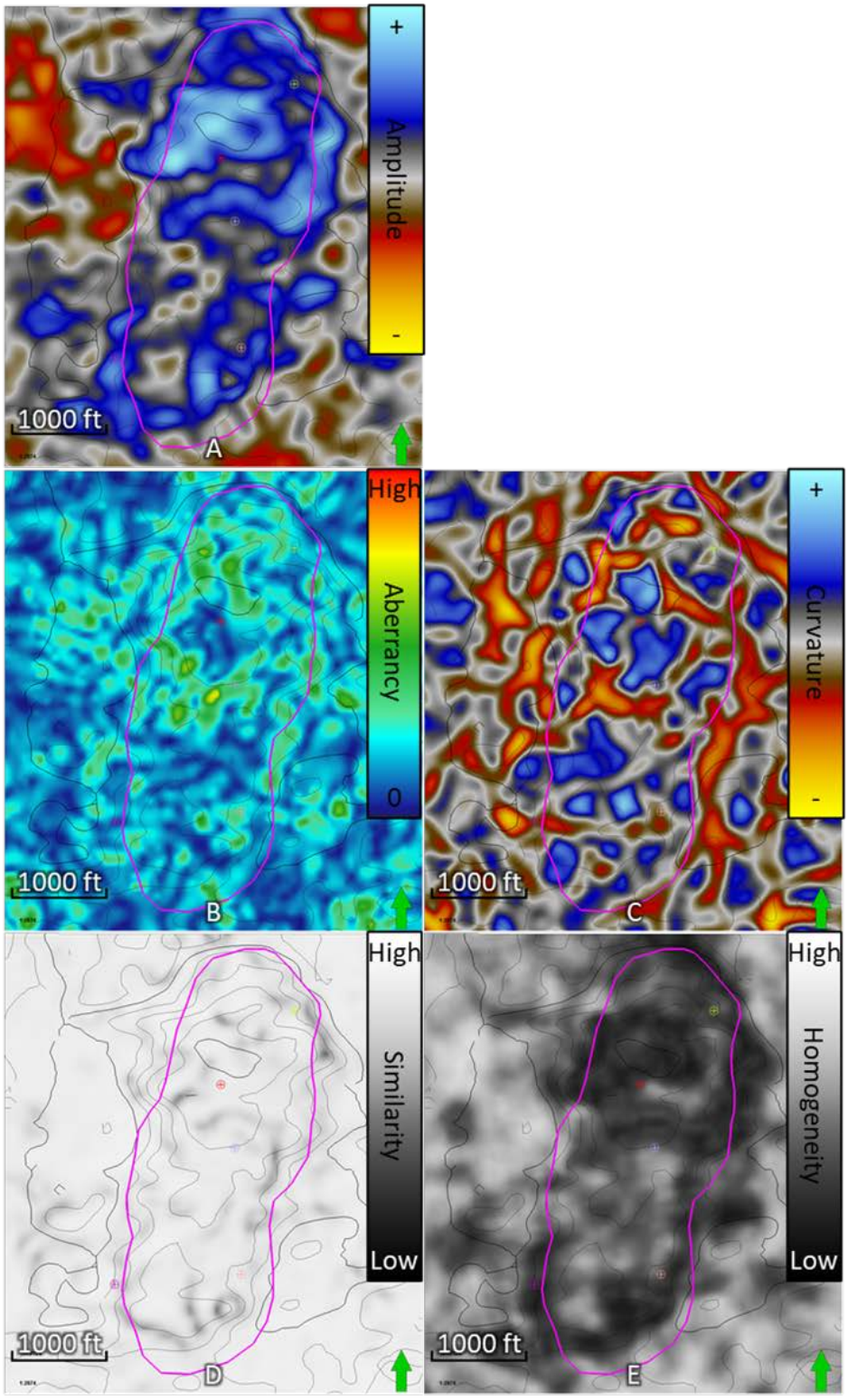


Figure 45: Gray horizon with extracted single structural attributes. A) PSTM amplitude B) Aberrancy C) Negative curvature D) ERS E) GLCM homogeneity Pink outline marks the outer reef boundary as defined by the A-1 Carbonate horizon.

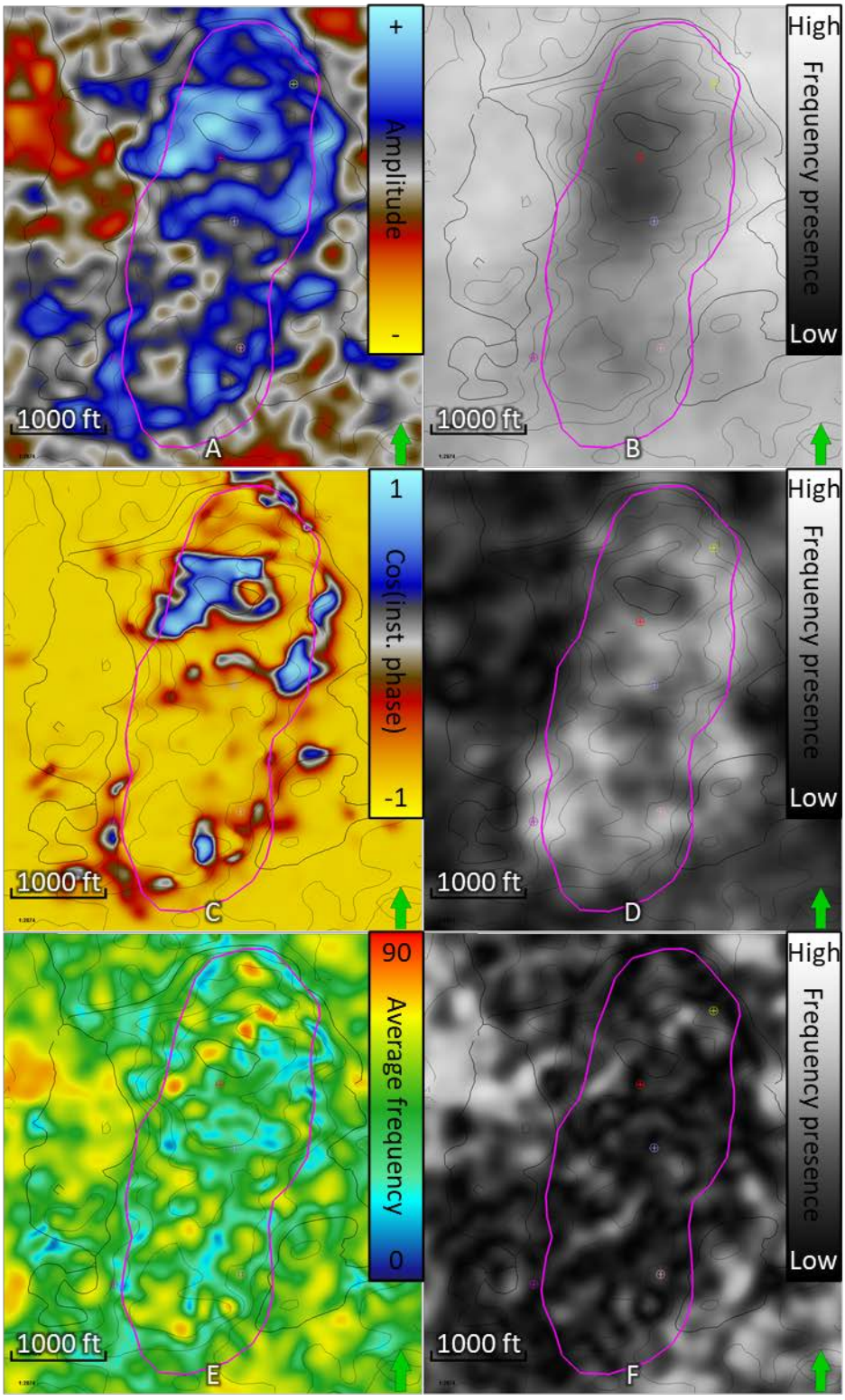


Figure 46: Gray horizon with extracted single frequency attributes. A) PSTM amplitude B) CWT 29 Hz C) Cosine of the instantaneous phase D) CWT 57 Hz E) Average frequency F) CWT 81 Hz Pink outline marks the outer reef boundary as defined by the A-1 Carbonate horizon.

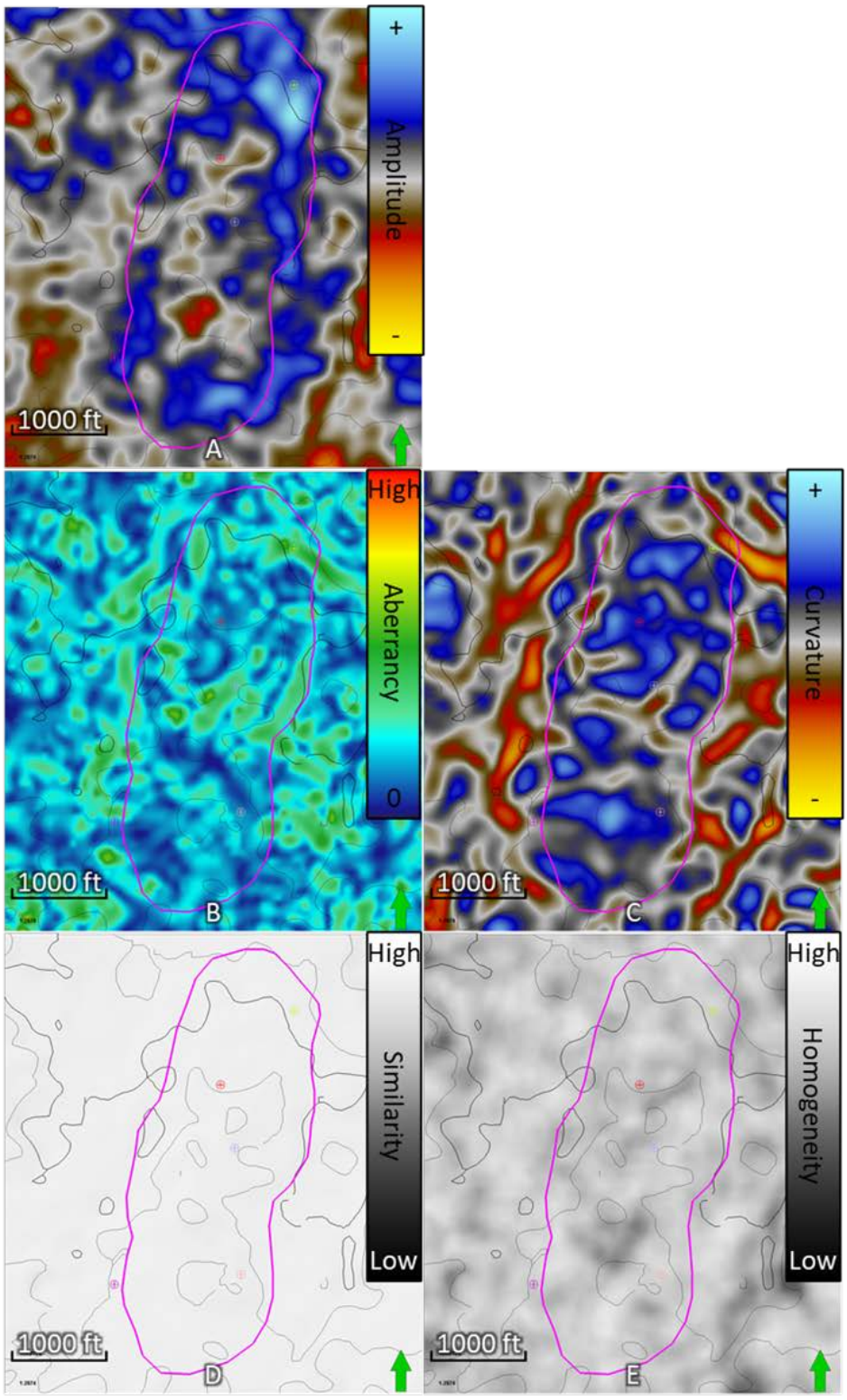


Figure 47: Clinton horizon with extracted single structural attributes. A) PSTM amplitude B) Aberrancy C) Negative curvature D) ERS E) GLCM homogeneity Pink outline marks the outer reef boundary as defined by the A-1 Carbonate horizon.

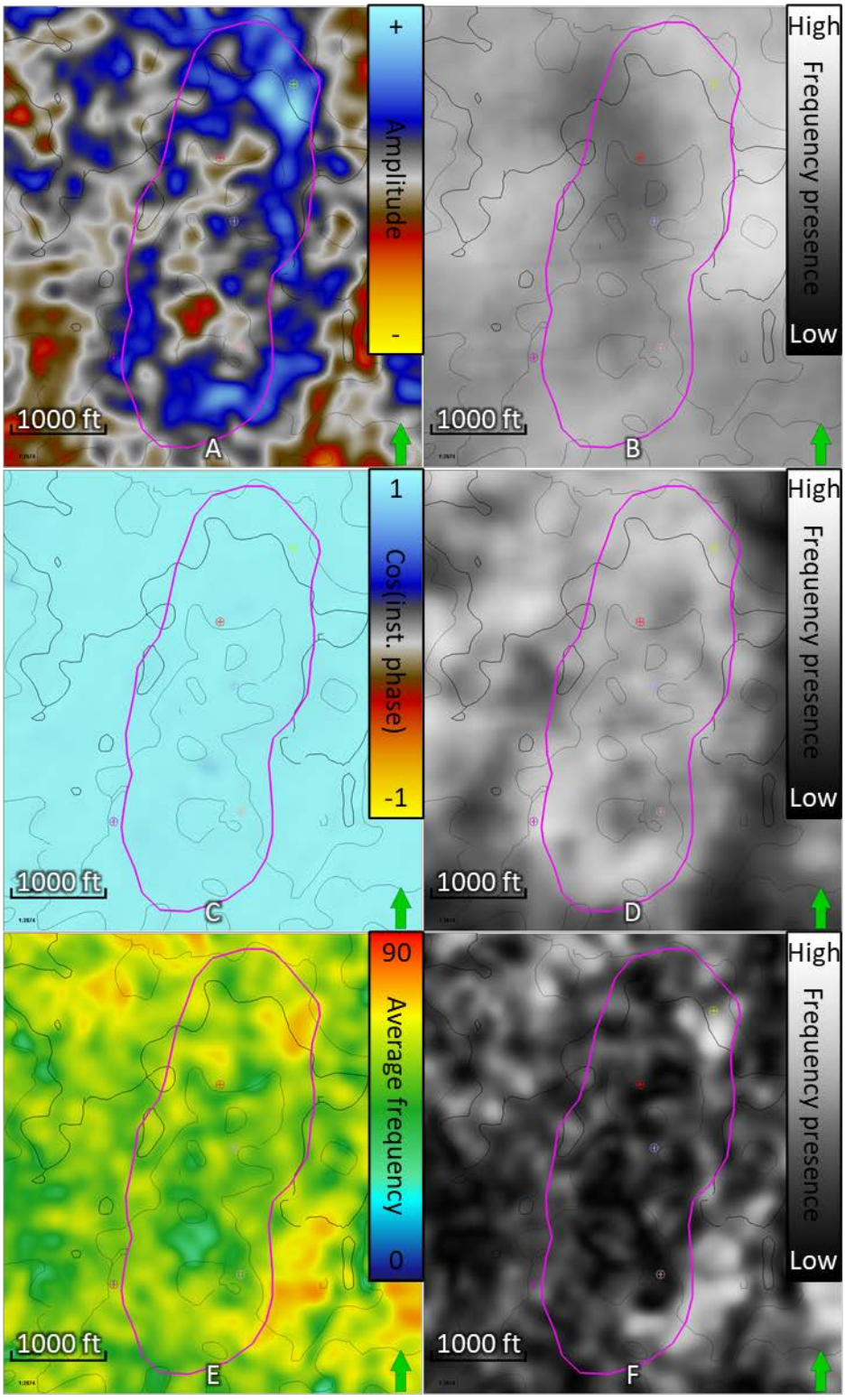


Figure 48: Clinton horizon with extracted single structural attributes. A) PSTM amplitude B) CWT 29 Hz C) Cosine of the instantaneous phase D) CWT 57 Hz E) Average frequency F) CWT 81 Hz Pink outline marks the outer reef boundary as defined by the A-1 Carbonate horizon.

Appendix B: Previous Puttygut SOM runs

In this appendix, the two previously mentioned SOM runs are documented. These are the two runs that utilized different amount of lateral data, one using all of the inlines and crosslines and the other only using a small subset of them, but were both vertically constrained between the A-2 Carbonate and the Clinton horizons. Since the boundaries for these SOM runs was the A-2 Carbonate and the Clinton horizons, they will not be shown.

Horizon slices of SOM run number one: Full inline and crossline extent

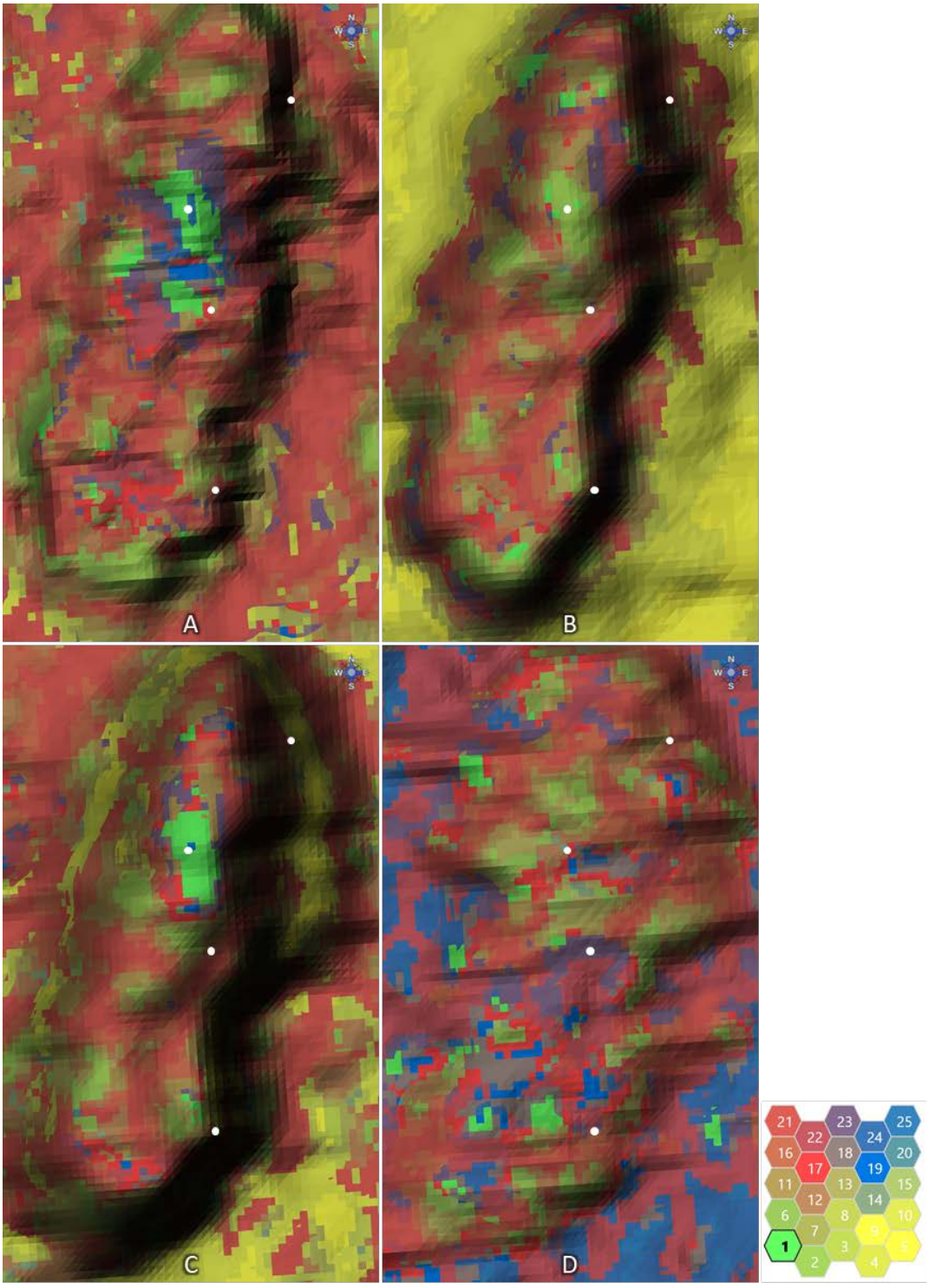


Figure 49: Structure SOM with full inline and crossline extent on: A) A-2 Anhydrite B) A-1 Carbonate C) Brown D) Gray

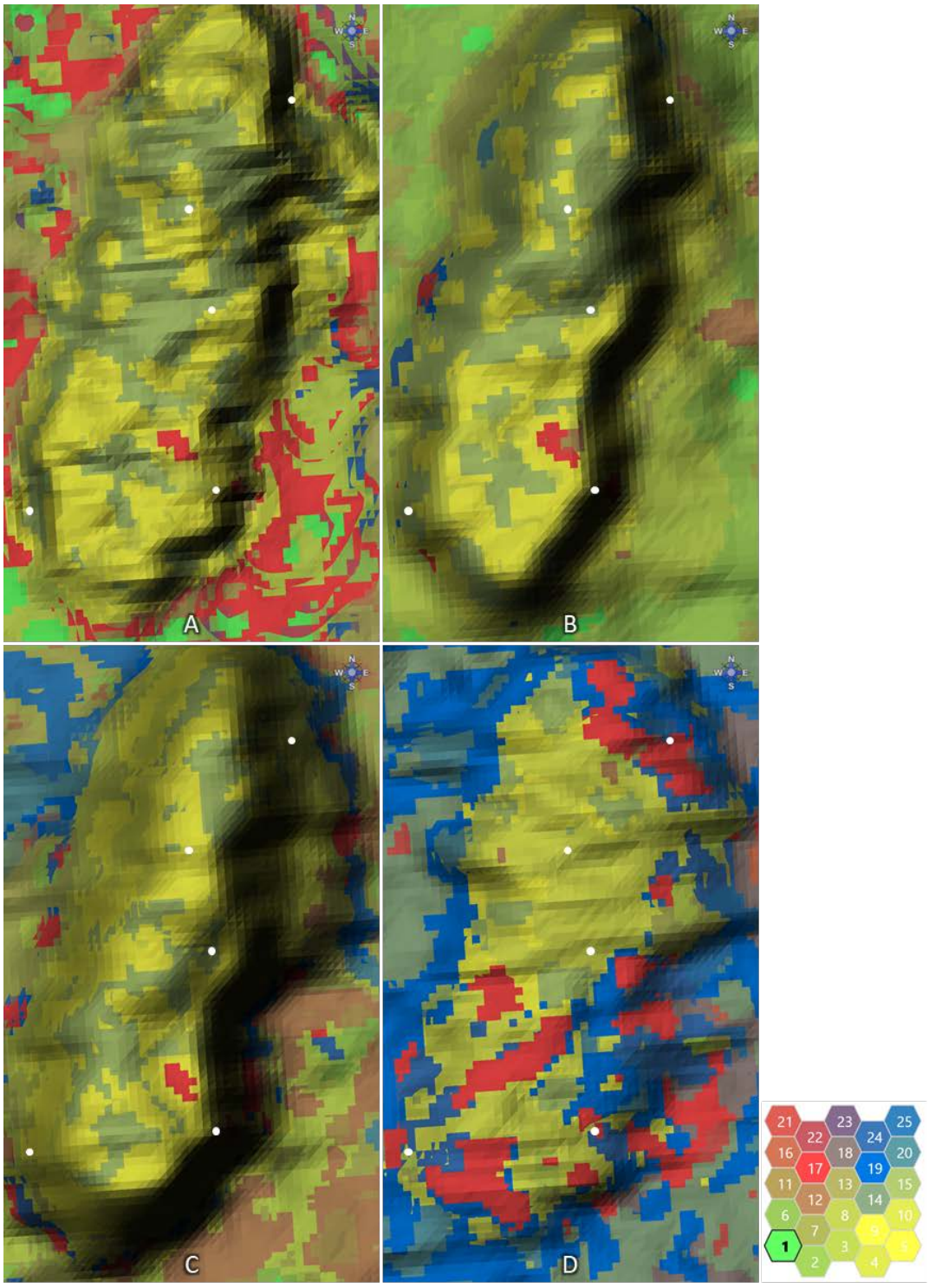


Figure 50: Frequency SOM with full inline and crossline extent on: A) A-2 Anhydrite B) A-1 Carbonate C) Brown D) Gray

Horizon slices of SOM run number two: Cropped inline and crossline extent

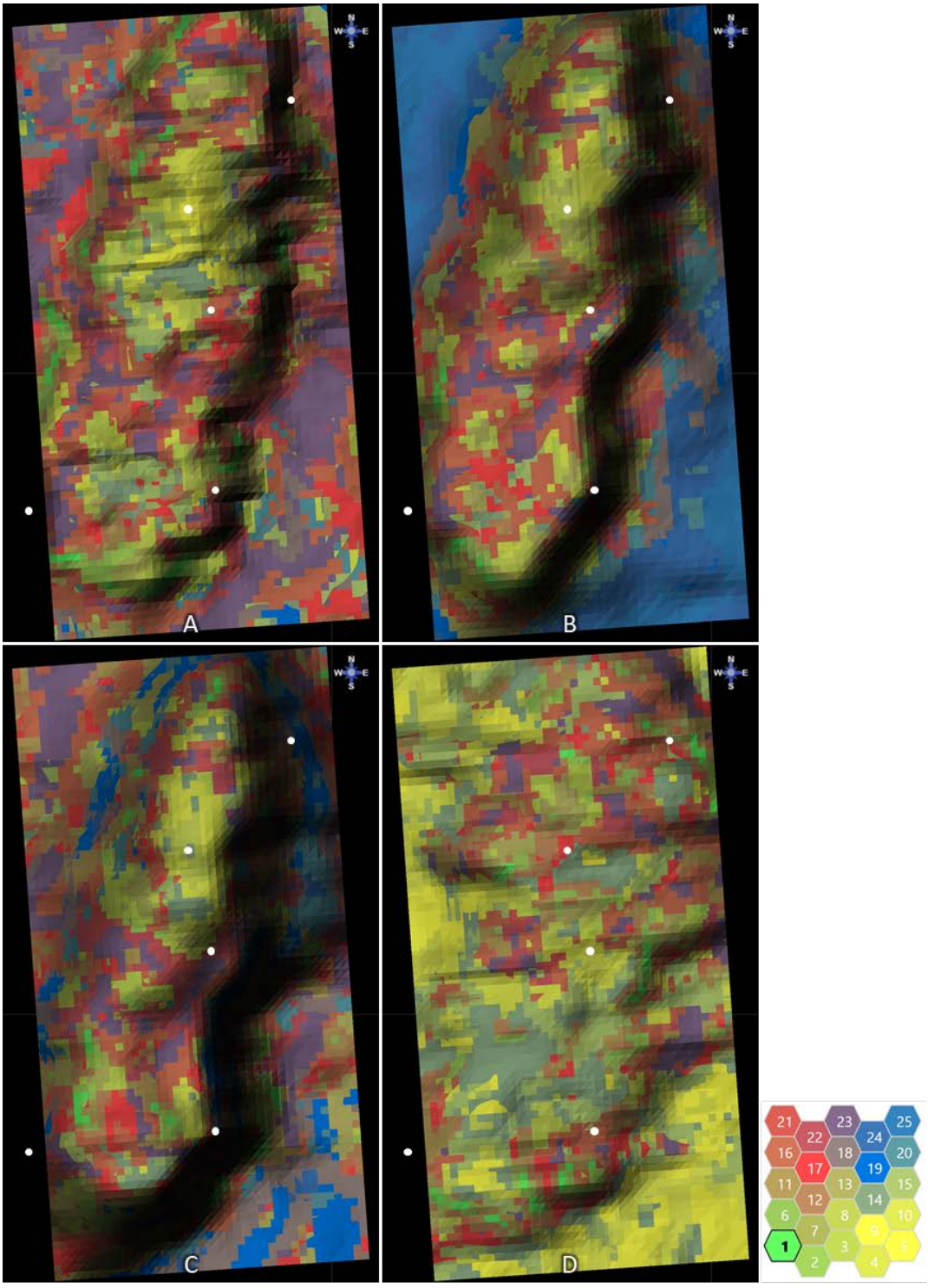


Figure 51: Structure SOM with cropped inline and crossline extent on: A) A-2 Anhydrite B) A-1 Carbonate C) Brown D) Gray

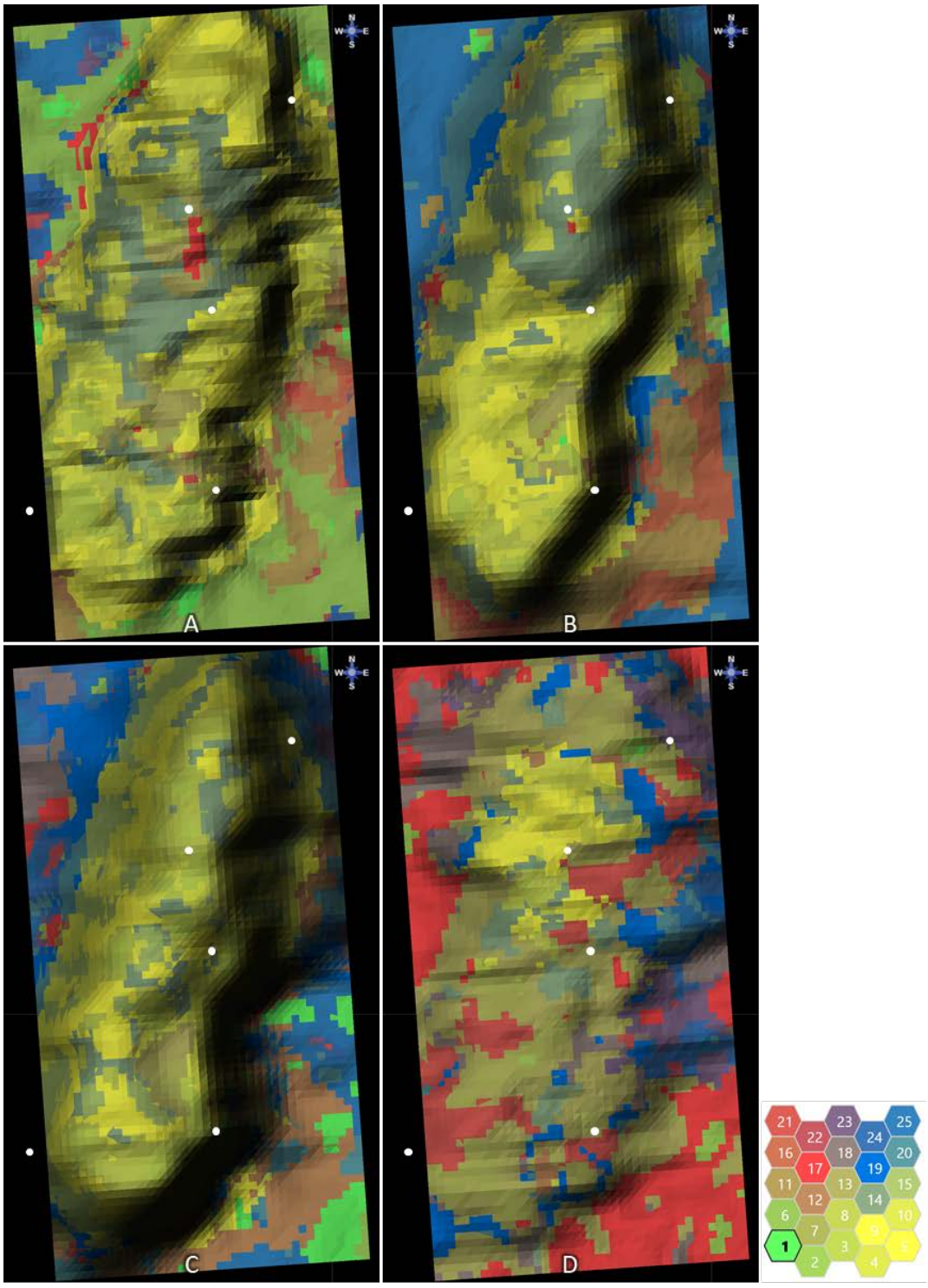


Figure 52: Frequency SOM with cropped inline and crossline extent on: A) A-2 Anhydrite B) A-1 Carbonate C) Brown D) Gray

Side by side of SOM runs one and two in vertical section

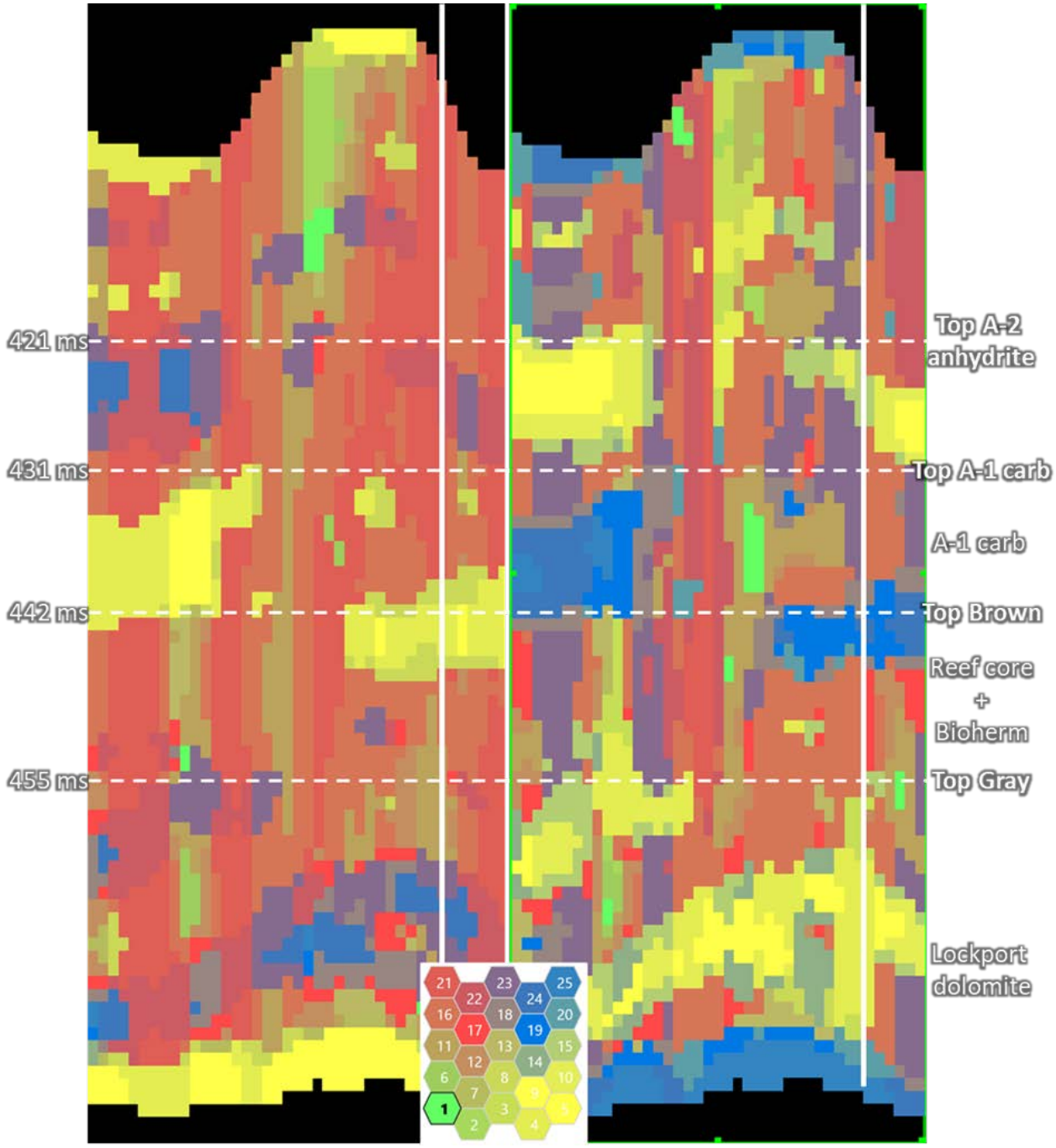


Figure 53: Inline 105, intersecting well P-106, of the full lateral extent SOM (left image) and the cropped lateral extent SOM (right image). Both images are displaying the SOMs created by using structural attributes.

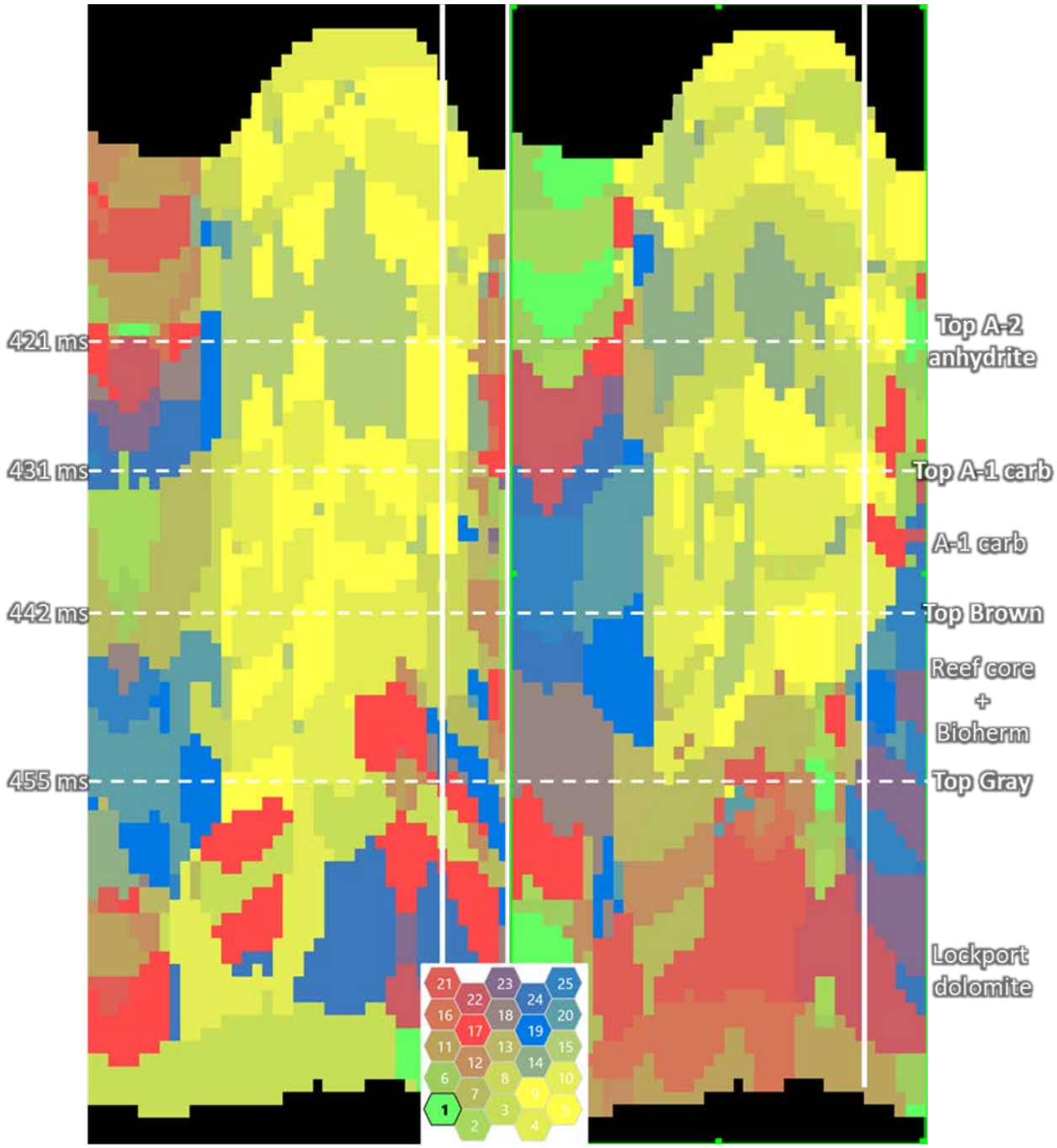


Figure 54: Inline 105, intersecting well P-106, of the full lateral extent SOM (left image) and the cropped lateral extent SOM (right image). Both images are displaying the SOMs created by using frequency attributes.

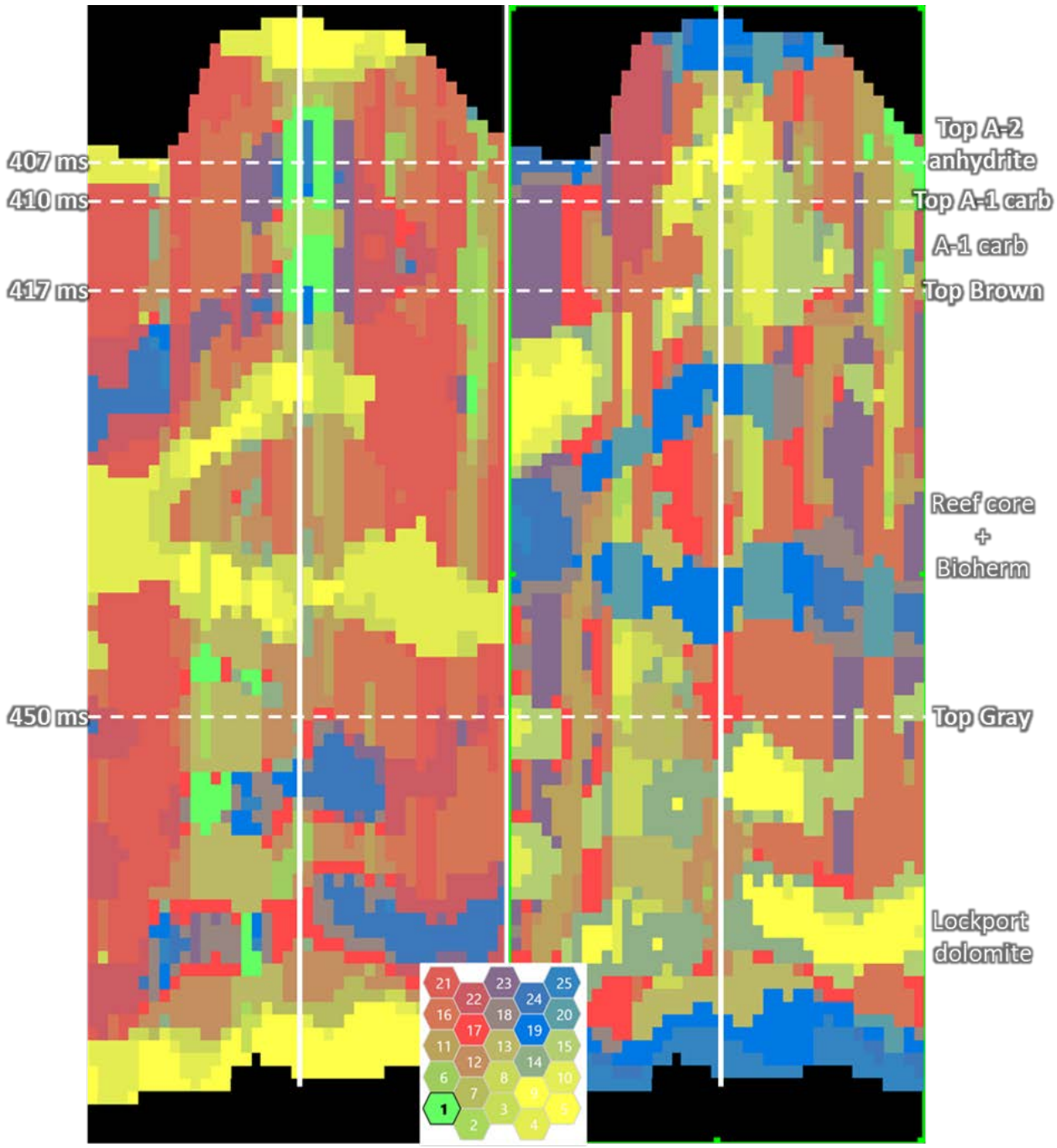


Figure 55: Inline 92, intersecting well P-201, of the full lateral extent SOM (left image) and the cropped lateral extent SOM (right image). Both images are displaying the SOMs created by using structural attributes.

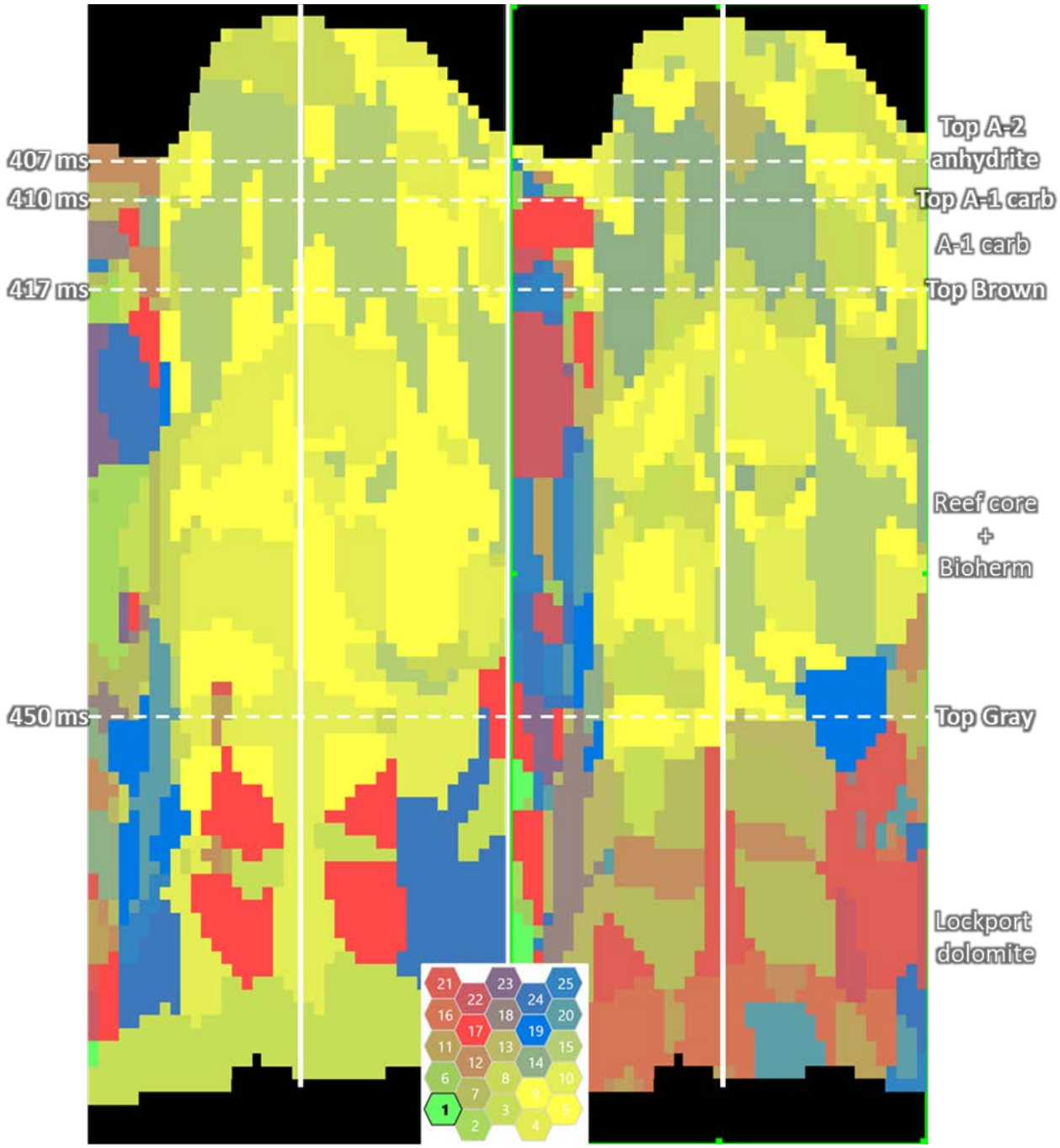


Figure 56: Inline 92, intersecting well P-201, of the full lateral extent SOM (left image) and the cropped lateral extent SOM (right image). Both images are displaying the SOMs created by using frequency attributes.

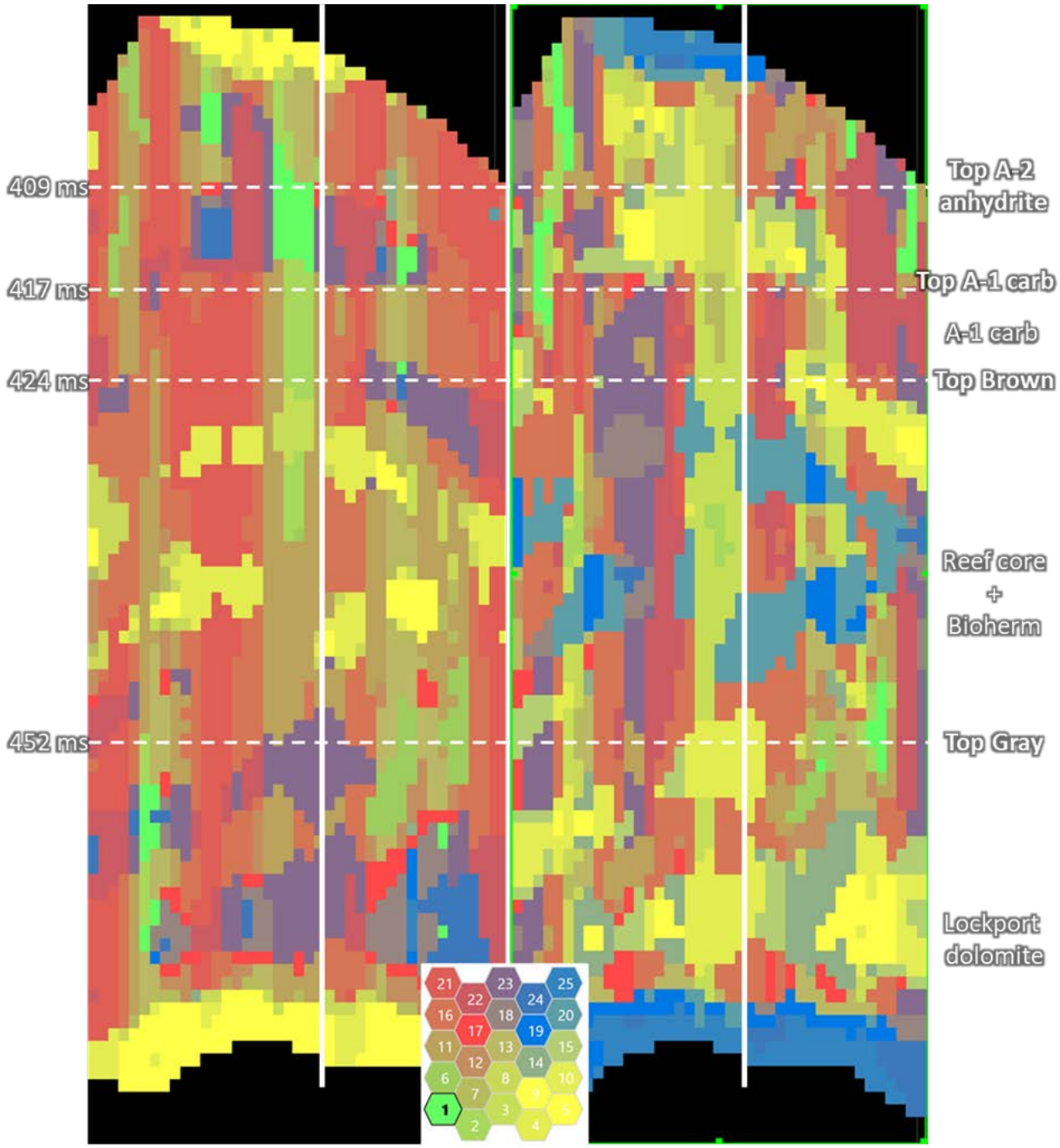


Figure 57: Inline 79, intersecting well P-102, of the full lateral extent SOM (left image) and the cropped lateral extent SOM (right image). Both images are displaying the SOMs created by using structural attributes.

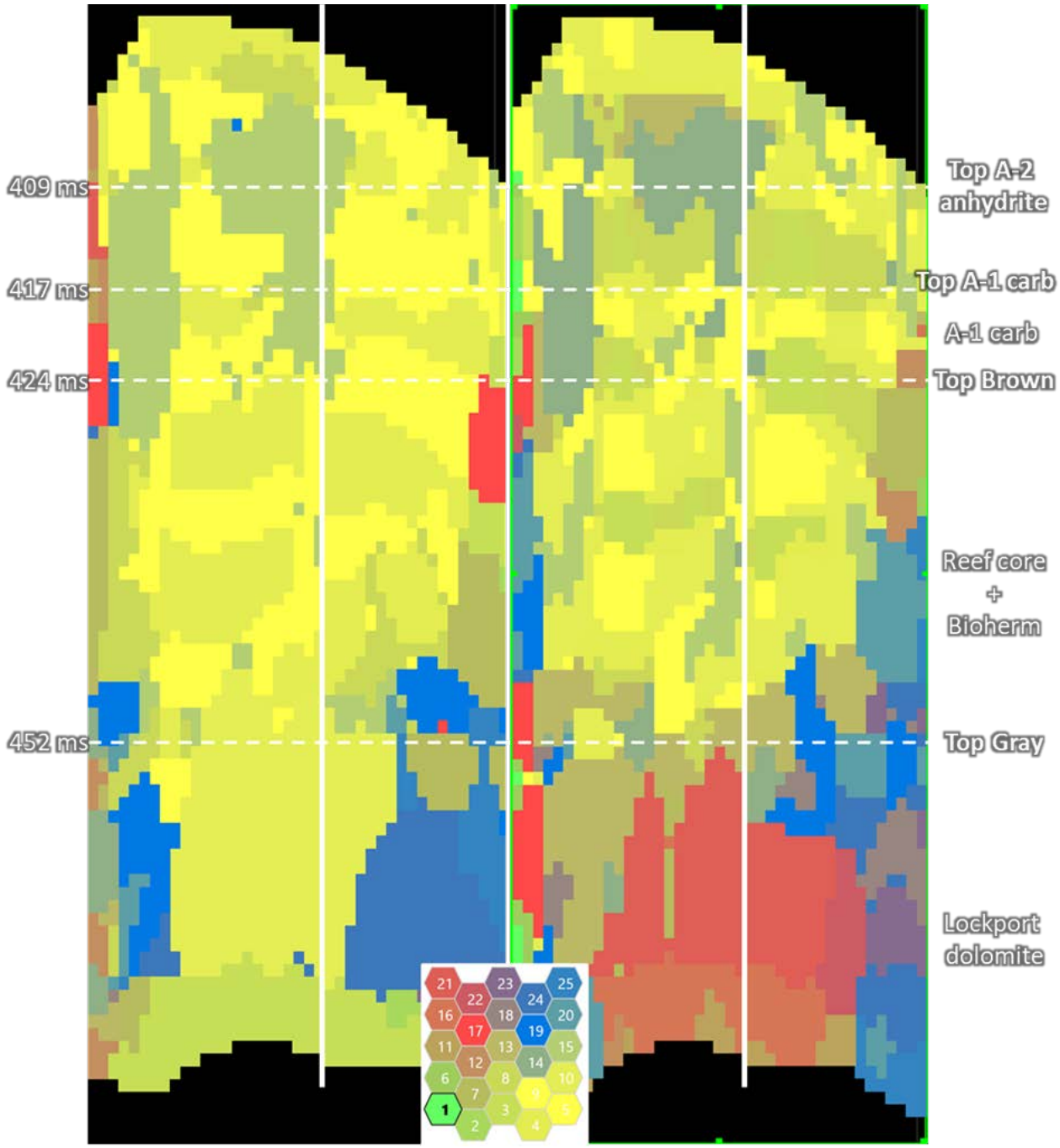


Figure 58: Inline 79, intersecting well P-102, of the full lateral extent SOM (left image) and the cropped lateral extent SOM (right image). Both images are displaying the SOMs created by using frequency attributes.

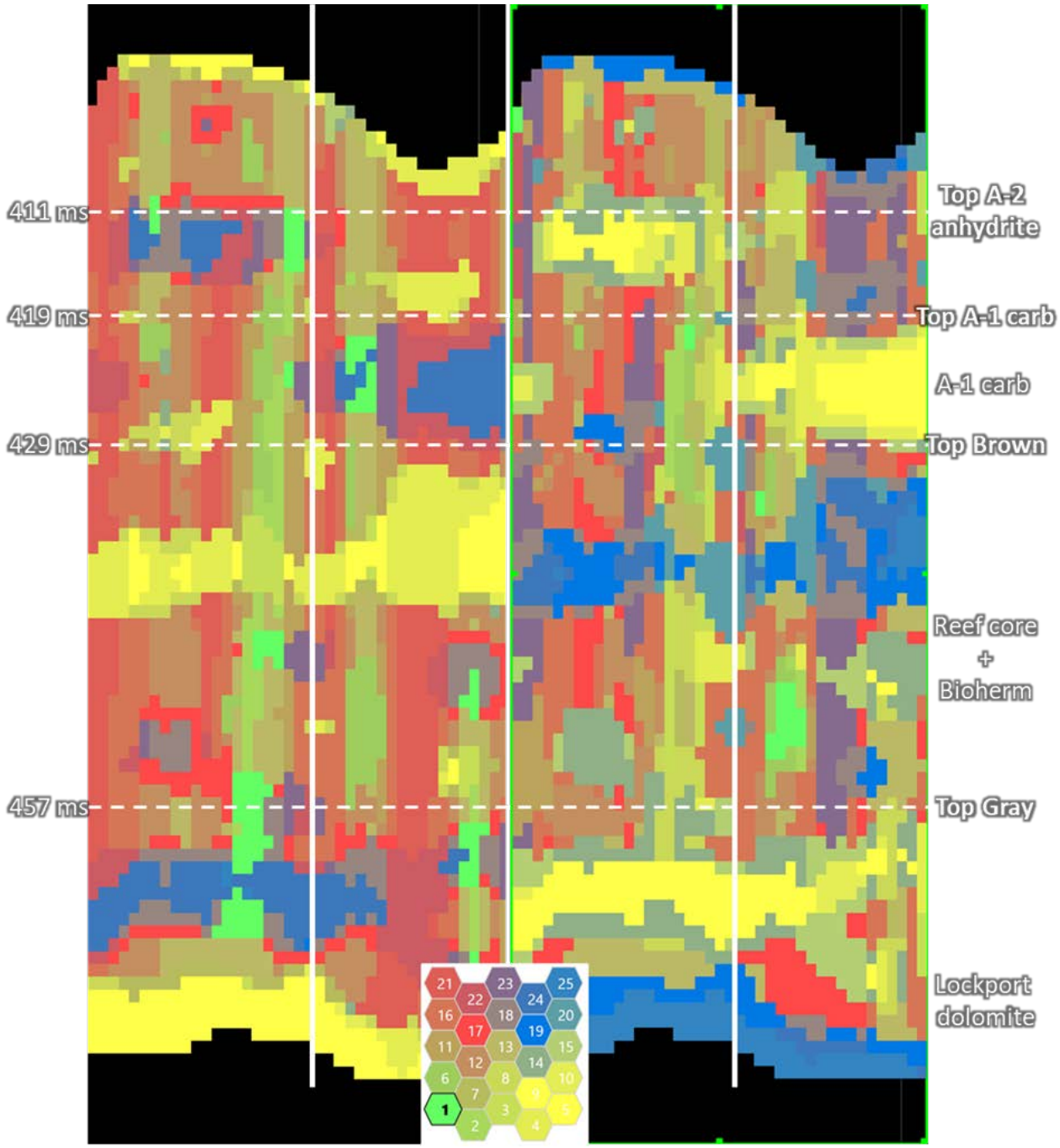


Figure 59: Inline 56, intersecting well P-103, of the full lateral extent SOM (left image) and the cropped lateral extent SOM (right image). Both images are displaying the SOMs created by using structural attributes

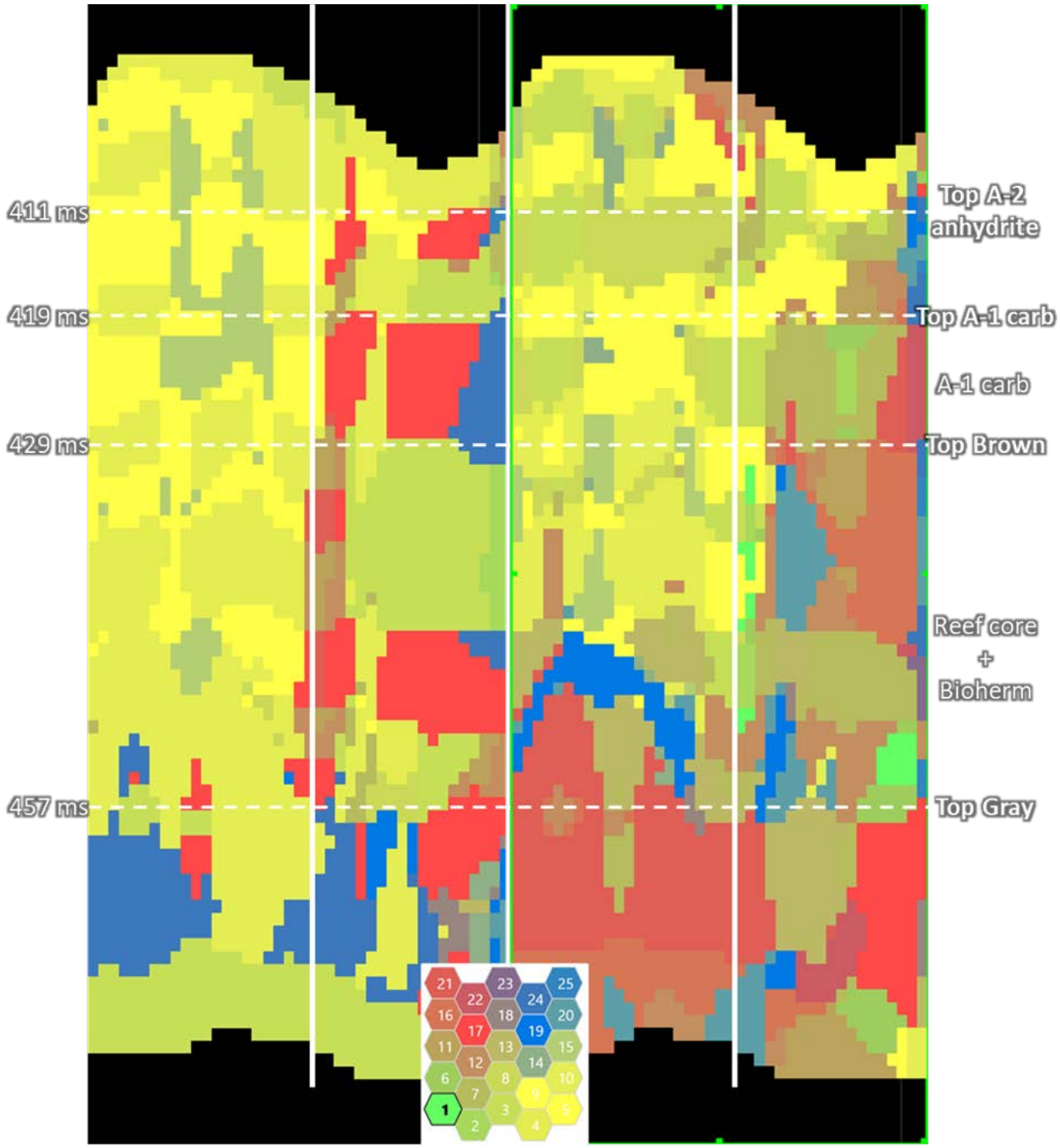


Figure 60: Inline 56, intersecting well P-103, of the full lateral extent SOM (left image) and the cropped lateral extent SOM (right image). Both images are displaying the SOMs created by using frequency attributes

Appendix C: Inline views of final Puttygut SOM

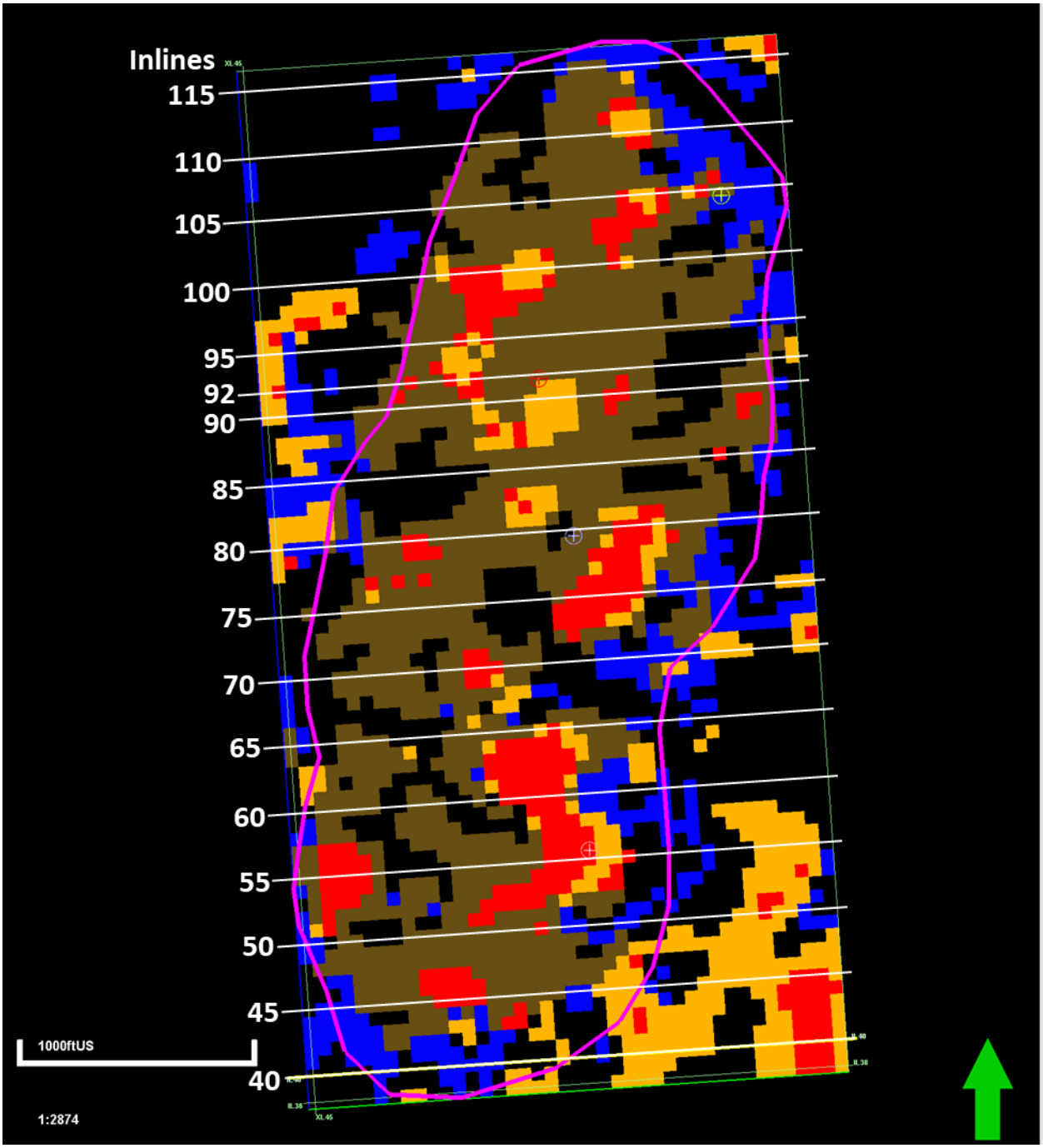


Figure 61: Base map showing inlines through Puttygut reef at an interval of five. Apart from Inline 92, which was included to show well P-201.

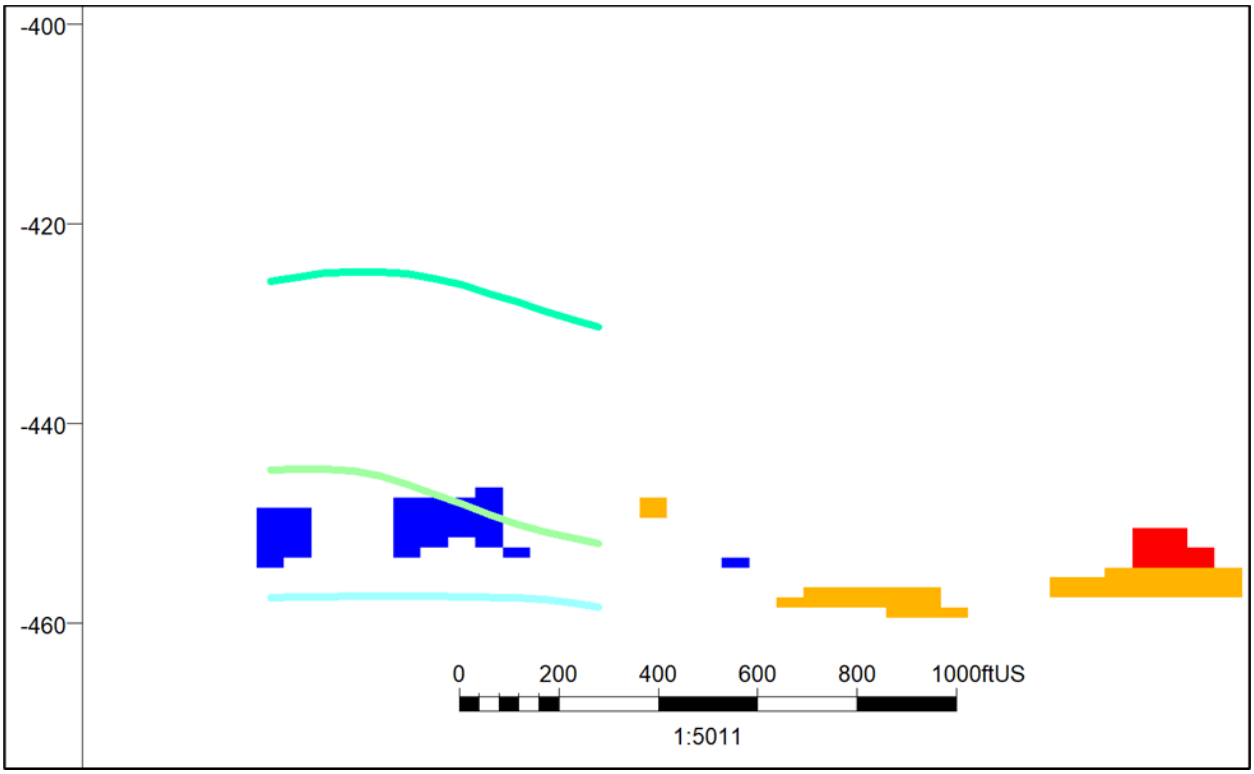


Figure 62: Inline 40

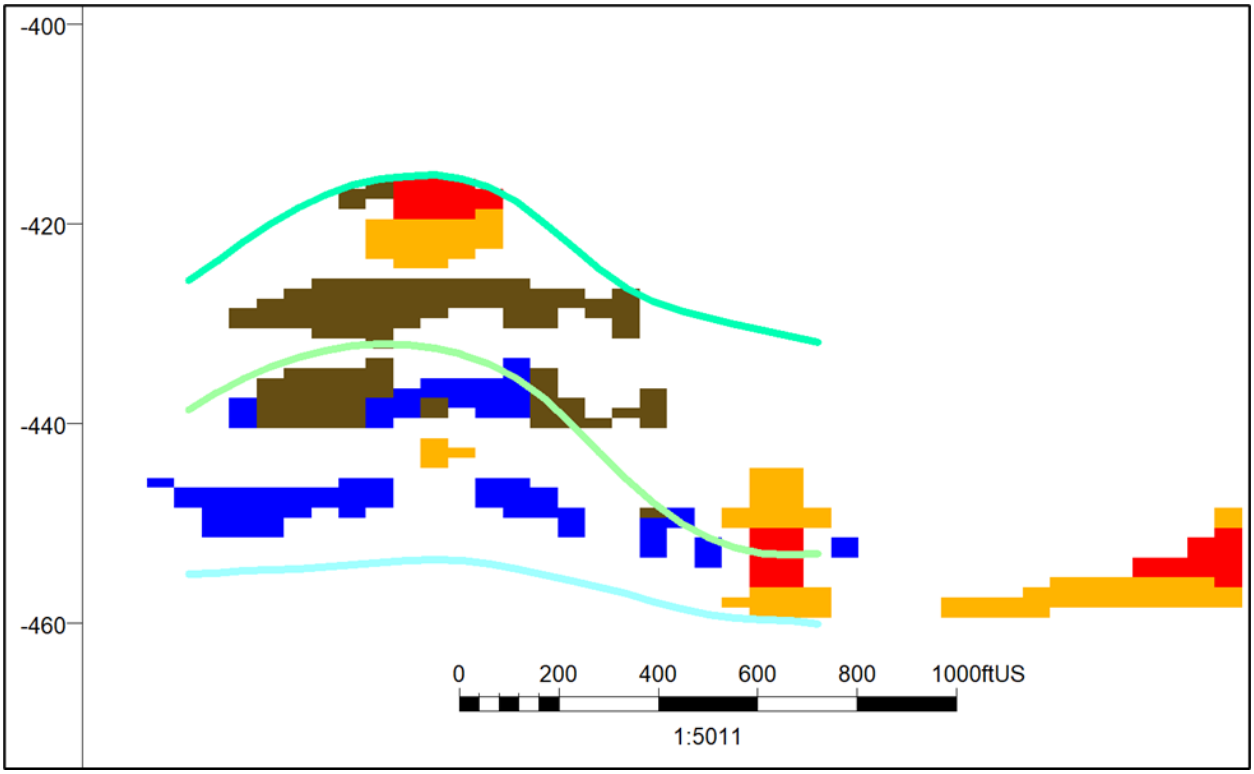


Figure 63: Inline 45

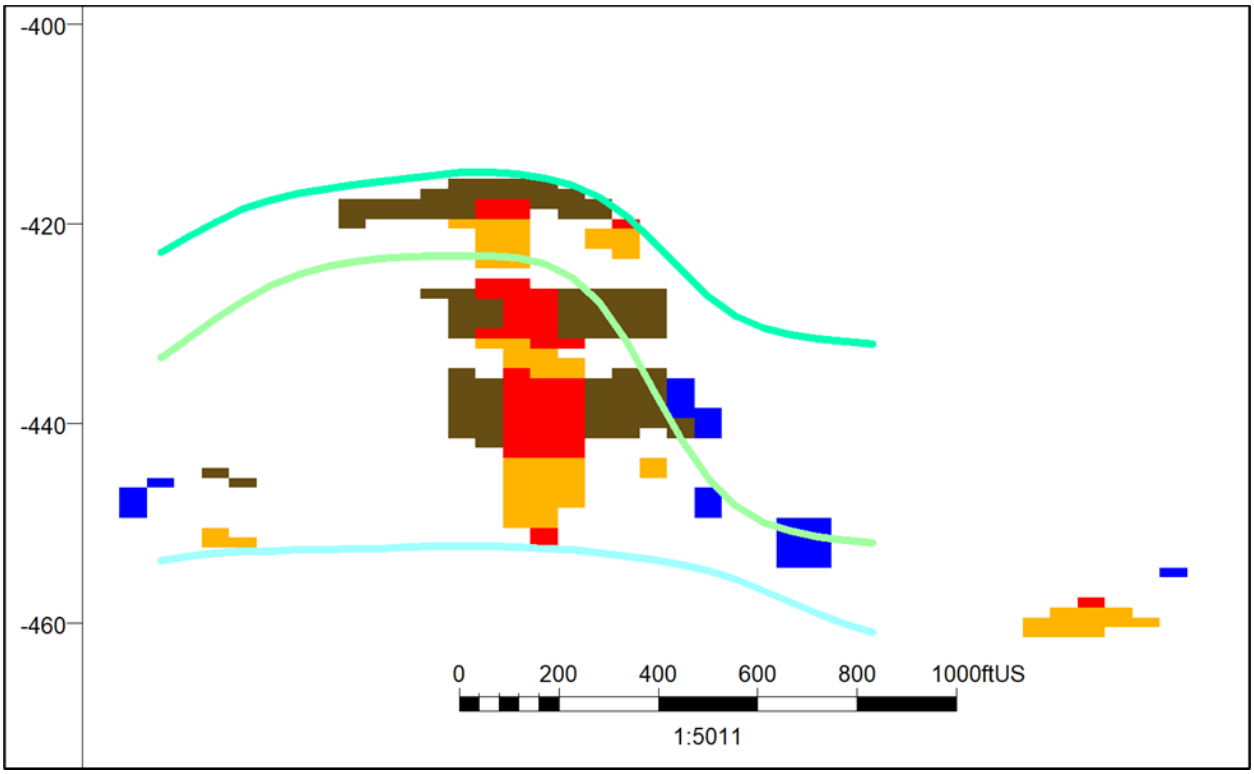


Figure 64: Inline 50

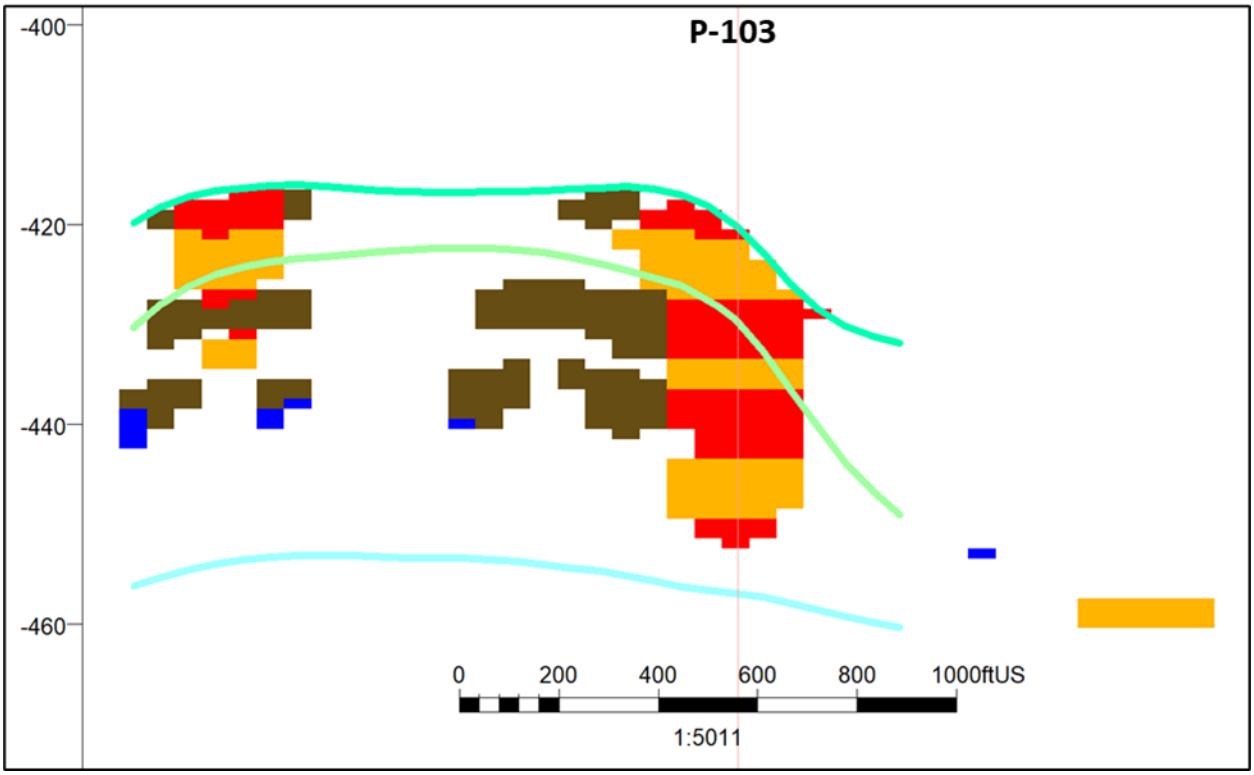


Figure 65: Inline 55

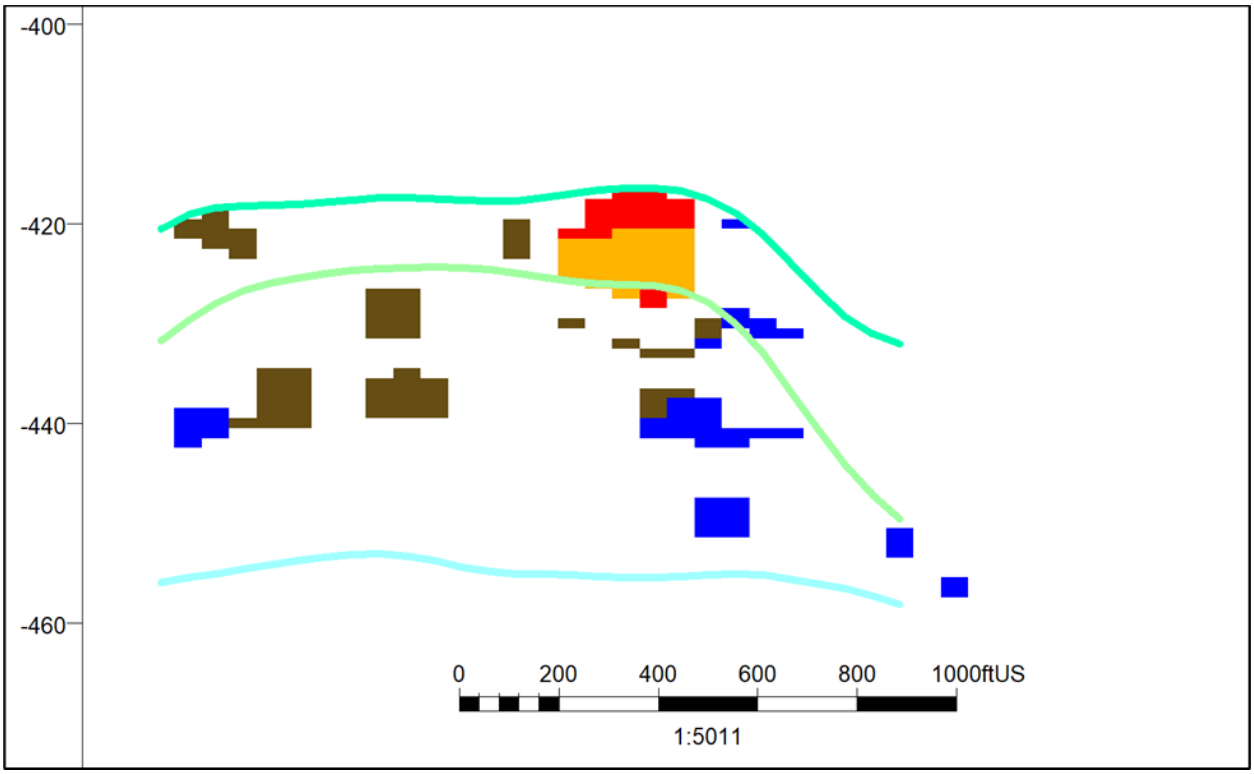


Figure 66: Inline 60

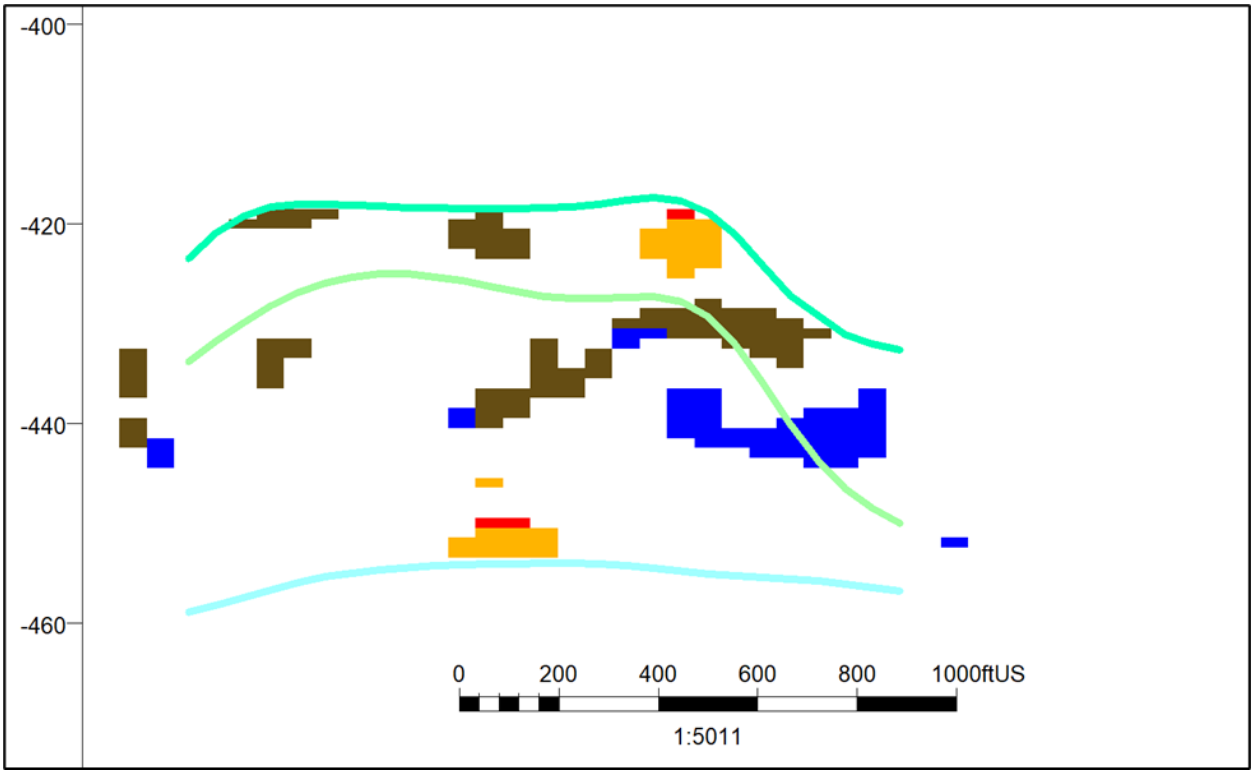


Figure 67: Inline 65

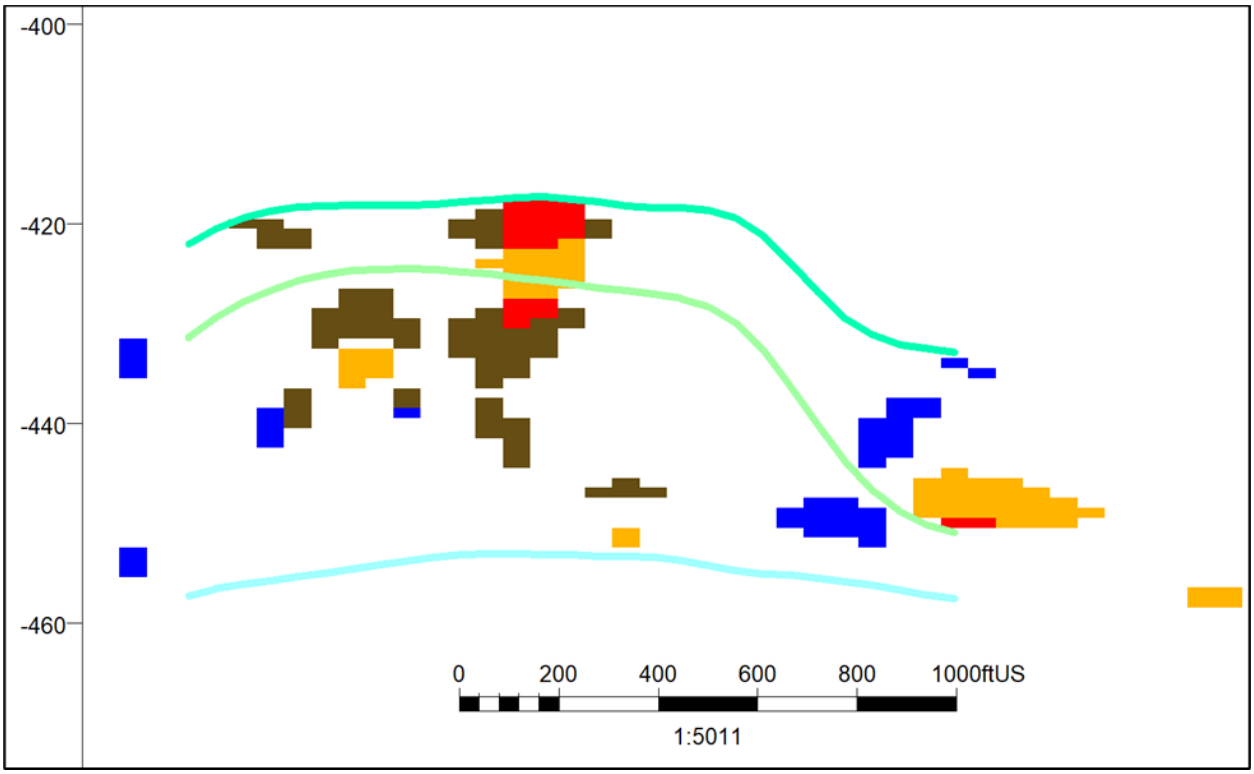


Figure 68: Inline 70

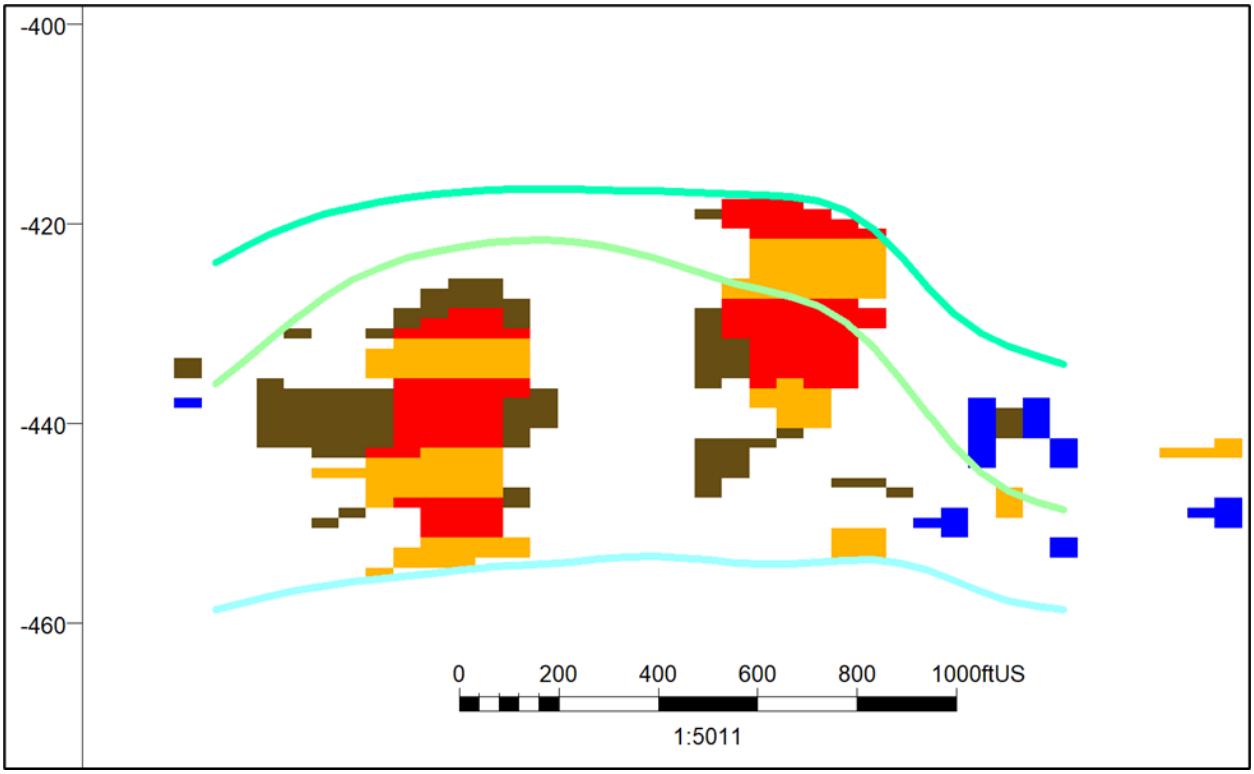


Figure 69: Inline 75

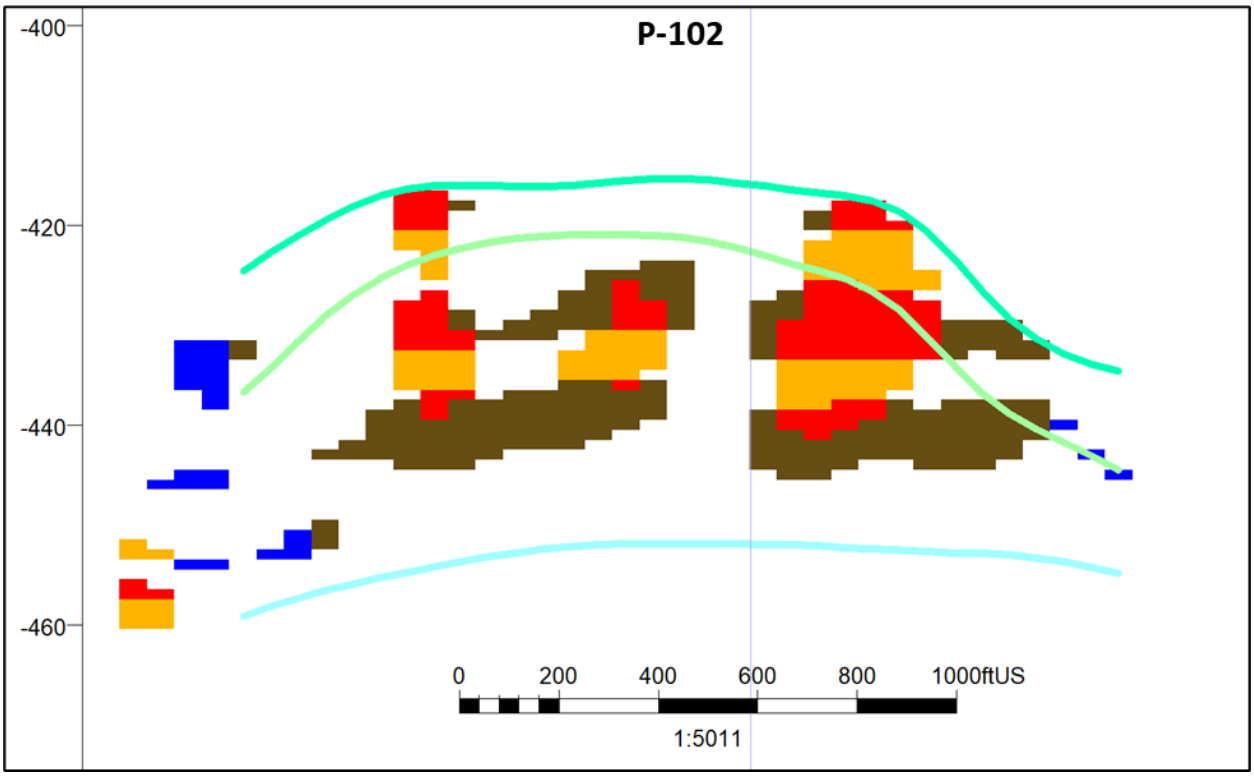


Figure 70: Inline 80. Vertical purple line is location of well P-102.

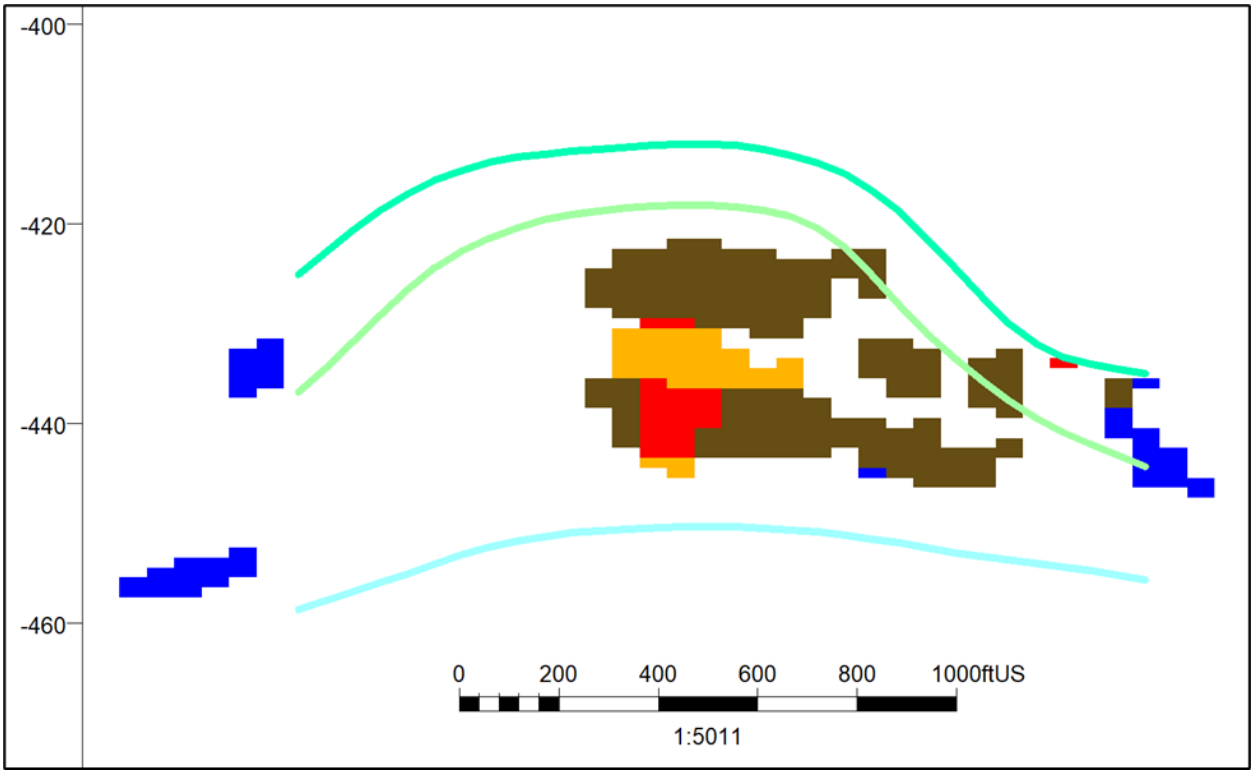


Figure 71: Inline 85

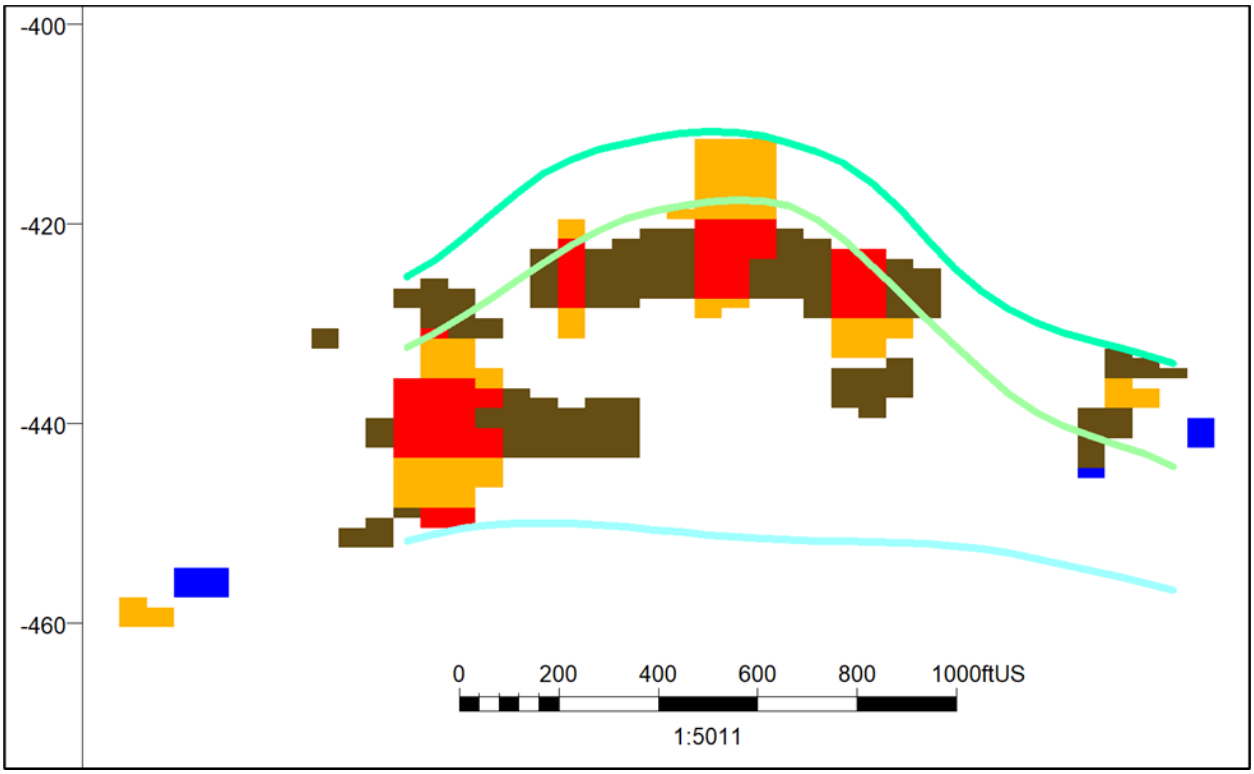


Figure 72: Inline 90

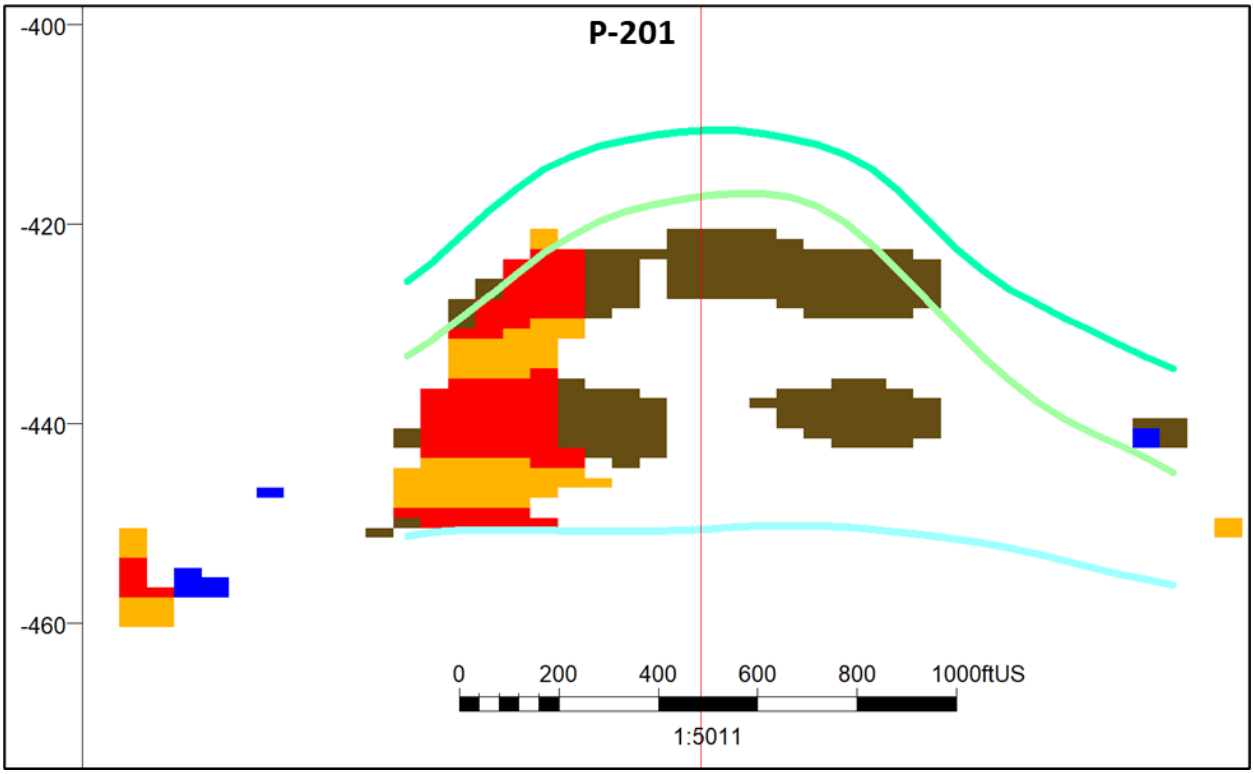


Figure 73: Inline 92. Vertical red line is location of well P-201.

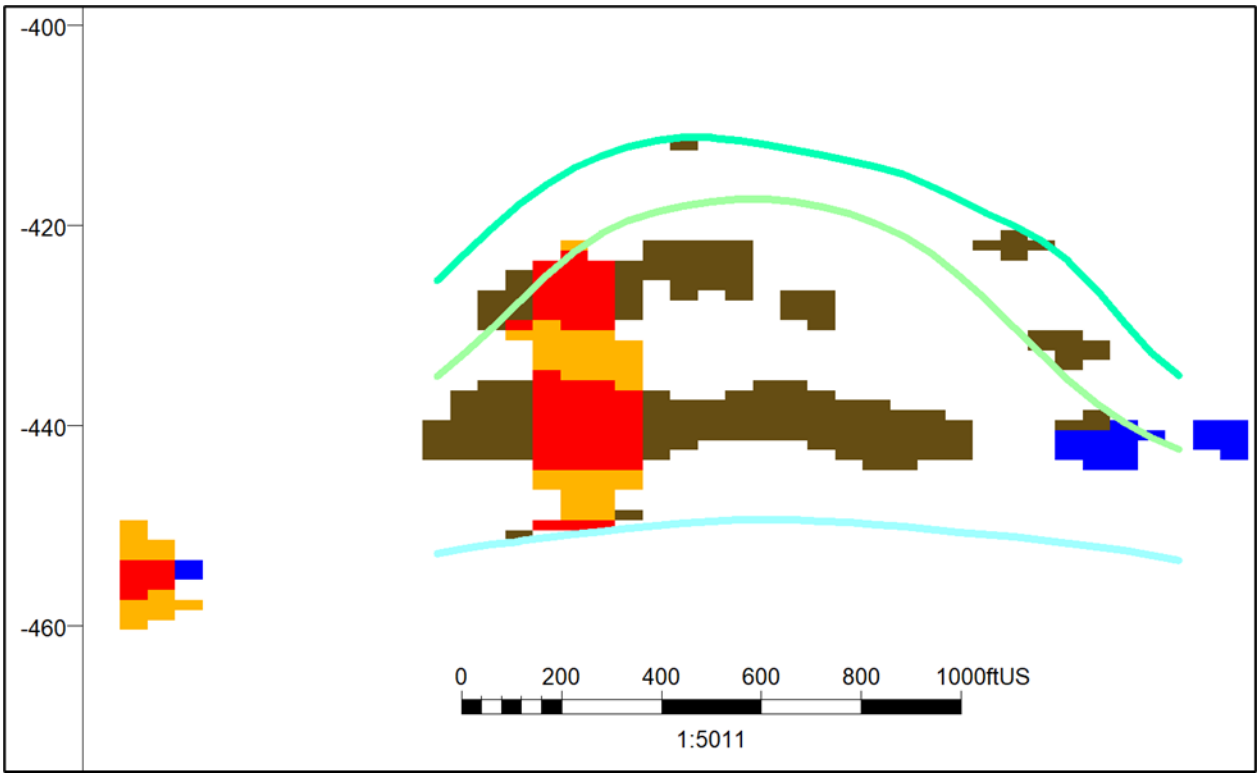


Figure 74: Inline 95

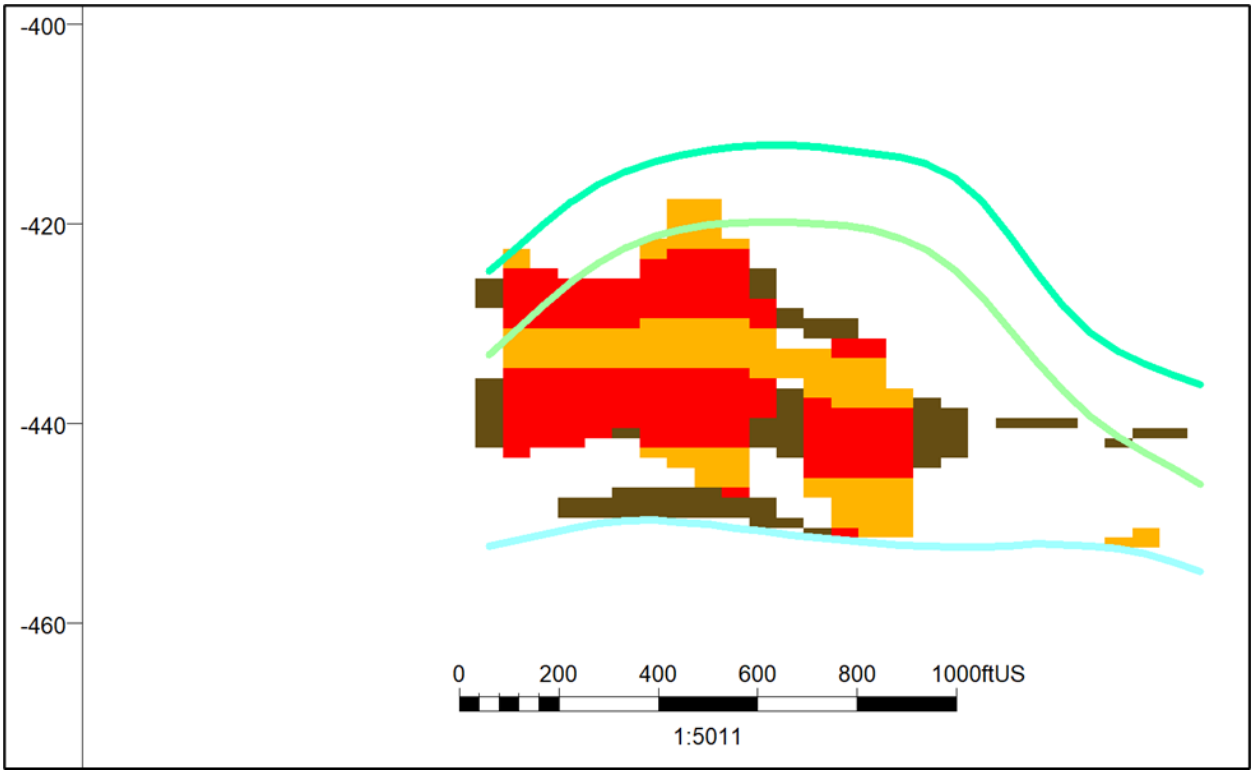


Figure 75: Inline 100

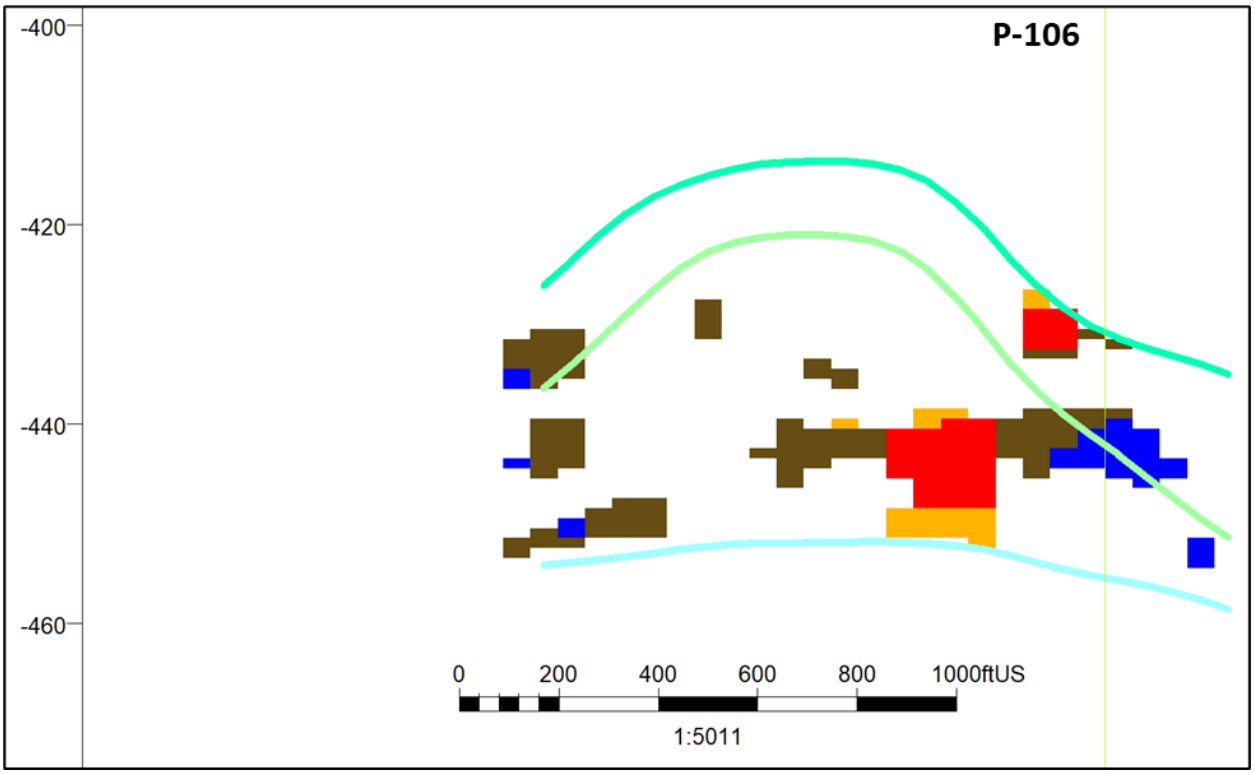


Figure 76: Inline 105. Vertical green line is location of well P-106.

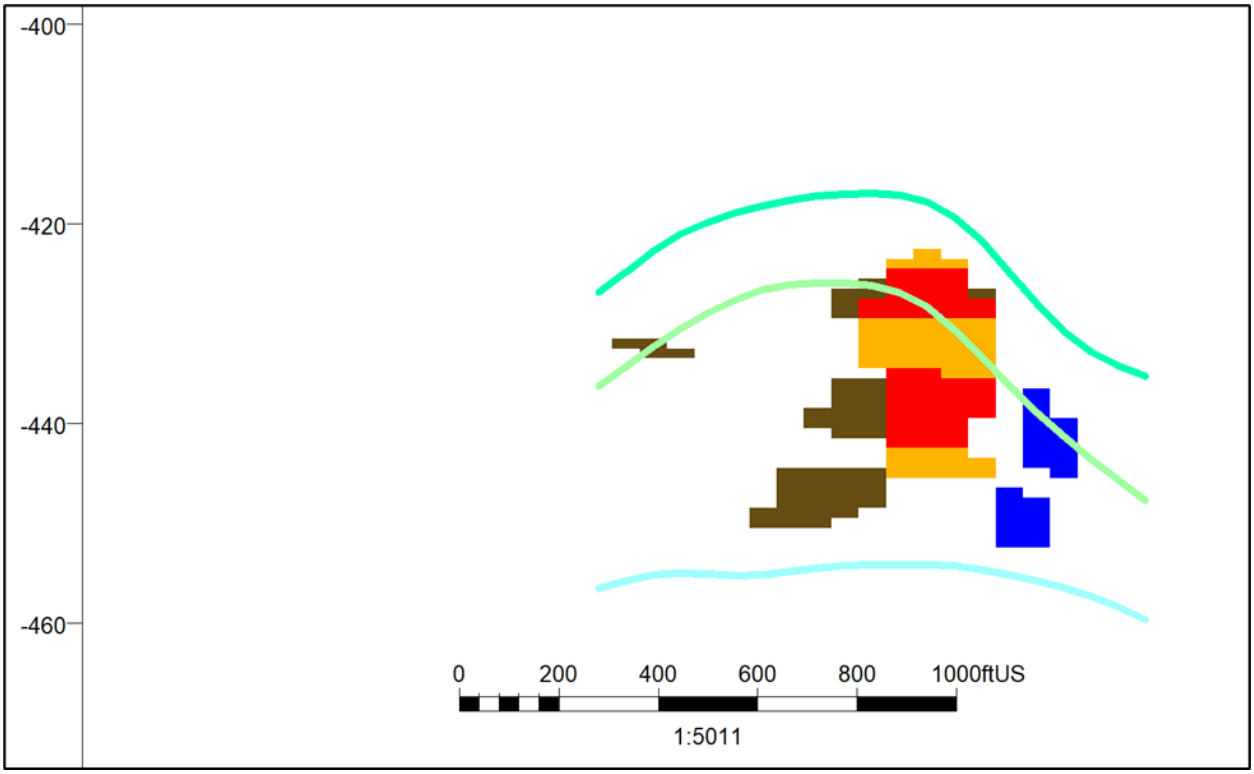


Figure 77: Inline 100

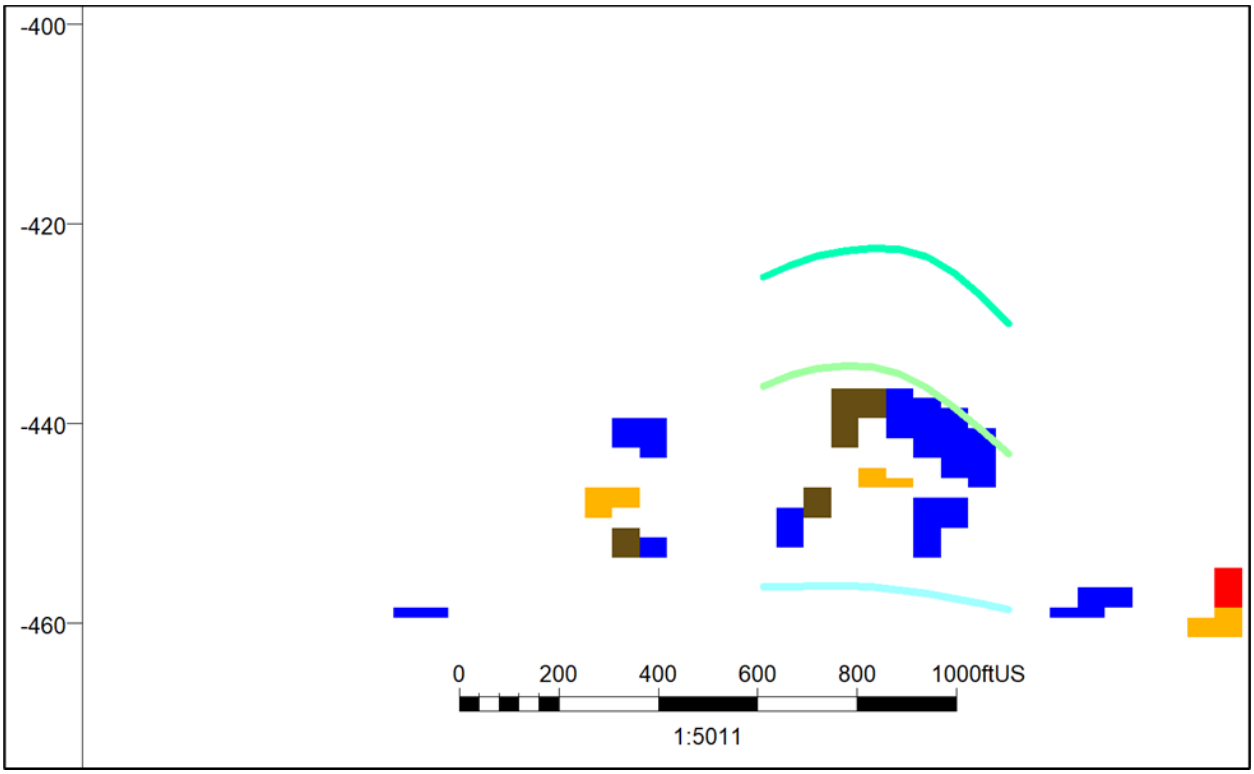


Figure 78: Inline 115

Appendix D: Well logs

Located in this section are the well logs of the four key wells used during the analysis of the Puttygut SOMs.

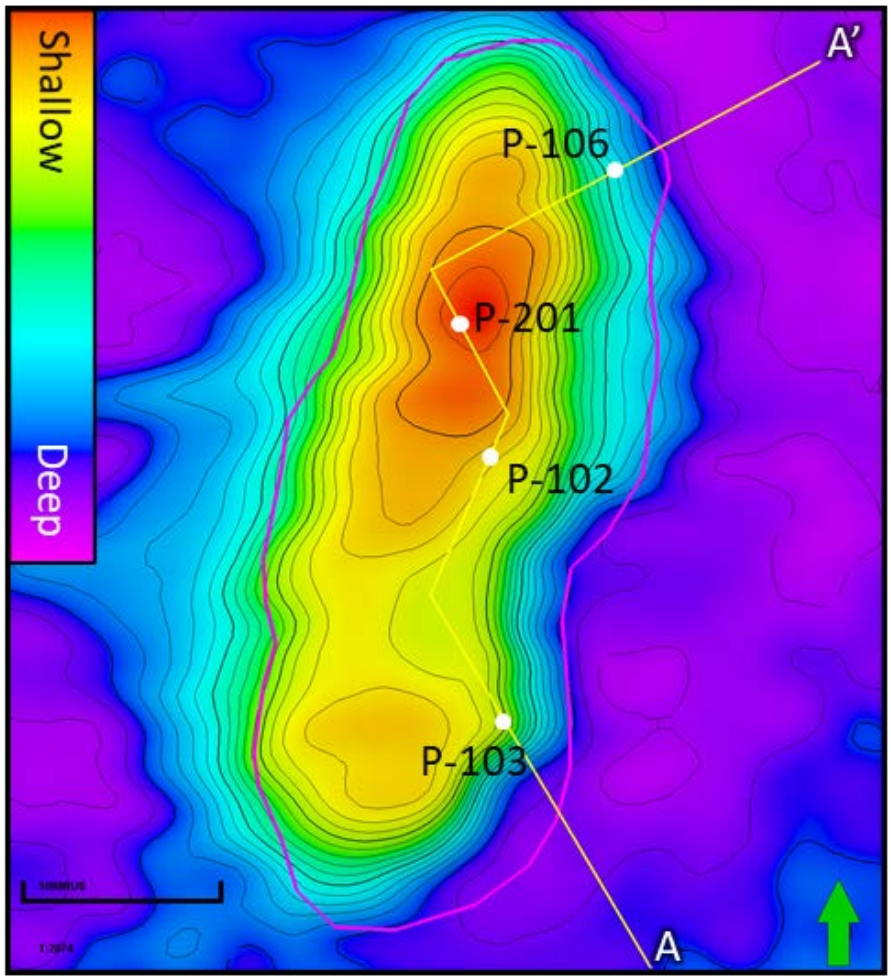


Figure 79: The locations of the four key wells in map view. The TWT map is of the Brown Formation.

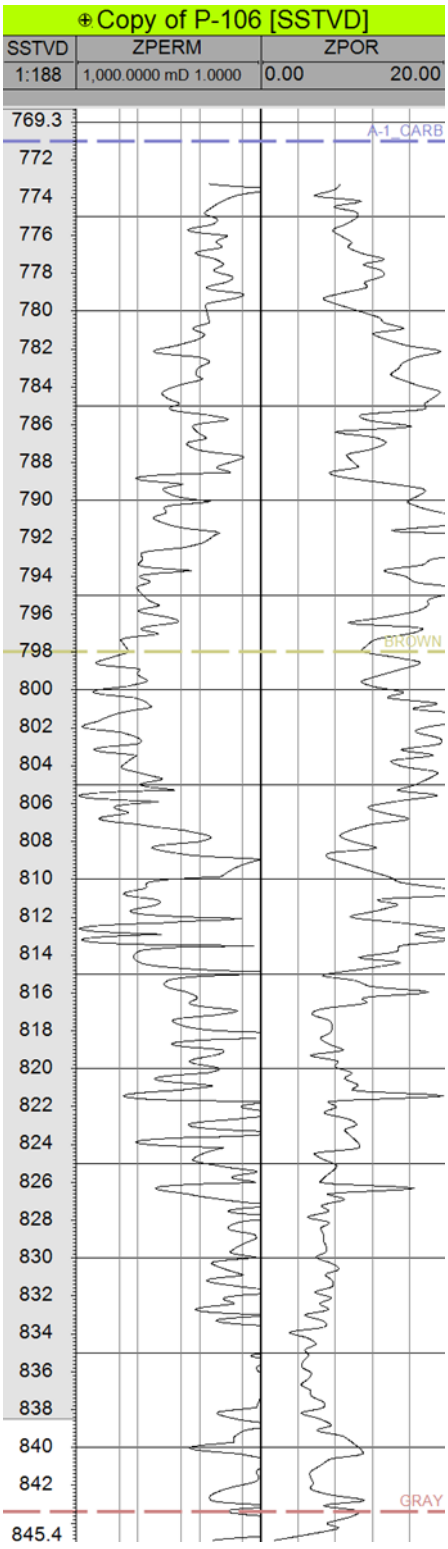


Figure 80: Permeability and porosity logs for well P-106

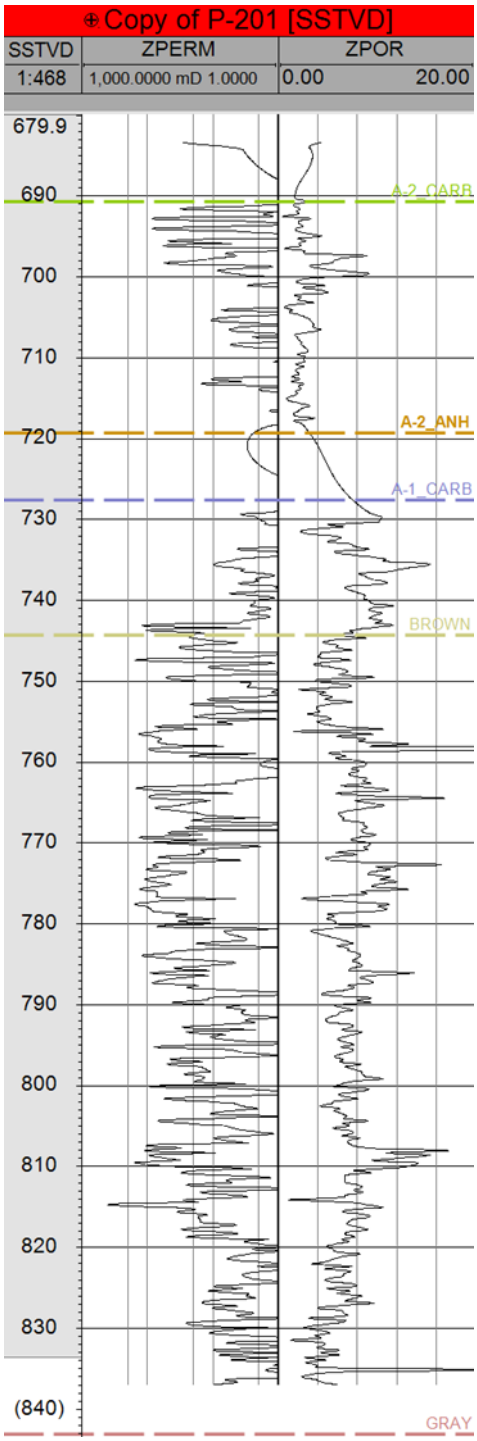


Figure 81: Permeability and porosity logs for well P-201

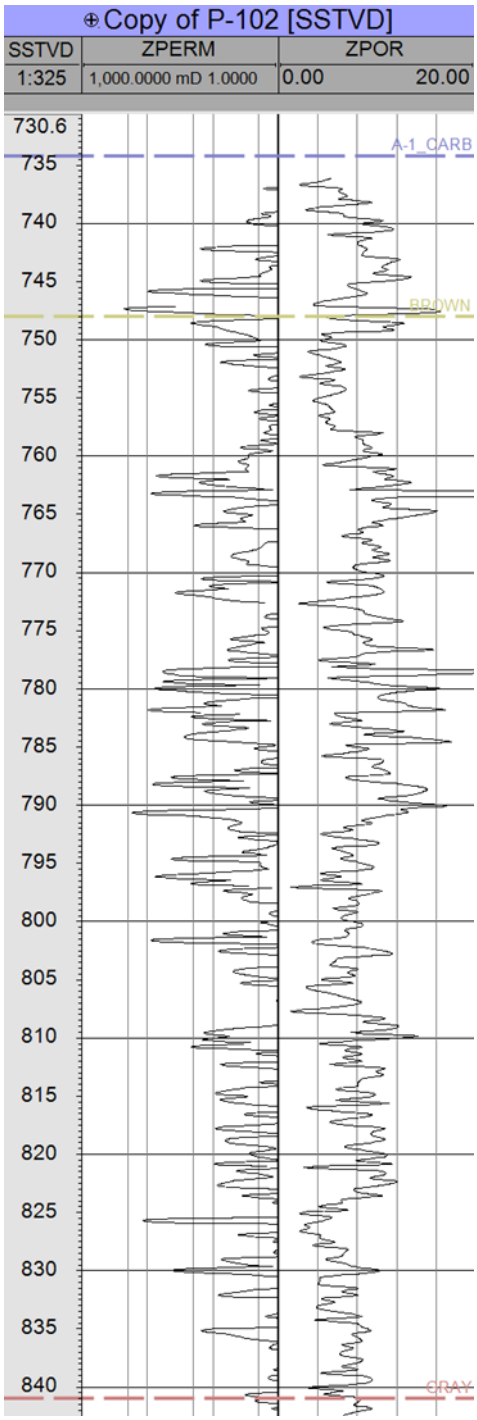


Figure 82: Permeability and porosity logs for well P-106

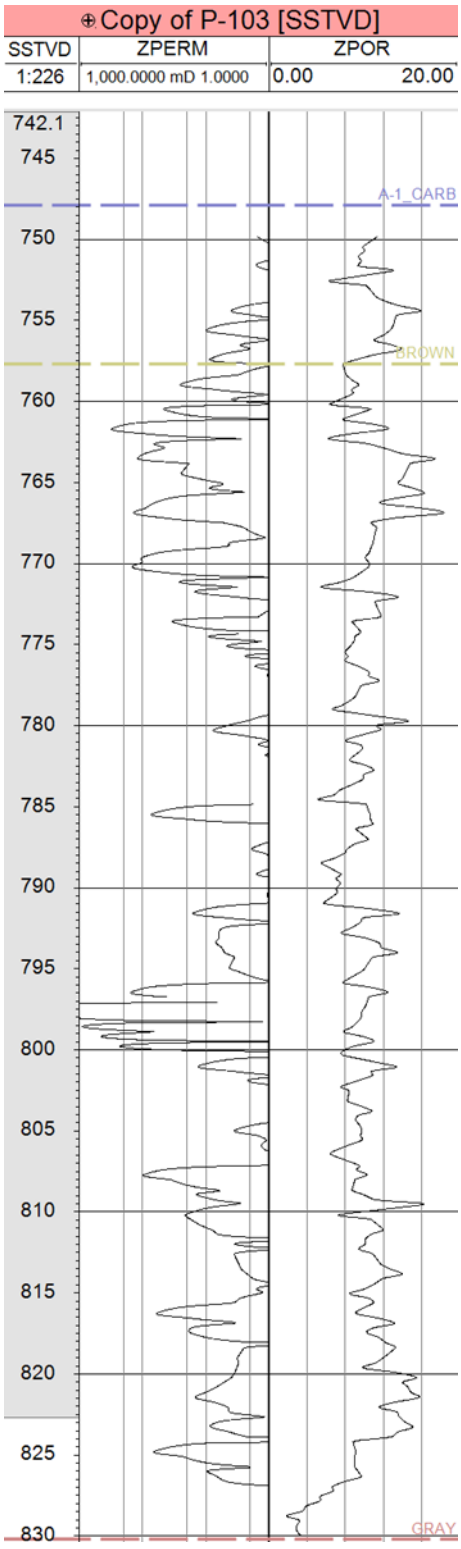


Figure 83: Permeability and porosity logs for well P-106

Appendix E: 3D survey design, acquisition parameters, and processing workflow

Puttygut acquisition parameters: Emerson Geophysical. Acquisition start and end date: 6/7/2019 to 6/14/2019. Field status: Injection. Field max inventory: 14,600 MMCF. Field inventory during survey: 9,400 MMCF. All information in this appendix was supplied by Consumers Energy.

Project:	Puttygut 3D
Type of survey:	3D
Recording system:	Sercel / E-Unite V3 (Wireless System)
Approximate square mileage:	2.72 MI^2
No. of channels:	1670
Fold:	High
Approx. receiver stations:	1670
Approx. source point:	1600
Sample rate:	1 ms.
Recording length:	2 sec.
Receiver stations intervals:	110' ft.
Source point intervals:	110' ft.
Bin Size:	55 ft.
Receiver line intervals:	440 ft.
Source line intervals:	440 ft. (Inline)
No. of shot holes/pattern:	1
Depth of shot holes:	6 ft.
Charge size:	150 gm
No. of large vibs.: 1	1 AHVIII 62,000 lb. HDW (County Rd.)
No. sweeps & Length:	4 - 8 sec. sweeps
Sweep Frequency:	12 Hz. to 150 Hz. Linear
No. of mini vibes: 1	1UNIVIB PLS 326 18,000 lb. HDW (CC use)
No of sweeps & length:	6 – 8 sec. sweeps
Sweep frequency:	12 Hz to 150 Hz linear
Geophone array:	6 geophones on the station over 25 ft. (10Hz)
High cut filter:	400 Hz
L/C filter/slope:	3 dB
Fixed gain setting:	12 dB 72 dB Nyquist
Notch filter setting:	Out
Spread configuration:	14 lines x Stations

Table 9: Puttygut acquisition parameters.

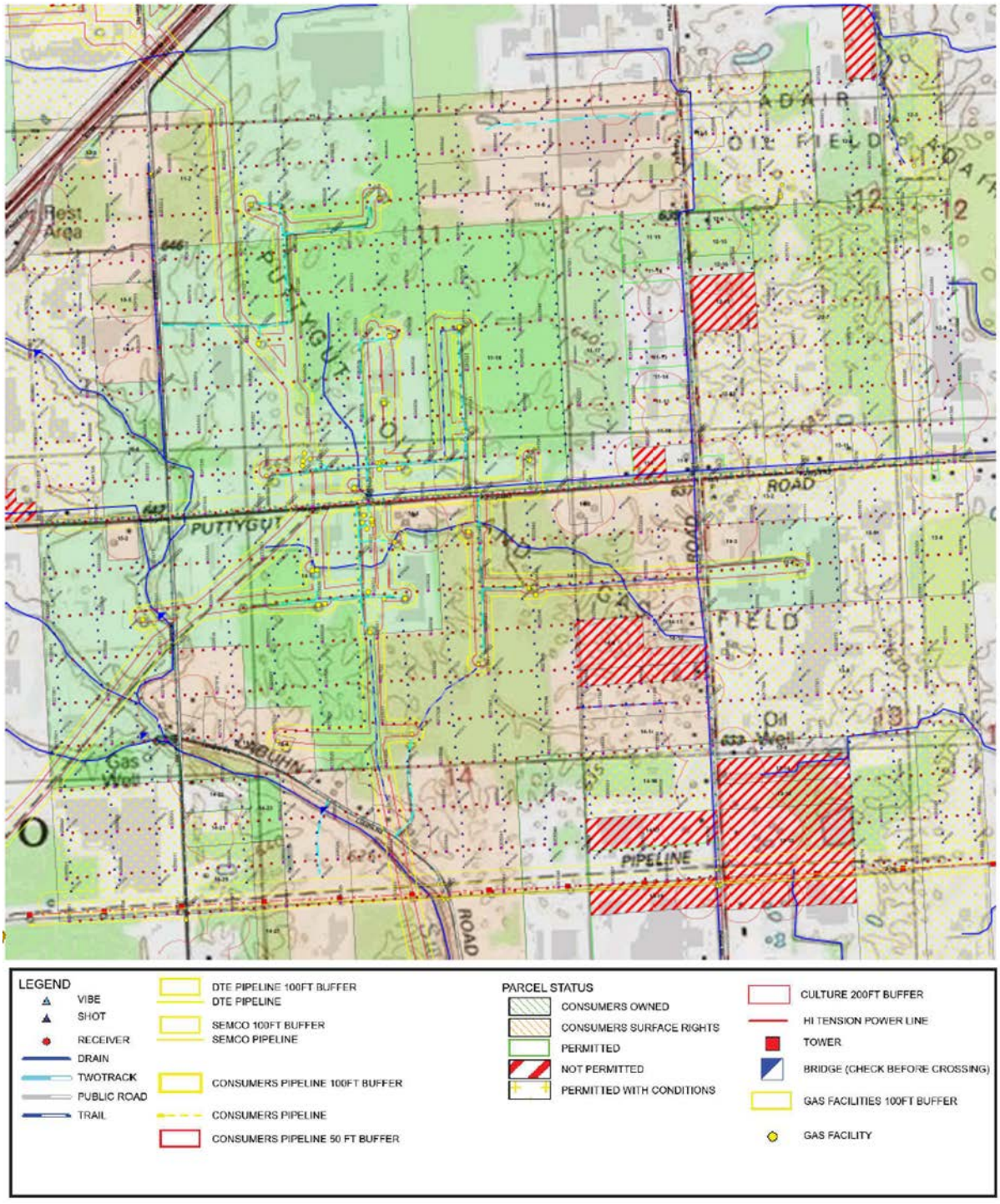


Figure 84: Puttygut pre-plot design.

Proposed BASIC PROCESSING FLOW (TBD by testing)

1. **Reformat field data to Internal Format**
2. **Spherical Divergence Correction and Trace/Spike/Noise Burst Edits**
3. **Refraction Analysis –*Every Record Picked***
   Utilizing XtremeGeo Flatirons Software
4. **Geometry QC and Correction**
5. **Geometry and Elevation/Refraction Statics Application**
6. **Surface-Consistent Deconvolution**
   Source, Receiver, Offset
7. **Zero Phase Spectral Whitening (*Optional*)**
8. **CMP Sort**
9. **Velocity Analysis (including VTI analysis/correction as necessary)**
   Program utilizes Stack Response, Gather and Semblance in Interactive Picking
10. **Surface-Consistent Automatic Reflection Statics (MaxPower, MASTT)**
11. **Iterate Steps 9 and 10 as necessary**
12. **Additional pre-stack Noise Attenuation as necessary (FDNS, FKK, SWNA, etc.)**
13. **MWNI 5D Interpolation/Regularization ** if needed-OVT****
14. **CMP Trim Statics**
15. **CMP Stack**
16. **Post Stack Filter/Scaling/Decon or Whitening Application**
17. **Post Stack Signal Enhancement –FXY Prediction Filter – as required**
18. **Final Stack Volume – output to SEGY**
19. **Post Stack Time Migration (Finite Difference or Kirchhoff) – "fasttrack" volume**
20. **Post Migration Signal Enhancement – FXY Prediction Filter – as required**
21. **Final Post Stack Migration – output to SEGY**
22. **Pre-stack Time Migration (PSTM) – Amplitude-preserving curved-ray Kirchhoff PSTM (with additional migration velocity analysis (data input from step 12)**
23. **Residual gathers, apply RNMO, Stack**
24. **Post Migration Signal Enhancement – FXY Prediction Filter – as required**
25. **Final PSTM Stack Volume – output to SEGY**

Figure 85: Sterling processing scope of work.

C 1 CLIENT: CONSUMERS ENERGY
C 2 PROJECT: PUTTYGUT 3D
C 3 AREA: ST CLAIR CO., MICHIGAN
C 4 PROCESSING: STERLING SEISMIC SERVICES, LTD JUNE 2019
C 5 DATASET: PRE-STACK MIGRATION
C 6 SAMPLE INTERVAL: 1.0 MSEC RECORD LENGTH: 3000 MS
C 7 DATUM: 1000 FEET REPL VELOCITY: 10000 F/S
C 8 SEGY IBM 32 FLOATING POINT
C 9 NON STANDARD HEADER INFO BYTES FORMAT
C10 INLINE NUMBER 9-12 INTEGER
C11 CROSS LINE NUMBER 13-16 INTEGER
C12 CDP NUMBER (STANDARD) 21-24 INTEGER
C13 TRACE FOLD 31-32 INTEGER
C14 DATUM 53-56 INTEGER
C15 CDP ELEVATION 57-60 INTEGER
C16 DATUM VELOCITY 91-98 INTEGER
C17 CDP X-COORDINATE 73-76 FLOATING POINT
C18 CDP Y-COORDINATE 77-80 FLOATING POINT
C19 CDP X-COORDINATE 81-84 INTEGER
C20 CDP-Y-COORDIANTE 85-88 INTEGER
C21 SURVEY REPRESENTATION
C23 INLINE 1-144 XLINE 1-171 CDPS 1-24624 Proj: MI SOUTH 2113 NAD27
C24 BINS: 55.0 X 55.0 FT INL: W/E XLN: S/N
C25 Lower Left: CDP 1 (I 1, X 1) X:2449907.8 Y:467885.0
C26 Upper Left: CDP 24454 (I 144, X 1) X:2449359.2 Y:475730.8
C27 Upper Right: CDP 24624 (I 144, X 171) X:2458686.5 Y:476383.0
C28 Lower Right: CDP 171 (I 1, X 171) X:2459235.0 Y:468537.2
C28 PROCESSING HISTORY:
C29 Geometry apply, Spherical Divergence Correction;
C30 Surface Consistent Amplitude Correction;
C31 Noisy trace removal; Minimum phase correction, Dyn/Vib Phase Match,
C32 Refraction/Elevation/Datum(floating) Statics Application,
C33 Surface Consistent Spiking Deconvolution 220ms Oper, .1 PW;
C34 Velocity Analysis, Surface Consistant Auto Statics,
C35 Source Noise Attenuation, Sort to CDP Bins, 2nd Velocity Analysis,
C36 Spectral Whitening, Surface Consistant Auto Statics #2,
C37 3rd Velocity Analysis, Final Datum Correction, CDP Flexbinning,
C38 Kirchhoff Migration, Migration Velocity Analysis, CDP Stack,
C39 FXY Deconvolution, Bandpass Filter, 3 Window Mean Scaling

Figure 86: Puttygut PSTM SEGY header.

References

Barnes, A., 2016, Handbook of Poststack Seismic Attributes: Geophysical References Series, 21, The Society of Exploration Geophysicists, Chapter 4, pages 47-48.

Barnes, A. E., 2000, Weighted average seismic attributes, GEOPHYSICS, 65(1), 275-285

Brock, J. C., Palaseanu-Lovejoy, M., Wright, C. W., Nayegandhi, A., 2008, Patch-reef morphology as a proxy for Holocene sea-level variability, Northern Florida Keys, USA, Coral Reefs, Vol.27(3), 555-568

Brock, T., Elenbaas, D., and G. Schmidt, 1995, Secondary Recovery in Michigan Reefs Summary Results, Recovery Achieved, In: Engineering Applications for Michigan: Society of Petroleum Engineers, Continuing Education Seminar Notes, Mt. Pleasant, Mi, 1995, 30 p.

Brown, A., 2011, Interpretation of Three-Dimensional Seismic Data, Seventh Edition: AAPG Memoir 42, 7th Edition/SEG Investigation in Geophysics, No. 9, pg. 247

Catacosinos, P., Daniels, P., and W. Harrison, 1991, Structure, stratigraphy, and petroleum geology of the Michigan Basin; interior cratonic basins. AAPG Memoir, v.51, 561-601

Chopra, S., and K. Marfurt, 2007a, Seismic attributes for prospect identification and reservoir characterization: SEG and EAGE.

Chopra, S., and K. Marfurt, 2007b, Volumetric curvature attributes add value to 3D seismic data interpretation, The Leading Edge, 26(7), 856-867

Eichkitz, C. G., Davies, J., Amtmann, J., Schreilechner, M. G., and P. de Groot, February 2105, Grey level co-occurrence matrix and its application to seismic data, First Break, 33, 71-77

Eichkitz, C. G., Schreilechner, M. G., de Groot, P. and J. Amtmann, March 2015, Mapping directional variations in seismic character using GLCM based attributes, Interpretation, 3(1), 13-23.

Garrett, J., 2016, A sequence stratigraphic model for the Silurian A-1 Carbonate and modeling of a Niagara-Lower Salina reef complex, Michigan Basin, U.S.A., M.S. thesis, Western Michigan University

Goloshubin, G., Dmitry S., Vjacheslav V., Gleb T., and L. Monir, 2008, Reservoir Permeability from Seismic Attribute Analysis, The Leading Edge, 27(3), 376-81

Huang, Y.-P., Geng, J.-H., Zhong, G.-F., Guo, T.-L., Pu, Y., Ding, K.-Y., and J.-Q., Ma., 2011, Seismic Attribute Extraction Based on HHT and Its Application in a Marine Carbonate Area, Applied Geophysics, 8(2), 125-133

Iturrarán-Viveros, U., 2012, Smooth regression to estimate effective porosity using seismic attributes, Journal of Applied Geophysics, 76, 1-12

Kohonen, T., 1995, Self-Organizing Maps, Springer Berlin Heidelberg

Kozlov, E., 2007, Seismic signature of a permeable, dual-porosity layer, GEOPHYSICS, 72(5), 281-291

Laudon, C., Stanley, S., and P. Santogrossi, 2019, Machine learning applied to 3D seaismic data from the Denver-Julesburg Basin imporoves stratigraphic resolution in the Niobrara, Unconventional resources technology conference, 337

Lichman, E., and G. Goloshubin, 2003, Unified approach to gas and fluid detection on instantaneous seismic wavelets: 73rd Annual International Meeting, SEG, ExpandedAbstracts, 1699–1702.

Michigan Department of Environmental Quality, 2019, Michigan Office of Oil, Gas, and Minerals. Oil and Gas Miner database. http://www.michigan.gov/deq (accessed 1 February 2019).

Nejad, M. R. S., Hassani, H., Khorasani, M. M., Javaherian, A., and M. R. Sokooti, 2009, The investigation of the spectral decomposition application in detecting reef reservoir on Abadan Plain, Iran, Australian Journal of Basin and Applied Sciences, 3(2), 866-874

Neumann, A. C., and I. Macintyre, Reef response to sea level rise: keep-up, catch-up or give-up: Proceedings of the 5th International Coral Reef Symposium, Tahiti (1985), pp. 105-110

NOAA Flower Garden Banks National Marine Sanctuary website, https://flowergarden.noaa.gov/ , accessed December, 2019.

Pramanik, A. G., V. Singh, Rajiv Vig, A. K. Srivastava, and D. N. Tiwary, 2004, Estimation of effective porosity using geostatistics and multiattribute transforms: A case study, GEOPHYSICS, 69(2), 352-372

Reich, C.D., Hickey, T.D., DeLong, K.L., Poore, R.Z., and Brock, J.C., 2009, Holocene core logs and site statistics for modern patch-reef cores—Biscayne National Park, Florida: U.S. Geological Survey Open-File Report 2009–1246, 26 p.

Rine, M., 2019, A new chronostratigraphic framework for the Silurian (Wenlockian) Niagara and Salina units of the Michigan Basin, Ph.D. dissertation, Western Michigan University

Roden, R. and D. Sacrey, 2015, Seismic pattern recognition in shale resource plays, E&P magazine

Roden, R., Smith, T.A., and D. Sacrey, 2015, Geologic pattern recognition from seismic attributes: Principal component analysis and self-organizing maps, Interpretation, Volume 3, Number 4, SAE59-SAE83

Roden, R. and C. Chen, 2017, Interpretation of DHI characteristics with machine learning, First Break, Issue 5, Volume 35, 55-63

Roden, R. and P. Santogrossi, 2017, Significant advancements in seismic reservoir characterization with machine learning, The First, Volume 3, 14-19

Roden, R., Smith, T. A., Santogrossi, P., Sacrey, D., and G. Jones, 2017, Seismic interpretation below tuning with multi-attribute analysis, The Leading Edge, 36, 330-339

Saadatinejad, M. R., Javaherian, A., and K. Sarkarinejad, 2012, Investigation of the various spectral decomposition methods to detect and explore hidden complex reef reservoir

structures and their hydrocarbon potentials in northwestern part of the Persian Gulf, Energy Exploration & Exploitation, 30(6), 867-888

Santogrossi, P., 2017, Classification/corroboration of facies architecture in the Eagle Ford group: A case study in then bed resolution, Unconventional resources technology conference, 2696775

Sarhan, M. A., 2017, The efficiency of seismic attributes to differentiate between massive and non-massive carbonate successions for hydrocarbon exploration activity, NRIAG Journal of Astronomy and Geophysics, 6(2), 311-325

Schot, S., 1978, Aberrancy: Geometry of the Third Derivative. Mathematics Magazine, 51(5), 259-275

Schuelke, J. S., Quirein, J. A., and J. F. Sarg, 1998, Reservoir architecture and porosity distribution, Pegasus Field, West Texas - An integrated sequence stratigraphic-seismic attribute study using neural networks, Geo-Triad ’98, 142-145

Sears, S., and F. Lucia, 1979, Reef-growth model for Silurian pinnacle reefs, northern Michigan reef trend, Geology v.7, 299-302

Skirius, C., Nissen, S., Haskell, N., Marfurt, K., Hadley, S., Ternes, D., Michel, K., Reglar, I., D’amico, D., Deliencourt, F., Romero, T., D’angelo, R., and B. Brown, 1999, 3-D seismic attributes applied to carbonates, The Leading Edge, 18(3), 384-93

Sukmono, S., Santoso, D., Samodra, A., Waluyo, W., and S. Tjiptoharsono, 2006, Integrating seismic attributes for reservoir characterization in Melandong field, Indonesia, The Leading Edge, 25(5), 532-538

Toelle, B. and Y. V. Ganshin, 2018, Porosity characterization in a Silurian reef, northern Michigan Basin, using azimuthal seismic data and potential impacts for enhanced oil recovery, The Geological Society of America, Special Paper 531, 157-173